

UNIVERSITY OF CALGARY

Interactions between Serum Albumin Proteins and Polystyrene Nanoparticles

by

Amanda Iris Bishop

A THESIS

SUBMITTED TO THE FACULTY OF GRADUATE STUDIES

IN PARTIAL FULFILLMENT OF THE REQUIREMENTS FOR THE

DEGREE OF MASTER OF SCIENCE

GRADUATE PROGRAM IN CHEMISTRY

CALGARY, ALBERTA

JULY, 2018

© Amanda Iris Bishop 2018

## Abstract

Nanoparticles (NPs) have become increasingly popular for several applications, especially regarding biomedical applications because of their unique properties. However, when a nanoparticle enters a biological medium, it is thought to become encapsulated in proteins and other biomolecules in a coating termed a “protein corona.” This coating is significant as it can change the identity and surface properties of the nanoparticle, thus affecting its fate within the biological medium. Studies on the formation of NP-protein complexes have been ongoing for years although the interactions are still not fully understood due to their dynamics and complexity. As a result, this hinders the use of NPs to their full potential in biomedical applications.

The studies performed in this thesis analyze the interactions of fluorescent polystyrene nanoparticles (FS) of two different sizes with bovine serum albumin proteins (BSA) by the technique of Two-Photon Excitation Cross-correlation Spectroscopy (TPE-FCCS). These interactions were explored both thermodynamically and kinetically to gain insight into the formation of the early hard corona and the kinetics of the formation of the BSA-FS complexes. The results suggested very low binding ratios and a mechanism of protein association dependent on the size of the sphere present in solution. The results also suggested an irreversible formation of BSA-FS complexes, in which the BSA appears to stack at the surface of the FS. These findings are significant as they challenge the current beliefs on the formation of a protein corona and perceived monolayer formation, and furthermore, provides a deeper understanding of NP-protein interactions.

## Acknowledgements

Graduate school is nothing like I had ever imagined, and I truly believe I would not have made it to this point if it wasn't for Dave taking a chance on me. Thank you, Dave, for giving me that chance. Thank you for allowing me to learn, to fail, and to pick myself back up and do it all over again while still being so supportive in the process. And also, for being a voice of reason in my project, teaching, and life endeavors, and for encouraging a work-life balance. I am extremely grateful and appreciative for all your guidance and help.

I would also like to thank my boyfriend, Thana, who has been there through much of my graduate degree, especially through the rough initial stages. Without his motivation, support, and strong belief in me, I don't think this thesis would have been finished. I cannot begin to express how grateful and thankful I am to have such a supportive and caring partner by my side.

My groupmates – past and present – have made my grad school journey so much more enjoyable, and I thank them dearly. To Amy, who set me up in the lab when I joined the Cramb group. To Rui, who I could always turn to for help with my project and for being a great inspiration to me. To Veritas, who was a shoulder to lean on during this thesis-writing process and for always brightening my day. To Wayne, teaching me how to process my data. To Hagar, for always bringing a smile to my face and being so positive! To Sarah, for sharing my love for the mountains and always being willing to lend a helping hand.

Lastly, I'd like to thank everyone else who helped me with my project and journey in some way: Dr. Max Anikovskiy, Dr. Ali Darbandi, Priya and Adrianna, everyone in the Chemistry office, and my family. I would also like to thank NSERC and Queen Elizabeth II Scholarships for the funding.

## Table of Contents

<b>Abstract</b> .....	ii
<b>Acknowledgements</b> .....	iii
<b>Table of Contents</b> .....	iv
<b>List of Tables</b> .....	vi
<b>List of Figures</b> .....	vii
<b>List of Symbols, Abbreviations and Nomenclature</b> .....	xii
<b>CHAPTER ONE: INTRODUCTION</b> .....	1
1.1 Motivation.....	1
1.2 Protein Corona.....	2
1.2.1 Hard and Soft Corona.....	2
1.2.2 Factors Driving Protein Adsorption.....	3
1.2.3 Specific NP Properties and Solution Conditions Influencing the NP-Protein Interactions.....	6
1.2.4 Protein Conformation Upon Adsorption to NP.....	8
1.2.5 Is the Corona a Protein Monolayer on an NP surface?.....	11
1.3 Fluorescent Polystyrene Nanoparticles.....	12
1.4 Bovine Serum Albumin.....	13
1.5 Techniques to Study Binding.....	16
1.5.1 Ultra-Violet Visible and Fluorescence Spectroscopy.....	16
1.5.2 Circular Dichroism.....	17
1.5.3 Gel Electrophoresis.....	17
1.5.4 Dynamic Light Scattering and Zeta Potentials.....	18
1.5.5 Isothermal Titration Calorimetry.....	19
1.5.6 Transmission Electron Microscopy.....	20
1.6 Direction of this Study.....	21
<b>CHAPTER TWO: MATERIALS, METHODS AND THEORETICAL BACKGROUND</b> .....	22
2.1 Introduction.....	22
2.2 Materials and Sample Preparation.....	22
2.3 Measurement of Binding via TPE-FCCS.....	24
2.3.1 Two-Photon Excitation Theory.....	24
2.3.2 Fluorescence Correlation and Cross-correlation Spectroscopy.....	28
2.3.2.1 Autocorrelation.....	28
2.3.2.2 Cross-correlation.....	33
2.3.3 TPE-FCS/FCCS Instrumentation.....	35
2.3.4 TPE-FCCS Nanoparticle-Protein Binding Experiments.....	37
2.3.4.1 Methods.....	37
2.3.4.2 FCCS Cross-Talk Correction.....	39

<b>CHAPTER THREE: EQUILIBIRUM BINDING RATIO DETERMINATION BETWEEN BOVINE SERUM ALBUMIN PROTEINS AND FLUOSPHERES.....</b>	<b>41</b>
3.1 Motivation.....	41
3.2 Results.....	42
3.2.1 Time Evolution and Equilibration of the BSA-FS Interactions.....	42
3.2.2 Approaches to Estimate the Protein-NP Binding Ratio at Equilibrium.....	50
3.2.3 Further Evidence to Support the Low Binding of Protein to NPs; Introduction to the Pseudo-Explicit Model.....	57
3.2.4 Transmission Electron Microscopy Images give Insight into the Binding Ratio.....	63
3.2.5 Unlabeled BSA Experiments for Insight into BSA-FS Binding.....	66
3.2.6 Stability of BSA-FS complexes in Culture Media.....	68
3.3 Discussion.....	69
3.3.1 Dynamics and Mechanism of the BSA-FS Interactions.....	69
3.3.2 Is there a Size-Dependency for the Binding Ratio between FS and BSA?.....	75
3.3.3 The Significance of the Estimated Binding Ratio.....	76
3.4 Conclusions.....	78
<b>CHAPTER FOUR: DYANMICS AND EQUILIBRIUM EVALUATION OF THE INTERACTIONS BETWEEN BOVINE SERUM ALBUMIN PROTEINS AND FLUOSPHERES.....</b>	<b>80</b>
4.1 Motivation.....	80
4.2 Results and Discussion.....	81
4.2.1 FS-BSA Interaction Kinetics.....	81
4.2.1.1 On-Rate Constant ( $k_{on}$ ) Determination.....	81
4.2.1.2 Association and Dissociation ( $K_A$ and $K_D$ ) Determination.....	87
4.2.1.3 Off-Rate Constant ( $k_{off}$ ) Determination.....	95
4.2.1.4 Insight into the BSA-FS Reaction Kinetics and Binding Mechanism.....	96
4.2.2 Fluorescence Intensity Changes in FS and BSA upon Mixing.....	100
4.2.3 Unlabeled FS Experiments for Insight into Energy Transfer to Labeled BSA.....	100
4.3 Global Discussion.....	106
4.3.1 Dynamics of the BSA-FS Interactions.....	106
4.3.2 Binding affinity of the BSA-FS Interactions.....	108
4.4 Conclusions.....	113
<b>CHAPTER FIVE: CONCLUSIONS AND GLOBAL PERSPECTIVE.....</b>	<b>116</b>
5.1 General Findings.....	116
5.2 Future Studies.....	118
<b>References.....</b>	<b>120</b>
<b>Appendix A.....</b>	<b>132</b>
<b>Appendix B.....</b>	<b>134</b>

## List of Tables

<b>Table 2.1</b> Tested mixtures and corresponding concentrations of BSA (nM) mixed with 1 nM red-labeled FS <sub>100</sub> or yellow-green-labeled FS <sub>200</sub> analyzed for the binding and kinetics studies. All mixtures were performed in triplicate.....	38
---	----

## List of Figures

**Figure 1.1** Schematic demonstrating the formation of a protein corona around an NP upon entering a biological medium. The surface of the NP (left) becomes surrounded by proteins and other biomolecules (depicted by the orange, blue, and green drawings) that form a weak outer layer, known as the “soft corona,” which are rapidly exchanging with the free proteins. Over time, the “hard corona” forms (right), where the exchange of proteins at the surface occurs much more slowly. The diagram is not to scale and does not accurately represent proportions of different entities in a biological medium.....3

**Figure 1.2** Crystal structure of bovine serum albumin showing the locations of the domains and sub-domains.<sup>78</sup> Reproduced with kind permission from Elsevier (Appendix B).....15

**Figure 2.1** Jablonski diagram showing one-photon excitation (OPE) and two-photon excitation (TPE), where  $S_0$ ,  $S_1$ ,  $T_1$ , and  $i$  denote the ground state, singlet excited state, triplet excited state, and intermediate state. Intersystem crossing (ISC) is denoted by the blue arrow.  $h\nu_f$  and  $h\nu_p$  represent fluorescence emission and phosphorescence emission, respectively.....26

**Figure 2.2** Illustration of the focused excitation volume using a one-photon excitation (OPE) process versus a two-photon excitation (TPE) process.....27

**Figure 2.3** Overview of Fluorescence Correlation Spectroscopy. (A) Fluorescent particles diffuse into and out of the excitation volume, which generate fluctuations in the detected fluorescence intensity signal. (B) The corresponding fluorescence intensity fluctuations tracked over time. (C) The resulting autocorrelation decay curve from the fluctuations in fluorescence intensity. The red line is the fitting with Equation 2.10.....32

**Figure 2.4** An example of the effect of concentration and diffusion on the resulting autocorrelation decay curves. Increasing the concentration of a fluorescent particle will lower the amplitude of the autocorrelation decay curve. Larger particles that diffuse more slowly out of the focal volume will shift the autocorrelation curve to the right.....33

**Figure 2.5** An example of the output of Fluorescence Cross-correlation Spectroscopy. (A) Shows the fluorescent count rate trajectories of two fluorescently-labeled entities, while (B) shows the corresponding cross-correlation decay curve, indicating that the two fluorescent entities are interacting with one another in solution.....35

**Figure 2.6** Schematic of the setup and instrumentation involved for the TPE-FCCS experimentation. A 100 fs pulsed titanium:sapphire laser, pumped by the Nd:VO<sub>4</sub> laser, is expanded to fill the back aperture of the objective lens. The band pass filter then separates the fluorescence emission signals that arise from the excitation volume. The dichroic optics directs the beam to and from the objective lens. The tube lens guides the emission signals to another dichroic optics, which allows for the separation of the signals into red and green emissions. These emissions pass to their respective filters, then to the avalanche photodiodes, which are analyzed by PC.....37

**Figure 2.7** An example of cross-talk or “bleed-through” in the emission detection filters. The spectral cut offs of the green and red emission filters are shown by the black and blue lines, respectively. The green curve corresponds to the emission spectrum of yellow-green dye labeling the FS<sub>200</sub>, where the long tail of its emission is seen to bleed into the red detection channel. The red curve corresponds to the emission spectrum of the Alexa Fluor® 594 dye labeling the BSA.....39

**Figure 3.1** Fluorescence count rate trajectories for (A) 1 nM red-labeled FS<sub>100</sub> and (B) 800 nM green-labeled BSA. (C) demonstrates the background signal from the PBS buffer alone. The green and red signals correspond to the signals detected in the green and red channels, respectively. The black lines represent the average fluorescence intensities.....43

**Figure 3.2** Apparent cross-correlation decay (A) and corresponding relative cross-talk (B) of red fluorescence (shown in red) to green fluorescence (shown in green) from a 1 nM sample of yellow-green-labeled FS<sub>200</sub>.....44

**Figure 3.3** Cross-correlation decay curves obtained at various time points upon mixing yellow-green FS<sub>200</sub> (1 nM) with red-labeled BSA (2000 nM).....46

**Figure 3.4** Cross-correlation curve amplitudes over various time points for a mixture of yellow-green FS<sub>200</sub> (1 nM) and red-labeled BSA (2000 nM).....47

**Figure 3.5** Autocorrelation decay curves for the red-labeled BSA (2000 nM) obtained at various time points upon mixing with yellow-green-labeled FS<sub>200</sub> (1 nM).....49

**Figure 3.6** Average number of BSA proteins per FS using Equation 3.13 for (A) the system composed of green-labeled BSA and red-labeled FS<sub>100</sub>, and (B) for the system composed of red-labeled BSA and yellow-green-labeled FS<sub>200</sub>. The concentration of FS in both systems was held at 1 nM. The errors correspond to the propagation of error calculations.....55

**Figure 3.7** Average number of BSA proteins per FS using Equation 3.13 employing larger concentration ratios of (A) green-labeled BSA with the red-labeled FS<sub>100</sub> and of (B) red-labeled BSA with the yellow-green-labeled FS<sub>200</sub> to determine if a saturation of BSA at the surface of the FS could be achieved. The errors correspond to the propagation of error calculations.....56

**Figure 3.8** Theoretical  $G_x(0)$  values calculated using Equation 3.10 for various combinations of bound and free BSA based on a mixture of red-labeled BSA (5000 nM) and yellow-green-labeled FS<sub>200</sub> (1 nM). The experimentally obtained  $G_x(0)$  for this system was between 0.05 and 0.06, which would theoretically correspond to an average of approximately 140 BSA proteins per FS<sub>200</sub> NP based on this estimation.....58

**Figure 3.9** (A) Theoretical  $G_p(0)$  values calculated using Equation 3.5 for various combinations of free and bound BSA based on a mixture of red-labeled BSA (5000 nM) and yellow-green-labeled FS<sub>200</sub> (1 nM). The experimentally obtained  $G_p(0)$  was found to be 0.008 for this system, which would theoretically correspond to an average of approximately 140 BSA proteins per FS. (B) shows the estimated value for  $G_p(0)$ , approximately 0.29, if all proteins were bound to FS.....59

**Figure 3.10** Average number of BSA proteins per FS as calculated using the pseudo-explicit model for (A) the system composed of green-labeled BSA and red-labeled FS<sub>100</sub>, and (B) for the system composed of red-labeled BSA and yellow-green-labeled FS<sub>200</sub>. The concentration of FS in both systems was held at 1 nM. Errors on the last points correspond to propagation errors from the calculations.....60

**Figure 3.11** Average number of BSA proteins per FS as calculated using the pseudo-explicit hypothetical model and employing larger concentration ratios of (A) green-labeled BSA with the red-labeled FS<sub>100</sub> and of (B) red-labeled BSA with the yellow-green-labeled FS<sub>200</sub> to determine if a saturation of BSA at the surface of the FS could be achieved. Errors on the last points correspond to propagation errors from the calculations.....61

**Figure 3.12** TEM images of (A) unstained red-labeled FS<sub>100</sub> alone and of (B) red-labeled FS<sub>100</sub> stained with uranyl acetate.....63

**Figure 3.13** TEM image of an equilibrated mixture of green-labeled BSA (800 nM) and red-labeled FS<sub>100</sub> (1 nM).....65

**Figure 3.14** Comparison of the estimated binding ratio of a mixture of 400 nM unlabeled and 400 nM BSA with 1 nM yellow-green FS<sub>200</sub> (red point) to a mixture of 800 nM labeled BSA with 1 nM yellow-green FS<sub>200</sub>. The red point better compares with the estimated binding ratio for a mixture of 400 nM labeled BSA with 1 nM FS, therefore suggesting the label on the BSA does not drive the interaction between the BSA and FS.....67

**Figure 3.15** Initial fluorescence intensity measurements of (A) red-labeled FS<sub>100</sub> in EBM-2 and (B) yellow-green-labeled FS<sub>200</sub> in EGM-2. The large peaks in these fluorescence intensity measurements are indicative of immediate agglomeration of the NPs in the media. After approximately two hours, the FS<sub>100</sub> (C) were visible in the media as large agglomerates, and the FS<sub>200</sub> (D) had completely precipitated out of the media, indicated by the absence of a fluorescence intensity signal.....69

**Figure 4.1** Cross-correlation curve amplitudes over various time points for a mixture of yellow-green FS<sub>200</sub> (1 nM) and red-labeled BSA (2000 nM). The red line corresponds to fitting with Equation 4.1.....81

**Figure 4.2**  $k_{on}$  rate constants determined for various initial concentrations of labeled BSA mixed with (A) red-labeled FS<sub>100</sub> (1 nM) and (B) yellow-green-labeled FS<sub>200</sub> (1 nM) in PBS. The errors were obtained from the fittings.....82

**Figure 4.3**  $k_{on}$  rate constants across all concentration ratios tested of BSA interacting with (A) red-labeled FS<sub>100</sub> and (B) yellow-green-labeled FS<sub>200</sub> in PBS. At the highest ratio, the concentration of FS<sub>100</sub> was dropped to 0.5 nM, while the concentration of FS<sub>200</sub> was dropped as low as 0.0625 nM. The errors were obtained from the fittings.....84

**Figure 4.4** (A)  $1/G_p(0)$  values tracked over the course of the experimental time, in seconds, for a mixture of 800 nM red-labeled BSA and 1 nM FS<sub>200</sub> in PBS. The red line represents the fitting of the data with Equation 4.2. (B) Linearized form of the data is displayed in panel (A).....85

**Figure 4.5**  $k_{on}$  rate constant values obtained from the decay curves of  $1/G_p(0)$  as a function of time for various mixtures of red-labeled BSA (200-5000 nM) and yellow-green-labeled FS<sub>200</sub> (1 nM) in PBS. The errors were obtained from the fittings.....86

**Figure 4.6**  $k_{on}$  rate constant values obtained from the decay curves of  $1/G_p(0)$  as a function of time for all tested mixtures of red-labeled BSA (200-5000 nM) and yellow-green-labeled FS<sub>200</sub> (ranging as low as 0.0625 nM and up to 1 nM) in PBS. The errors were obtained from the fittings.....87

**Figure 4.7** The linearized Hill plot for the equilibrated system composed of the (A) red-labeled FS<sub>100</sub> (1 nM) and green-labeled BSA and (B) yellow-green-labeled FS<sub>200</sub> (1 nM) and red-labeled BSA. The x-intercepts of these plots allowed for the determination of the approximate  $K_D$  value for the system.....89

**Figure 4.8**  $K_A$  values determined using the “sites bound” approach for BSA (ranging 200 nM to 5000 nM) interacting with (A) red-labeled FS<sub>100</sub> (1 nM) and (B) yellow-green-labeled FS<sub>200</sub> (1 nM). The errors shown on a few points correspond to the propagation of errors from the calculations.....91

**Figure 4.9**  $K_A$  values determined for the higher concentration ratios of BSA to FS using the “sites bound” approach for BSA (200 to 5000 nM) interacting with (A) red-labeled FS<sub>100</sub> (0.5 to 1 nM) and (B) yellow-green-labeled FS<sub>200</sub> (0.0625 to 1 nM). The errors shown on a few points correspond to the propagation of errors from the calculations.....92

**Figure 4.10** Plot of the log ( $K_A$ ) from the values determined through the “sites bound” approach as a function of the log (Protein concentration) ranging from 200 to 5000 nM, for the system composed of BSA interacting with FS<sub>200</sub> (1 nM).....94

**Figure 4.11** Examples of the average fluorescence intensity changes over the total experiment time for a mixture of (A) 400 nM green-labeled BSA interacting with 1 nM red-labeled FS<sub>100</sub> and (B) 3500 nM green-labeled BSA interacting with 1 nM red-labeled FS<sub>100</sub>. The BSA proteins are denoted by the green squares, and the FS<sub>100</sub> are denoted by the red circles. As seen in both examples, the average fluorescence intensities of both entities remain relatively constant over the total experimental time.....101

**Figure 4.12** Examples of the average fluorescence intensity changes over the total experiment time for a mixture of (A) 800 nM red-labeled BSA interacting with 1 nM yellow-green-labeled FS<sub>200</sub> and (B) 5000 nM red-labeled BSA interacting with 1 nM yellow-green-labeled FS<sub>200</sub>. The BSA proteins are denoted in red, and the FS<sub>200</sub> are denoted in green. As seen in these examples, the average fluorescence intensities of the BSA changes depending on its concentration, while the fluorescence intensity of the FS<sub>200</sub> drops slightly in both cases.....103

**Figure 4.13** (A) Normalized fluorescence intensity changes for the yellow-green-labeled FS<sub>200</sub> upon being mixed with red-labeled BSA (red circles) and pseudo-explicit binding ratio for this FS-BSA system (black circles). (B) shows a blow-up of the observed change in fluorescence intensity for the FS as the ratio of protein to FS increases. Interestingly, there appears to be a re-generation of fluorescence intensity after a ratio of approximately 10,000 : 1.....105

**Figure A1** Examples of various fittings of  $G_x(0)$  data as a function of time for mixtures of 1 nM red-labeled FS<sub>200</sub> with (A) 800 nM BSA, (B) 2400 nM BSA, (C) 3500 nM BSA, and (D) 5000 nM BSA. The line corresponds to the fitting with Equation 4.1.....132

**Figure A2** Examples of various fittings of  $G_x(0)$  data as a function of time for mixtures of 1 nM yellow-green-labeled FS<sub>200</sub> with (A) 800 nM BSA, (B) 2000 nM BSA, (C) 3500 nM BSA, and (D) 5000 nM BSA. The red line corresponds to the fitting with Equation 4.1.....133

## List of Symbols, Abbreviations and Nomenclature

<b>Symbol</b>	<b>Definition</b>
APD	Avalanche photodiode
BSA	Bovine serum albumin
$c$	Speed of light
$\langle C \rangle$	Average concentration of diffusing emitter
$C_i$	Concentration of emitter $i$
CD	Circular dichroism
Cys	Cysteine
$D$	Diffusion constant
DLS	Dynamic light scattering
$\langle F \rangle$	Average fluorescence intensity
FCCS	Fluorescence cross-correlation spectroscopy
FCS	Fluorescence correlation spectroscopy
$F_i^{cal}$	Average fluorescence intensity of calibration green particles in green detection channel
$F_j^{cal}$	Average fluorescence intensity of calibration green particles in red detection channel
$f_p$	Laser repetition rate
fs	Femtosecond
FS	FluoSphere
FS <sub>100</sub>	FluoSphere 100 nm in diameter
FS <sub>200</sub>	FluoSphere 200 nm in diameter
$G(0)$	Autocorrelation amplitude at time zero
$G(\tau)$	Autocorrelation function/decay
$G_p(0)$	Autocorrelation amplitude for the proteins
$G_s(0)$	Autocorrelation amplitude for the spheres
$G_x(0)$	Cross-correlation amplitude at time zero
$G_x(\tau)$	Cross-correlation function
GS	Ground state
HSA	Human serum albumin
$i$	Intermediate virtual state
IR	Infrared
ISC	Intersystem crossing
ITC	Isothermal titration calorimetry
$K_A$	Association constant
$K_D$	Dissociation constant
$k_{on-auto}$	On-rate constant from autocorrelation amplitude values
$k_{on-cross}$	On-rate constant from cross-correlation amplitude values

$k_{\text{off}}$	Off-rate constant
$k_{\text{on}}$	On-rate constant
$k_{\text{stack}}$	On-rate constant for the stacking of protein onto a surface-bound protein
$n$	Binding ratio
$N_i$	Number of emitter $i$
NA	Numerical Aperture
NP	Nanoparticle
$N_{\text{protein}}$	Number of proteins
$N_s$	Number of spheres
OPE	One-photon excitation
$\langle P \rangle$	Average laser power
P	Protein
$P_A$	Fractional occupancy
PBS	Phosphate buffered saline
pI	Isoelectric point
PS	Polystyrene
$r_0$	Laser beam waist
S	Sphere
$S_0$	Ground state
$S_1$	Singlet excited state
$T_1$	Triplet excited state
Ti-Sapph	Titanium sapphire
TEM	Transmission electron microscopy
TPE	Two-photon excitation
Trp	Tryptophan
UV-Vis	Ultraviolet-visible
$V_{\text{eff}}$	Effective volume of excitation
$z_0$	Beam radius in the z-direction
ZP	Zeta potential
$\Delta H$	Enthalpy change
$\Delta S$	Entropy change
$\delta F(t)$	Temporal fluorescence intensity fluctuations
$\hbar$	Reduced Planck's constant
$h\nu_f$	Fluorescence emission
$h\nu_p$	Phosphorescence emission
$\kappa$	Bleed-through ratio of green dye into red detection channel
$n_a$	Number of photons absorbed per fluorophore per laser pulse
$\eta_i$	Brightness of emitter $i$
$\delta$	Two-photon absorption cross-section

$\tau$	Lag time
$\tau_D$	Residence time of a diffusing molecule in the excitation volume
$\tau_p$	Laser pulse duration
$\lambda$	Wavelength

## CHAPTER ONE: INTRODUCTION

### 1.1 Motivation

Nanoparticles (NPs) have become increasingly popular and utilized in biomedical applications, such as for drug delivery, imaging, diagnostics, and therapeutics, because of their unique properties including their small sizes, surface-tunability, as well as the various compositions available. However, the interactions that occur when a NP enters a biological system are still not fully understood, which hinders the usage of NPs to their full potential for these applications. NPs are thought to become encapsulated in proteins and other biomolecules upon entry into a biological system, forming what is known as a “protein corona.”<sup>1-4</sup> The formation of the protein corona therefore affects the size and surface chemistry of the NP, which in turn affects how a cell “sees” the NP.<sup>4-6</sup>

In the past few decades, many studies have been performed to further investigate the interactions between NPs and proteins – in particular, between NPs and proteins from the blood serum – with an emphasis on identifying the proteins involved in the protein corona and the amount of proteins adsorbed to a variety of different NP surfaces.<sup>1, 2, 7</sup> However, many studies use a combination of indirect techniques to determine the presence and size of the protein corona, and there are very few kinetic studies that have been performed. Confident and conclusive quantitative analysis of the number of proteins that adsorb to an NP surface, determined using direct measurement techniques such as fluorescence cross-correlation spectroscopy, is important for the understanding of the formation of the protein corona.<sup>8-10</sup> Kinetics studies are important for the determination of the rate and mechanism of the formation of the protein corona, which can provide insight on the time evolution of the protein corona in a biological system. Both equilibrium and

kinetics studies in conjunction will provide a deeper understanding of the time-dependence, mechanism, and amount of proteins that interact with an NP upon entering a biological environment. This will allow for better design of NPs for future usage in biomedical applications.

## **1.2 Protein Corona**

### **1.2.1 Hard and Soft Corona**

When a NP enters a biological medium, it may become encapsulated with proteins and other biomolecules, forming a “protein corona,” as depicted in Figure 1.1. The formation of the protein corona is likely a dynamic process in which the proteins and biomolecules adsorbed to the NP surface are continuously exchanging with others in the biological environment. Effectively, the proteins and biomolecules “dress” the NP are loosely described as being composed of two layers: a “soft” corona and a “hard” corona.<sup>1, 2, 8, 11-14</sup> The soft corona is thought to be formed first by proteins and biomolecules that have lower binding affinities for the NP and that are either abundant in the medium or diffuse rapidly on and off the surface. Over time, the soft corona is replaced by the hard corona, which is composed of proteins and biomolecules that have a higher binding affinity for the NP. Because of these stronger interactions between the proteins and biomolecules with the NP, it can be easier to isolate and identify specific components of the hard corona. The hard corona is considered to be more important, since ultimately, a cell will interact with the protein corona decorating the surface of the NP.<sup>5, 15, 16</sup> Moreover, the factors influencing the first steps of hard corona formation have yet to be examined. Therefore, the studies presented in this thesis focus specifically on the formation of the hard corona formed by interactions between the protein and NP surface.

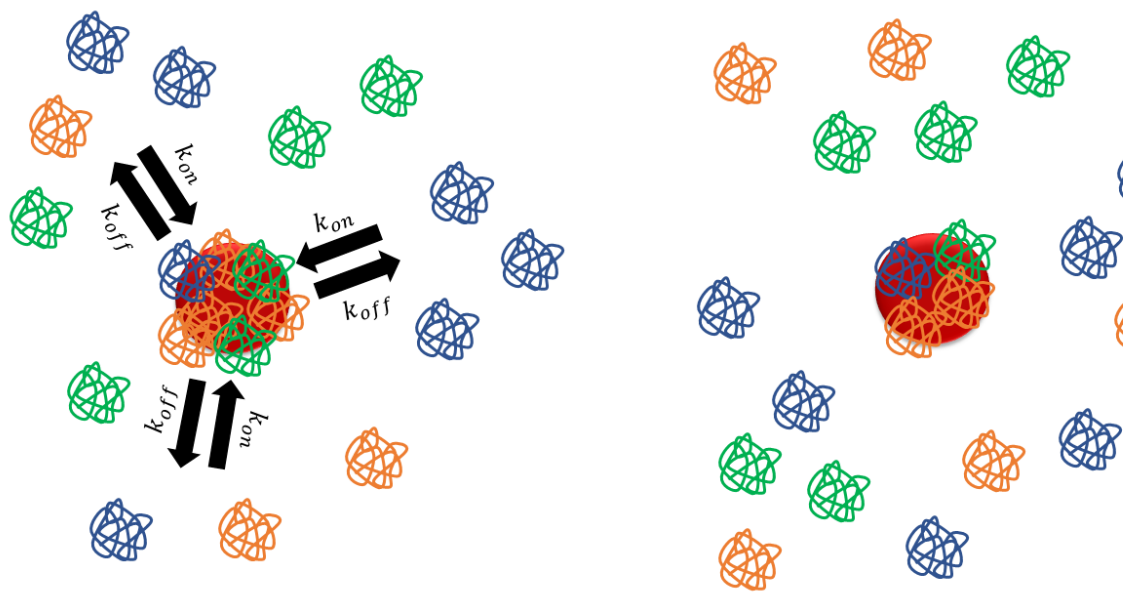


**Figure 1.1** Schematic demonstrating the formation of a protein corona around an NP upon entering a biological medium. The surface of the NP (left) becomes surrounded by proteins and other biomolecules (depicted by the orange, blue, and green drawings) that form a weak outer layer, known as the “soft corona,” which are rapidly exchanging with the free proteins. Over time, the “hard corona” forms (right), where the exchange of proteins at the surface occurs much more slowly. The diagram is not to scale and does not accurately represent proportions of different entities in a biological medium.

### 1.2.2 Factors Driving Protein Adsorption

There are two main factors that have been reported to influence the association of proteins with NPs: the hydrophobic effect<sup>17-20</sup> and electrostatic forces<sup>20-22</sup>. Although some studies attribute the formation of a protein corona based on a single factor, it is likely a combination of these factors that drive the formation of a protein corona.

One study performed by Gessner *et al.* investigating the influence of polystyrene (PS) surface hydrophobicity on plasma protein adsorption found that decreasing the hydrophobicity of the NPs was met with decreased plasma protein adsorption.<sup>19</sup> Therefore, this led the authors to conclude that the main driving force for the interaction was a result of the hydrophobic effect.<sup>19</sup> Another study performed by Monopoli *et al.* compared plasma

protein adsorption between “hydrophobic” sulfonated PS NPs and hydrophilic silica NPs and concluded that hydrophobic interactions were the driving force for the adsorption onto the PS NPs.<sup>20</sup> Their reasoning for this conclusion was that the release of the hydration shell from the NP surface as well as possible conformational changes in the adsorbed proteins led to a large entropic gain, and therefore, that the dehydration process would prevail over electrostatic repulsion.<sup>20</sup>

Other groups have suggested that the main driving force for the formation of a protein corona is a result of electrostatic forces. Studies performed by Gessner *et al.*<sup>21</sup> and Luck *et al.*<sup>22</sup> concluded the driving force for protein plasma adsorption as Coulombic after studying PS NPs with higher surface charge densities. Both studies concluded that NPs with increasing surface charge densities would show increased protein adsorption because of electrostatic interactions. Another study analyzing the interaction between bovine serum albumin and a water-soluble cationic fluorescent conjugated polymer conducted by Li *et al.* also concluded the interaction was driven by electrostatic forces.<sup>23</sup> Under their conditions (pH = 7.4, using a Tris-HCl buffer), the polymer and serum albumin would be oppositely charged, which was suggestive of a possible electrostatic driving force. The authors made this conclusion after analyzing the interaction while varying the ionic strength of the medium through the addition of NaCl<sup>23</sup>, which should lower the effect of any electrostatic interaction between the protein and polymer and result in lower adsorption.<sup>24</sup> Li *et al.* did observe fewer interactions between the two entities, leading them to conclude the interactions were governed by electrostatic forces.

Based on the changes in enthalpy ( $\Delta H$ ) and entropy ( $\Delta S$ ) for a given protein-NP interaction, it is thought that the force driving the interaction can be predicted.<sup>25, 26</sup> For

example, an interaction producing a  $\Delta H > 0$  and  $\Delta S > 0$  is suggestive of a hydrophobic driving force; a  $\Delta H < 0$  and  $\Delta S < 0$  is suggestive of van der Waals and hydrogen bonding being the driving forces; and a  $\Delta H < 0$  and  $\Delta S > 0$  is suggestive of an electrostatic driving force.<sup>25, 26</sup> This approach was used in a study performed by Mariam *et al.*, where they investigated the interactions between gold nanoparticles and bovine serum albumin proteins.<sup>26</sup> They found positive values for both  $\Delta H$  and  $\Delta S$ , and therefore concluded a hydrophobic driving force.<sup>26</sup>

It can be difficult to state with certainty that there is a single governing driving force for the interaction between an NP and proteins, as the interactions can be dependent on the conditions in solution, NP properties, and method of analysis. For example, Satzer *et al.* wanted to determine if the interaction between bovine serum albumin and myoglobin with silica NPs was purely driven by electrostatic interactions.<sup>24</sup> To do so, they added of 1M NaCl to their buffer and observed a decrease of myoglobin adsorption and an increase in serum albumin adsorption to the NPs. The authors concluded that the electrostatic force, although predominant for the interaction between myoglobin and NPs, was not the only contributing force driving the adsorption. Furthermore, they concluded that interaction between serum albumin and the silica NPs was of a hydrophobic nature. This demonstrates that, depending on the conditions, the “driving force” for the interaction can change. Ross *et al.*, in their publication, suggested analyzing each step of the association process, where the combination of steps is a result of a combination of electrostatic, hydrophobic, hydrogen bonding, and van der Waals forces.<sup>25</sup>

### 1.2.3 Specific NP Properties and Solution Conditions Influencing the NP-Protein Interactions

Several other factors influence how NP and proteins interact within a biological medium, which include the NP characteristics (for example, surface hydrophobicity, surface charge, and size)<sup>1, 2, 12, 18, 19, 21, 22, 27-35</sup>, the pH of the medium<sup>2, 17, 33, 36-41</sup>, and the temperature<sup>36, 42-45</sup>. Many studies have investigated the influence of NP characteristics on protein adsorption and specifically, plasma protein adsorption, including the effect of fluorescent labels on protein adsorption.

Müller *et al.* investigated the effect of plasma protein adsorption as a result of surface hydrophobicity changes from the fluorescent labeling of polystyrene NPs.<sup>18</sup> They compared commercially obtained unlabeled and labeled PS NPs to those they synthetically prepared and analyzed the difference in surface hydrophobicity. They found that the unlabeled NPs (commercial and house-made) were more hydrophobic than the labeled NPs. According to their results, the increased hydrophobicity of the unlabeled NPs led to higher plasma protein adsorption to the NP surfaces when compared to the labeled NPs.<sup>18</sup> Similar studies conducted by both Gessner *et al.*<sup>19</sup> and Luck *et al.*<sup>22</sup> focusing on differences in plasma protein adsorption due to differing surface hydrophobicities of a variety of PS NPs also uncovered similar results – increased NP surface hydrophobicity led to greater plasma protein adsorption. Gessner *et al.* stated that their study demonstrated that not only surface hydrophobicity, but also the functional groups present at the NP surface, have an effect on protein adsorption.<sup>19</sup> In a later study, Gessner *et al.* found that proteins with a pI < 5.5 preferentially adsorbed to NPs with basic functional groups, while proteins with a pI > 5.5 preferentially adsorbed to NPs bearing acidic functional groups.<sup>27</sup> More recently,

Kokkinopoulou *et al.* found that the adsorption of proteins was much greater for negatively charged NPs when compared to positively charged and unfunctionalized NPs.<sup>28</sup>

Another study performed by Gessner *et al.* investigated the effect of surface charge density on plasma protein adsorption on the surfaces of latex particles.<sup>21</sup> They synthesized latex particles with a range of different surface charge densities while keeping a constant particle size and surface hydrophobicity. Their study suggested that increasing the surface charge density resulted in increased plasma protein adsorption and furthermore, that the qualitative protein adsorption pattern did not change significantly between the NPs.

The authors Lundqvist *et al.* studied the effect of size and surface charge of NPs on plasma protein adsorption. They found that larger proteins tended to adsorb to larger NPs and that NP size and surface charge affected the composition of the formed protein coronas.<sup>29</sup> A more recent study by Lundqvist *et al.* found that not only the size of the NP affects the composition of the protein corona, but the surface curvature, the biological environment and abundance of proteins in the environment under study also effects the composition of the corona around the NPs.<sup>30</sup> It has been reported that a larger protein coverage tends to form on larger NPs<sup>2</sup> and conversely, less protein coverage on smaller NPs as a result of higher surface curvature.<sup>1, 31</sup>

The pH of the environment can also affect the interactions between NPs and proteins. Under certain pH conditions, proteins and functionalized NPs will take on different conformations because of protonation and deprotonation, which can affect how the proteins and NPs interact. Increasing the pH in a system where the interactions are driven primarily by electrostatic forces will result in weaker protein adsorption on negatively charged NPs because of increased electrostatic repulsion.<sup>36</sup> Several studies have

also stated that NPs may adsorb proteins most optimally in a narrow range around the pI of the protein, at which point the proteins would have a net charge of zero, and the interactions would be driven primarily by the hydrophobic effect.<sup>2, 17, 37, 38</sup>

Although the effects of temperature on protein-NP interactions have not been extensively studied, the effect of temperature may be of great relevance for *in vivo* applications since body temperature varies for different parts of the body.<sup>43</sup> In a recent study, Bhunia *et al.* analyzed the interaction between bovine serum albumin proteins and ZnO NPs under different temperatures (20°C, 30°C, 37°C, and at 42°C).<sup>44</sup> They found that the adsorption of proteins to the NP surfaces decreased with increasing temperature and further that the proteins would unfold at higher temperatures<sup>44</sup>, which has also been reported by other groups<sup>42</sup>. Another study investigating the interactions between gold NPs and bovine serum albumin reported similar results – a decrease in bovine serum albumin adsorption with increasing temperature to 45°C.<sup>36</sup> There is a definite need for more studies investigating the effect of temperature on adsorption and adsorption kinetics, especially for future use of NPs in biomedical applications.

#### **1.2.4 Protein Conformation Upon Adsorption to NP**

Since protein function is directly linked to protein conformation, it is important to know if protein adsorption to an NP surface maintains the native protein conformation or alters it, and if upon desorption of the protein, the change in conformation is reversible or irreversible. A change in protein conformation may occur because of the interaction with an NP surface and is influenced by properties of the surface and by properties of the protein itself. Such a change in protein conformation that may occur upon binding could be due to the intrinsic stability or flexibility of the protein<sup>36, 46-48</sup>, the surface curvature and chemistry

of the NP<sup>3, 24, 46</sup>, the concentration of protein on the surface<sup>45, 46, 49</sup>, and the ionic strength and pH of the medium<sup>2, 39, 45, 46, 50</sup>. The flexibility of a protein depends on the hardness (ability to maintain the native form) or softness (readily undergoes conformational changes) of the protein, which in turn, depends on the structural build (for example, number of disulfide bridges or stabilizing sites) and thermodynamics (balance between enthalpy and entropy contributions).<sup>46</sup> Duan *et al.* found that proteins with high flexibility (such as  $\beta$ -casein and human serum albumin) had the greater conformational changes in their secondary structures upon adsorption to polystyrene NPs.<sup>47</sup> A study performed by Satzer *et al.* used circular dichroism to observe conformational changes dependent on the size of silica NP to which the proteins – bovine serum albumin and myoglobin – were adsorbed.<sup>24</sup> Both proteins showed a decrease in  $\alpha$ -helical structure upon adsorption to particles above 150 nm in size, and these results were attributed to the larger particles having less surface curvature and therefore, a flatter surface for protein-NP interaction.<sup>24</sup> However, the influence of surface curvature on inducing conformational changes upon protein adsorption is not well-defined, as other studies have reported the opposite trend – greatly curved NP surfaces inducing conformational changes.<sup>33, 46, 51</sup> The extent of NP hydrophobicity and hydrophilicity has also been reported to induce protein conformational changes, where the adsorption of proteins to hydrophobic NPs have showed a greater change in secondary structure.<sup>32, 36</sup>

The abundance of proteins in the system being tested could also influence or induce a conformational change due to molecular crowding of the surface of the NP.<sup>46</sup> Two studies, both analyzing different concentrations of proteins adsorbing to silica NPs, found that at low protein concentrations, the proteins unfolded to a much greater extent than at

higher concentrations of proteins present in the system.<sup>45, 49</sup> It was also observed that the protein would unfold faster at lower protein surface concentrations, and this was attributed to there being more interfering protein-protein interactions at higher protein surface concentrations.<sup>45</sup>

As previously discussed, the pH of the medium will determine the conformation (either protonated, deprotonated, or neutral) that the protein and NP functional groups will undertake. The pH of the medium can ultimately affect the state of the amino acids involved in hydrogen bonding and electrostatic interactions. One study performed by Vertegel *et al.* observed that the percentage of  $\alpha$ -helicity of lysozyme upon adsorption to silica NPs decreased from 40% to 5% under pH conditions of 6.9 and 5.0, respectively.<sup>50</sup> As for ionic strength of the medium, Wu *et al.* reported observing greater extent of protein unfolding at higher ionic strength.<sup>45</sup>

The reversibility of the conformational changes in protein structure upon adsorption is of importance to determine the bio-functionality of the proteins upon desorption from the NP surface. It has been suggested that the reversibility of the conformational changes depend on the surface properties and nature of the NP to which the protein was adsorbed. Norde *et al.* observed irreversible changes (decreased  $\alpha$ -helicity and increased  $\beta$ -structure) in protein conformation of bovine serum albumin upon desorption from hydrophobic polystyrene NPs, but also observed the protein regain its native conformation upon desorption from hydrophilic silica NPs.<sup>52</sup> Many groups have observed conformational changes in protein structure upon adsorption to an NP surface, as described in the preceding paragraphs; however, future studies must be performed to further explore the reversibility of these changes and predict the outcomes on protein bio-functionality.

### 1.2.5 Is the Corona a Protein Monolayer on an NP surface?

The formation of a protein corona monolayer around an NP has been reported by many groups<sup>5, 53-56</sup>, where the geometrical dimensions of the NP and protein are used to identify the thickness of the resulting corona. These studies suggest that the reported increase in radius of the NP is a result of protein adsorption, where the thickness of the layer corresponds to the geometric dimensions of the protein under study. One example of this is in the study performed by Walczyk *et al.* where they used 100 nm carboxy-coated polystyrene NPs incubated with human plasma and using transmission electron microscopy imaging and dynamic light scattering observed a 10 nm increase in radius.<sup>5</sup> They attributed this increase in radius to the formation of a thin plasma-derived layer around the NPs. Other studies have suggested the formation of thick coronas and multiple shell formation at the NP surface.<sup>24, 57, 58</sup> In a study performed by Payne *et al.*, the authors calculated that bovine serum album proteins covered 230% of the surface of 60 nm carboxy-terminated PS NPs, where 100% meant the formation of a monolayer.<sup>57</sup> They assumed that the protein would bind end-on as opposed to face-on, which is not the protein's typical mechanism of binding.<sup>59</sup>

Other studies have suggested the formation of a less dense protein corona and incomplete coverage of the NP surface.<sup>14, 28, 60</sup> Landfester *et al.* calculated a 27% and 54% surface coverage of bovine serum albumin for carboxy-coated PS NPs of 190 nm in diameter at pH values of 3 and 6, respectively.<sup>60</sup> They stated that a full coverage of these NPs could not be achieved because of the repulsion that existed between the negatively-charged protein and NPs.<sup>60</sup> Kokkinopoulou *et al.* describe observing the formation of a less dense protein corona around unfunctionalized, amino- and carboxy-functionalized

polystyrene NPs after being washed and imaged using transmission electron microscopy.<sup>28</sup> The biggest issue with many of the reports thus far is the lack of use of quantitative techniques<sup>8</sup> and proper control experiments in the case of the transmission electron microscopy images – both of which should be considered in order to obtain direct support of the formation of a protein corona.

### **1.3 Fluorescent Polystyrene Nanoparticles**

FluoSpheres (FS) are fluorescently-labeled polystyrene nanospheres. These particles were chosen since have not been studied as intensively reported on in literature in relation to their kinetics and early hard corona formation. FS NPs are spherical particles that are formed using an amorphous polymer – in this case, polystyrene. The FS employed in the experiments in this thesis were purchased from Invitrogen and come as a 2% suspension in water, or 0.02 g/mL concentration, and pre-loaded with a fluorescent dye. The fluorescent dye that the manufacturers use is proprietary but is designed to show little to no photobleaching. The manufacturers label the particles by first swelling them in a solvent containing the hydrophobic dye, which can then enter the polystyrene matrix. The FS are then placed into an aqueous environment, which reverses the swelling of the particles and effectively traps the dye within the polystyrene. The manufacturers claim that once this process is complete, the dye is not exposed to the outside environment, unless the particles are subjected into an organic solvent that can result in particle swelling.

The FS's that were employed in the experiments in this thesis were carboxylate-modified, though there are a variety of surface modifications that can be chosen for these particles, such as amino and sulfate modifications. The carboxy-terminated FS NPs have a known density of pendent carboxylic acids on their surface. The manufacturers did not

specify how the NPs were functionalized, but preparation methods such as dispersion polymerization<sup>61</sup>, use of supercritical CO<sub>2</sub><sup>62</sup>, ionic liquids<sup>63</sup>, and by free radical precipitation polymerization of acrylic acid with or without a cross-linking agent in organic solvents<sup>64, 65</sup> have been previously reported.

Fluorescently labeled and unlabeled polystyrene microspheres are employed in applications such as instrument calibration (for example in microscopy and flow cytometry), as cell biology tracers, and in immunoassays.<sup>66</sup> Previously, experiments within our group have utilized these particles to study the uptake of FS in angiogenic tissues of chicken embryo chorioallantoic membrane<sup>67</sup> because they are well-established tools for determination of blood flow.<sup>68, 69</sup>

#### **1.4 Serum Albumin Proteins**

Serum albumins are the most abundant proteins in blood serum in mammals.<sup>70, 71</sup> Albumins are the principal carriers of fatty acids that are otherwise insoluble in the circulating plasma.<sup>70, 71</sup> Because of their low cost, stability, and availability, serum albumins are very popular and well-described proteins; therefore, this made serum albumin an ideal protein of choice for the experiments presented in this thesis.

Mammalian serum albumin proteins are chemically very similar. Their amino acid sequence contains a high percentage of cysteine (35%) and 17 disulfide bridges, one free thiol (Cys 34), and tryptophan residues.<sup>70, 72</sup> The disulfide bridges contribute to the stability of the 3-D protein structure while the free thiol can be used as a modification site to covalently bind a fluorescent dye.<sup>72, 73</sup> The tryptophan residues give the serum albumin proteins their intrinsic fluorescence.<sup>74, 75</sup> The albumin protein structure is predominantly  $\alpha$ -helical and the remaining polypeptide occurring in turns between subdomains with no  $\beta$ -

sheets.<sup>75, 76</sup> Both human serum albumin (HSA) and bovine serum albumin (BSA) share 76% sequence homology; therefore, HSA and BSA are considered to have a similar conformation.<sup>72, 77</sup>

Albumin proteins are described as heart-shaped molecules that can be approximated by an equilateral triangle with a height of roughly 3 nm and a width of roughly 8 nm, shown in Figure 1.2<sup>70, 72, 78</sup> Albumin proteins are composed of three homologous domains (I, II, and III). Each domain is further divided into two subdomains (ie. IA, IB) that share common structural motifs. The six subdomains are primarily helical and cross-linked by disulfide bridges. There are two principal binding regions, located in the subdomains IIA and IIIA. Within the binding region, there is an asymmetric distribution of hydrophobic and hydrophilic residues; therefore, this creates a hydrophobic surface on one side of the subdomain and a positively charged surface on the other side, respectively. As a result, serum albumin generally has a higher affinity for small and negatively-charged hydrophobic molecules.<sup>71</sup>

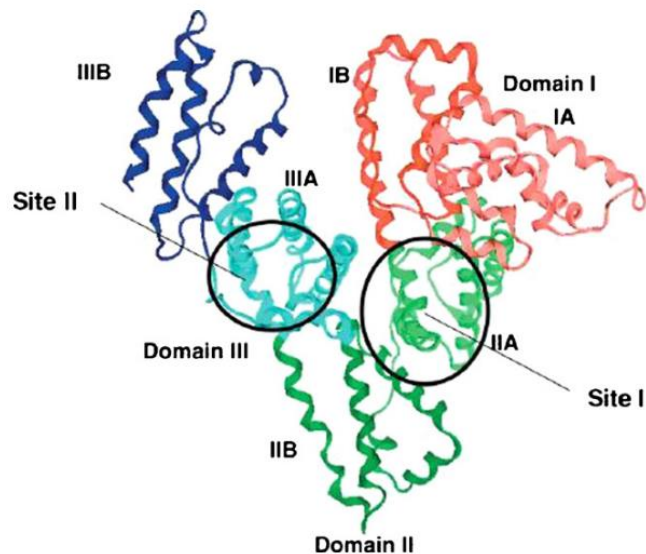


**Figure 1.2** Crystal structure of bovine serum albumin showing the locations of the domains and sub-domains.<sup>78</sup> Reproduced with kind permission from Elsevier (Appendix B).

The tryptophan residues within the serum albumin structure possess intrinsic fluorescence, and this property is often exploited to investigate the adsorption of albumin proteins onto NP surfaces. HSA has one tryptophan residue (Trp-214) while BSA has two tryptophan residues (Trp-134, located on the surface of the molecules in the first domain, and Trp-212, located in a hydrophobic binding pocket in the second domain). These residues can act as fluorophores that are capable of fluorescence quenching induced by molecular interactions with a quencher molecule. As a result, a change in the fluorescence emission intensity peak or a shift in the emission wavelength of the albumin proteins is measured upon interaction with NPs. These changes are indicative of either binding to the NP surface and further, can involve a change in the hydrophobicity of the tryptophan environment upon binding, often due to partial unfolding of the protein structure.<sup>74</sup>

## **1.5 Techniques used to Study Binding**

### **1.5.1 Ultra-Violet Visible and Fluorescence Spectroscopy**

UV-Vis and fluorescence spectroscopy are two of the most popular techniques used for the analysis of protein and NP interactions.<sup>7</sup> UV-Vis is a very quick technique with easy sample preparation. These techniques allow for the observation of spectral changes such as shifts or broadening of absorption or emission peaks for either NP or protein upon being mixed. Such changes can provide insight about the environment of the complexes; however, the results from UV-Vis alone are often not enough to draw comprehensive conclusions and must be paired with other techniques for support of the results. Oftentimes, fluorescence spectroscopy is used in conjunction with UV-Vis, where the changes in fluorescence intensity are monitored.<sup>14, 36, 57</sup> The technique of fluorescence spectroscopy is highly sensitive and can allow for the determination of the binding affinity of proteins to an NP surface and further, access to the binding ratio between proteins and NPs. However, this technique also has its limitations. To analyze for fluorescence intensity changes, there must be intrinsic fluorescence or the molecules under study must be labeled with a fluorophore, which could interfere with the interactions between the protein and NPs. The technique of fluorescence spectroscopy is not the most direct method to measure the interactions between proteins and NPs, since it is assumed that the change in intensity is related to the presence of interactions.<sup>79, 80</sup> Careful control experiments and pairing the results with results with other, preferentially direct and quantitative techniques would provide more support for the presence of interactions between proteins and NPs.

### **1.5.2 Circular Dichroism**

Circular dichroism (CD) has been employed to study the change in protein conformation upon adsorption to an NP surface.<sup>7, 24, 57, 80</sup> It is important to understand if and how proteins change upon adsorption to an NP surface, as these changes could affect the function of the protein within a biological system. Since protein molecules are chiral, the CD signal corresponds to different adsorptions of left- and right-circularly polarized light by the proteins. CD can therefore be indicative of a change in the secondary structure of a protein, since all possess their own CD features in the UV region. However, the technique is limited, as CD can only provide information on changes in the secondary structure of the proteins but cannot provide information on changes of the individual amino acids making up the protein.<sup>14</sup> CD signal also only reflects an average of the total changes that occurred in the protein upon adsorption to an NP surface, and furthermore, is not suitable for the measurement of complex protein mixtures.<sup>14</sup>

### **1.5.3 Gel Electrophoresis**

Gel electrophoresis is a popular and widely used technique for the separation and identification of proteins and has been often employed in analyzing the proteins that form the protein corona around NPs.<sup>4, 14, 18-22, 29</sup> This technique is quick, reliable, inexpensive, and highly used because both the identity and amount of each protein from the protein corona can be determined. The technique involves the migration of proteins through a gel, where the speed of the protein migration depends on its size, shape, and charge. Both 1-D and 2-D gels are frequently employed in gel electrophoresis to determine the identity and amount of a protein involved in formation of a protein corona. One of the most commonly used 1-D gels is sodium dodecyl sulfate polyacrylamide electrophoresis (SDS-PAGE). The

SDS-PAGE first detaches the proteins from the NP surface, which are then separated based on their molecular weight while in a denatured state. In 2-D gels, proteins are separated by both their isoelectric points (pI) and molecular weights (MW).<sup>21, 22</sup>

Although this technique is widely used, it does come with some limitations. As the number of different proteins in solution increases, this can increase the complexity of the system and result in poor separation. Furthermore, the removal of the proteins from the NP surface for analysis purposes could alter the properties of the protein, which would not be representative of the protein corona. Conversely, not separating the proteins from the NP surface and separating the complexes can also be challenging – if a distribution of complexes were present in solution, it is possible that the separation will be poor due to streaking. Or, if there was a low binding ratio of protein to NPs, then this technique would further not provide any useful results. Ultimately, this technique has low detection sensitivity and does not provide quantitative results.<sup>14</sup>

#### **1.5.4 Dynamic Light Scattering and Zeta Potentials**

Dynamic light scattering (DLS) has been used in many studies to analyze the change in size of the hydrodynamic radius of an NP upon protein absorption. Although this technique is fast, nondestructive, nonperturbative, and inexpensive, it is not always reliable and is not entirely quantitative.<sup>53</sup> DLS measurements can be affected by many factors, including NP polydispersity, the size and/or shape of the NP, and the formation of the hydration shells.<sup>81</sup> Therefore, cautious interpretation of the results obtained using DLS is necessary. Oftentimes, DLS is paired with the results obtained from measurement of zeta potentials (ZP) to determine the binding ratio of proteins onto an NP surface. ZP is the electric potential that forms when ions present in solution surround a diffusing particle in

what is known as the hydrodynamic shear. Therefore, ZP measures the electric potential at the shear boundary and is an indirect measurement of a particle's overall surface charge. These measurements have been used to analyze for changes in surface potential as proteins adsorb onto an NP surface, as well as for the stability of the complexes that are formed. However, one major limitation to this technique is that the ionic strength of the buffer employed affects the ZP measurements.<sup>81, 82</sup> Both DLS and ZPs are challenging techniques to employ for the characterization of heterogeneous and highly complex samples, or samples that have a large background, and these techniques are not suitable for the measurement of polydispersed samples.<sup>14</sup>

### **1.5.5 Isothermal Titration Calorimetry**

The technique of isothermal titration calorimetry is predominantly used to determine the strength of the interaction between the proteins to an NP surface, as it has long been used to accurately measure ligand-binding properties.<sup>1, 31, 57, 60, 79</sup> The technique involves the titration of one entity into another at a constant pressure, and the change in heat released or absorbed is monitored relative to a reference cell, which adjusts the temperature accordingly between the cells so that they remain at a constant temperature. A resulting binding curve is obtained through repeated injections, which provides the stoichiometry, affinity, and enthalpy change of the binding of the protein to the NP surface. Careful control experiments to determine whether any protein-protein interactions or NP-NP interactions influence the results must be performed prior to these measurements. One limitation of this technique is the need for high concentration of protein for titration into the NP solution, which can be difficult to achieve without any occurrence of agglomeration.<sup>14</sup> The studies in this thesis analyzed the interactions between NPs and

proteins at the highest possible concentration before agglomeration of the proteins would dominate. At the concentrations levels explored in this thesis, ITC was not a suitable option for investigation of the interactions, as the concentrations were too low. ITC would further not be a suitable or fruitful method of choice for experiments indicating a low binding ratio between the proteins and NPs, as the amount of heat absorbed or released may be too low to detect.<sup>80</sup>

### **1.5.6 Transmission Electron Microscopy**

A transmission electron microscopy (TEM) image forms from the interactions between an accelerated electron beam being transmitted through a sample and being scattered by nuclei. TEM has been employed in some studies to visualize the shape and structure of NPs as well as complexes between NPs and proteins.<sup>5, 6, 12, 14, 28</sup> Currently, it is the highest resolution imaging technique – up to several Angstroms. The limitations around this technique are largely focused around sample preparation. Prior to being imaged, some samples are fixed in a solution or dried overnight, which could affect the interactions between the NPs and proteins because of the change in environment.<sup>14</sup> The drying process could also affect and change the placement of the proteins around the surface of the NP. Oftentimes, a staining agent is used to image the proteins more clearly, but the staining agent can provide severe artifacts and can also adsorb to the surfaces of NPs depending on the functional groups present. Therefore, careful control experiments with and without the staining agent must be performed to ensure that the proper conclusions are drawn from the images obtained.

## 1.6 Direction of this Study

As described in the previous sections, studies have not yet achieved a concrete understanding of the interactions between NPs and proteins in a biological medium, especially regarding the kinetics and mechanism of the first steps in hard corona formation. To enhance the understanding of the interactions between proteins and NPs, studies should employ techniques that provide direct measurements of quantitative data focusing on the thermodynamics and kinetics of the interactions – doing so will allow for the usage of NPs to their fullest potential in biological applications. This thesis study aims to provide an example of such, by starting simplistically with the analysis of a single type of protein interacting with a specific NP surface, in hopes that the simplicity of the knowledge gained can build towards a more complex study and understanding of these interactions in the biological medium. We would like to emphasize that this study aims to understand the first steps in the binding process between proteins and NPs that form the hard corona. This work does not intend to mimic a biological system, but rather is our attempt at breaking down the complexity of the protein corona formation that has been shown to form around NPs.

This study focuses on the interactions between bovine serum albumin proteins with FS of two different sizes primarily by using Two-Photon Excitation Cross-Correlation Spectroscopy (TPE-FCCS). This technique is advantageous as it enables a non-destructive *in-situ* exploration of NP-protein interactions without requiring any previous sample preparation. The theory behind TPE-FCCS, the instrumentation, materials, and experimental procedures will be described in Chapter 2. In subsequent Chapters 3 and 4, the thermodynamics and kinetics of this specific interaction are analyzed and discussed.

## **CHAPTER TWO: MATERIALS, METHODS AND THEORETICAL BACKGROUND**

### **2.1 Introduction**

The studies described in this thesis aim to examine the interactions between the surfaces of fluorescently-labeled polystyrene microspheres with fluorescently-labeled bovine serum albumin proteins, to quantify the binding ratio between BSA and FS, and further, to understand the kinetics/equilibrium of the protein association to the nanoparticle. Unlike many techniques that are currently used to describe the association of proteins to the surface of a nanoparticle (such as DLS, ITC, gel electrophoresis – previously discussed in Chapter 1), the technique of Two-Photon Excitation Fluorescence Cross-correlation Spectroscopy (TPE-FCCS) can directly measure the occurrence of binding of fluorescently-labeled species in solution and can also monitor freely diffusing species in solution. This technique is therefore extremely powerful and offers the advantage of performing these studies in buffered media, which allows the study to be more physiologically relevant. Copious amounts of information can be extracted from a single TPE-FCCS experiment, which can allow for a deep characterization of the system under study. This chapter will introduce TPE-FCCS, optics, and instrumentation background, as well as sample sourcing and preparation.

### **2.2 Materials and Sample Preparation**

Fluorescent polystyrene NPs (FluoSpheres or FS) and unlabeled polystyrene NPs were purchased from Invitrogen and were used as received for all the protein binding experiments. Fluorescent NPs of two different sizes and fluorescent labels were chosen to study for the binding experiments. The first set of NPs (F8811) chosen were 200 nm in

diameter, modified with a carboxylate surface functionality, and contained a yellow-green fluorescent label ( $\lambda_{em} = 515$  nm). The second set of NPs (F8801) chosen were 100 nm in diameter, also modified with a carboxylate surface functionality, and contained a red fluorescent label ( $\lambda_{em} = 605$  nm). The FS stock solutions were stored in the fridge at 4 °C. Prior to each use, the FS's were sonicated (Branson 1510 Ultrasonic Cleaner) for 2 x 10-minute periods, with 1-2 minute resting in between, to ensure monodispersity. Diluted FS solutions were prepared in phosphate buffered saline (PBS 10X [1.37 M sodium chloride, 0.027 M potassium chloride, 0.080 M sodium phosphate dibasic, 0.020 M potassium phosphate monobasic], Ambion, pH = 7.4). All glassware, pipet tips, vials, and the buffer solution were autoclaved before use. The FluoSpheres were characterized using DLS and TEM imaging, and were found to be within the manufacturer's specifications.<sup>83</sup>

Unlabeled bovine serum albumin (BSA), BSA Alexa Fluor® 594 conjugate (A13101,  $\lambda_{em} = 617$  nm), and BSA Alexa Fluor® 488 conjugate (A13100,  $\lambda_{em} = 520$  nm) were purchased from Thermofisher Scientific and used for the binding experiments. The unlabeled BSA was used as received. Stock solutions of the fluorescently-labeled BSA were prepared by dissolving in 1 mL of PBS (10X, pH = 7.4). The stock solutions were stored at -4 °C. Upon experimentation, the stock solutions were vortexed (VWR Analog Vortex Mixer, speed setting 3) to ensure homogeneity prior to preparation of the experimentally used, diluted solutions.

For the binding experiments involving the red-labeled 100 nm diameter FS (FS<sub>100</sub>) and green-labeled BSA, the concentration of FS used was either 0.5 nM or 1 nM, and the concentration of BSA ranged from 400 nM to 5000 nM. The binding experiments involving the yellow-green-labeled 200 nm diameter FS (FS<sub>200</sub>) with red-labeled BSA, the

concentration of FS ranged between 0.0625 nM to 1 nM, and the concentration of BSA ranged from 200 nM to 5000 nM. Experiments attempting to analyze for possible energy transfer between NPs and red-labeled BSA used a concentration of 1 nM unlabeled NPs and 800 nM red-labeled BSA in PBS. The experiment using unlabeled and red-labeled BSA with FS<sub>200</sub> involved preparation of a 1:1 unlabeled to labeled BSA solution (400 nM each) and a 1 nM solution of FS<sub>200</sub>. Measurements for all experiments were taken within one minute after mixing the BSA with the FS solution by pipet in a chamber slide (made in-house by the glass shop at the University of Calgary) with a size 0 coverslip (Ted Pella, Inc.) glued at the bottom of the chamber. Detailed methods for the experiments performed in this thesis are provided later in the Methods section of this Chapter.

## **2.3 Measurement of Binding via TPE-FCCS**

### **2.3.1 Two-Photon Excitation Theory**

In 1931, Maria Göppert-Mayer was the first to publish and propose two-photon quantum transmission theory in her doctoral dissertation.<sup>84, 85</sup> Göppert-Mayer's theories were not experimentally tested until 1961, when Kaiser and Garrett measured the fluorescence of CaF<sub>2</sub>:Eu<sup>2+</sup>.<sup>84</sup> Referencing Göppert-Mayer, Kaiser and Garrett displayed a log-log plot of fluorescence intensity versus intensity with a resulting slope of two, which was indicative of two-photon excitation.<sup>84</sup> Then, in 1990, the invention of the titanium sapphire femtosecond pulsed laser allowed the commercialization of two-photon excitation for a wide range of research fields.<sup>84, 85</sup>

One-photon excitation (OPE) and two-photon excitation (TPE) are photophysically similar, shown in Figure 2.1. In OPE, a molecule absorbs one photon of energy, which

excites the molecule into any one of many vibrational levels within the excited electronic state (typically  $S_1$  or  $S_2$ ). The photon must have high enough energy such that it spans at least the energy gap between the ground state (GS or  $S_0$ ) and the first excited state ( $S_1$ ). In TPE, a molecule absorbs two photons simultaneously, which excites an electron into an excited energy level. In this process, the molecule is thought to pass through an intermediate state ( $i$ ), known as a “virtual” state, because this state is not an eigenstate of the molecule in the absence of an external electric field.<sup>84</sup> The relaxation process for OPE and TPE occurs the same way for a molecule in the excited state. According to Kasha’s rule, fluorescence will only occur when an electron relaxes to the GS from the lowest vibrational level of the excited electronic state, which is also the most probable transition. Alternatively, once the molecule is in the lowest vibrational level in the excited state, the molecule can undergo an intersystem crossing (ISC) to the triplet state ( $T_1$ ), and emit a photon via phosphorescence, which returns the molecule to the ground state. In the case of TPE, since two photons were absorbed, the photon of light that is released during the relaxation will be the same as it was for OPE.

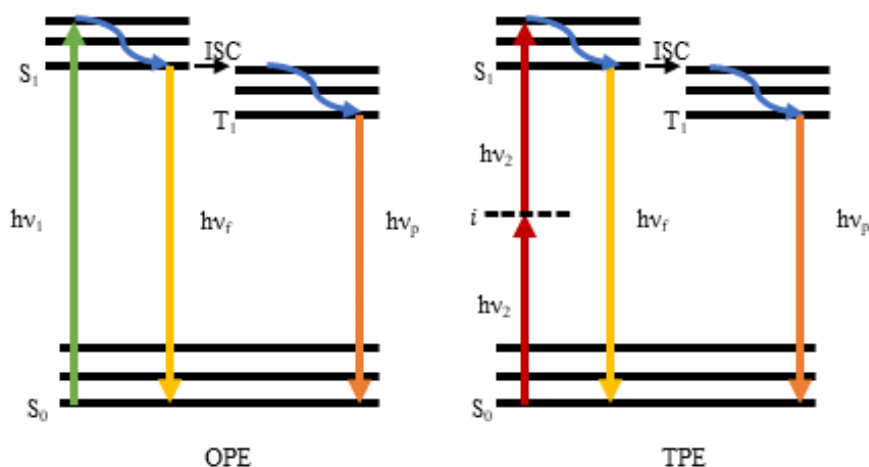


**Figure 2.1** Jablonski diagram showing one-photon excitation (OPE) and two-photon excitation (TPE), where  $S_0$ ,  $S_1$ ,  $T_1$ , and  $i$  denote the ground state, singlet excited state, triplet excited state, and intermediate state. Intersystem crossing (ISC) is denoted by the blue arrow.  $h\nu_f$  and  $h\nu_p$  represent fluorescence emission and phosphorescence emission, respectively.

The probability of the simultaneous absorption of two photons is orders of magnitude smaller than that for single photon excitation. Therefore, for a TPE process to occur, it is necessary to have a high density of photons both spatially and temporally. This can be achieved by tightly focusing pulsed laser light.

The efficiency of TPE, also thought of as the number of photons that are absorbed per fluorophore per laser pulse  $n_a$ , is given by Equation 2.1 below <sup>86</sup>

$$n_a \approx \frac{\langle P \rangle^2 \delta}{\tau_p f_p^2} \left( \frac{(NA)^2}{2\hbar c \lambda} \right)^2 \quad \text{Equation 2.1}$$

where  $\langle P \rangle$  is the average laser power at the sample,  $\delta$  is the two-photon absorption cross-section in  $\text{cm}^4/\text{photon}$  at wavelength  $\lambda$ ,  $\tau_p$  is the pulse duration of the laser,  $f_p$  is the laser repetition rate,  $NA$  is the numerical aperture of the objective lens,  $\hbar = h/2\pi$  where  $h$  is Planck's constant, and  $c$  is the speed of light.

TPE has several advantages over OPE, with the first being the confined excitation volume, on the femtoliter scale. The confined ovoid interrogation volume (Figure 2.2) improves the ability to detect fluctuations in fluorescence, which are temporally autocorrelated using fluorescence correlation spectroscopy (FCS). The confined interrogation volume also limits the region of photodamage and heating effects such that heat can be dissipated easily in a diffusing solution. TPE systems also use excitation wavelengths in the near-IR range (700-1100 nm) and therefore exploits the “optical window” of tissue – meaning that the absorbance of light is orders of magnitude less than UV and Visible light, which are required for OPE to occur.<sup>86,87</sup> Lastly, for Rayleigh scatters (scattering particles that are smaller than the wavelength of light), the scattering cross-section is inversely proportional to the fourth power of the wavelength.<sup>88</sup> This implies that longer wavelengths of light scatter less, and this allows for greater depth of penetration of the light.<sup>86, 89, 90</sup>

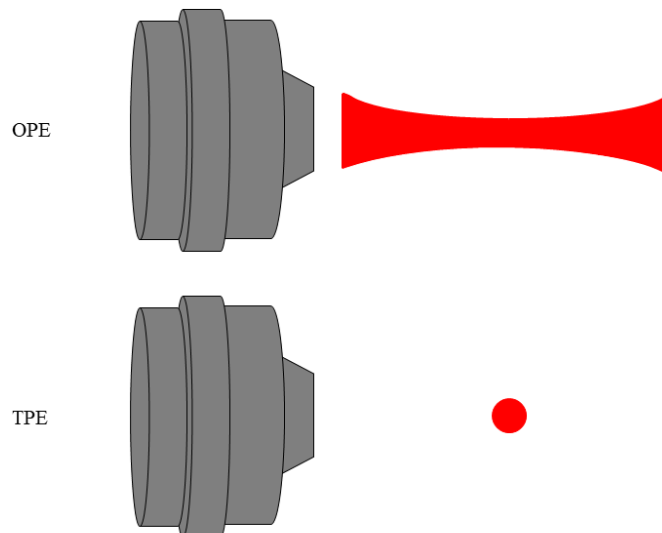


**Figure 2.2** Illustration of the focused excitation volume using a one-photon excitation (OPE) process versus a two-photon excitation (TPE) process.

### 2.3.2 Fluorescence Correlation and Cross-correlation Spectroscopy

Fluorescence correlation spectroscopy (FCS) was first developed in the 1970's at Cornell University to analyze the diffusion and chemical kinetics of DNA-drug intercalation.<sup>9, 10</sup> FCS differed from other classical relaxation techniques in that the experimentalist would not induce any perturbation of the system. In the 1990's, confocal laser scanning microscopy was combined with FCS which allowed for the detection of single molecules and increased the signal-to-noise ratio.<sup>91</sup> Fluorescence cross-correlation spectroscopy (FCCS) is an extension of FCS and analyzes the temporal fluorescence intensity fluctuations of bound fluorescent entities diffusing within the excitation volume.<sup>92, 93</sup> Similarly to FCS, FCCS allows for measurement of the fluorescence intensity changes upon binding but is a more powerful technique to study molecular binding. FCCS can provide information on the change in number of both reactant and complexed fluorophores upon a binding event. TPE-FCCS has been successfully employed to study membrane fusion<sup>94</sup> and ligand-receptor binding<sup>92</sup>.

#### 2.3.2.1 Autocorrelation

Autocorrelation analysis is performed when an experimentalist wants to focus on a single species of fluorescent particles. At ambient temperature, incessantly small fluctuations in fluorescence intensity will be observed due to Brownian motion of molecules in the focal volume. The average fluorescence intensity,  $\langle F \rangle$ , in a certain time window is expressed in photons per second per TPE volume.  $\langle F \rangle$  is dependent on the concentration ( $C$ , in moles per liter) and brightness ( $\eta$ , in emitted photons per second per mole) of every fluorescent entity in solution,  $i$ , shown in Equation 2.2<sup>95</sup>.

$$\langle F \rangle = \sum_i \eta_i C_i \quad \text{Equation 2.2}$$

These fluctuations in the fluorescence signal intensity within the excitation volume are temporally autocorrelated, which provides a measure of the self-similarity of the fluorescence signal after lag time,  $\tau$ . The normalized autocorrelation function is described in Equation 2.3<sup>92</sup>,

$$G(\tau) = \frac{\langle \delta F(t) \cdot \delta F(t + \tau) \rangle}{\langle F(t) \rangle^2} \quad \text{Equation 2.3}$$

where  $\tau$  represents the lag time, and  $\delta F(t)$  represents the instantaneous fluorescence signal minus the average fluorescence signal (Equation 2.4), assuming a constant excitation power.<sup>10</sup>

$$\delta F(t) = F(t) - \langle F(t) \rangle \quad \text{Equation 2.4}$$

The amplitude of the autocorrelation function,  $G(0)$ , results in the following manipulation of Equation 2.3:

$$G(0) = \frac{\langle \delta F(t) \cdot \delta F(t + 0) \rangle}{\langle F(t) \rangle^2} = \frac{\langle \delta F(t)^2 \rangle}{\langle F(t) \rangle^2} \quad \text{Equation 2.5}$$

The number of fluorescent molecules,  $N$ , in the focal volume at any given time is governed by the Poissonian distribution and is proportional to the number of emitter molecules,  $F(t)$ , in the focal volume. Therefore,  $\langle \delta F(t)^2 \rangle$  can be substituted for  $\langle \delta N^2 \rangle$ , which is also known as the variance. The variance is equal to the average number of fluctuating particles,  $\langle N \rangle$ , demonstrated by Equation 2.6.<sup>96</sup> However, it is important to note that this equation is only valid when there is only one type ( $N$ ) of fluorescent species in solution.

$$G(0) = \frac{\langle \delta N^2 \rangle}{\langle N \rangle^2} = \frac{\langle N \rangle}{\langle N \rangle^2} = \frac{1}{\langle N \rangle} \quad \text{Equation 2.6}$$

A 3-dimensional Gaussian intensity profile is the most common way to express what occurs in the focal volume of a tested sample. To express the normalized three-dimensional autocorrelation function for one species of molecules, two relationships must first be considered. The first is the relationship between the residence time of a diffusing molecule in the excitation volume,  $\tau_D$ , and the diffusion coefficient,  $D$ , shown in Equation 2.7<sup>10</sup>,

$$\tau_D = \frac{r_0^2}{\alpha \cdot D} \quad \text{Equation 2.7}$$

where  $\alpha$  is equal to 4 for OPE and 8 for TPE, and  $r_0$  is the laser beam radius at its focus, which perpendicular to the direction of laser propagation (obtained from calibration measurements of the focal volume).<sup>10</sup> Using this expression, as well as the definition for the effective focal volume,  $V_{eff}$ , below allows the calculation of an autocorrelation function that describes a single species moving freely in solution:

$$V_{eff} = \left(\frac{\pi}{2}\right)^{\frac{3}{2}} \cdot r_0^2 \cdot z_0 \quad \text{Equation 2.8}$$

$$G(\tau) = \frac{1}{V_{eff} \cdot \langle C \rangle} \cdot \frac{1}{1 + \left(\frac{\tau}{\tau_D}\right)} \cdot \frac{1}{\sqrt{1 + \left(\frac{r_0}{z_0}\right)^2 + \frac{\tau}{\tau_D}}} \quad \text{Equation 2.9}$$

where  $\langle C \rangle$  is the concentration of the diffusing emitter molecules and  $z_0$  is the depth of the excitation focal volume, in the direction of the laser propagation (obtained from calibration measurements of the focal volume). The first term in Equation 2.9 is equal to the inverse

of the average number of particles in the focal volume,  $N$ . Therefore, assuming a Gaussian TPE volume, collected autocorrelation curves can be fitted using Equation 2.10.<sup>92</sup>

$$G(\tau) = G(0) \cdot \left(1 + \frac{8D\tau}{r_0^2}\right)^{-1} \cdot \left(1 + \frac{8D\tau}{z_0^2}\right)^{-\frac{1}{2}} \quad \text{Equation 2.10}$$

An illustrative overview of FCS is demonstrated in Figure 2.3. Figure 2.3 (A) shows fluorescent particles diffuse in and out of the excitation volume which creates fluctuations in the fluorescence intensity signal.<sup>97</sup> These fluctuations generate the plot in (B), also known as the count rate trajectory, which tracks the change in fluorescence intensity signal over time. Figure 2.3 (C) depicts the autocorrelation decay curve that results from the fluctuations in fluorescence intensity signal from the average fluorescence intensity. The decay curve represents the probability distribution that a fluorophore, present in the focal volume at time ( $t = 0$ ), will still be present in the focal volume at a later time ( $t + \tau$ ).<sup>98</sup> When the lag time of a particle is very small,  $\tau$  roughly 0.01 to 0.1 ms, the autocorrelation function plateaus because the fluorescent molecule has not yet diffused out of the excitation volume. At this point, the autocorrelation amplitude is at its maximum. As the lag time increases for faster diffusing particles, the probability of finding the original emitter in the focal volume decreases. Thus, when an emitter has a lag time greater than 100 ms, the probability approaches zero for this experiment.

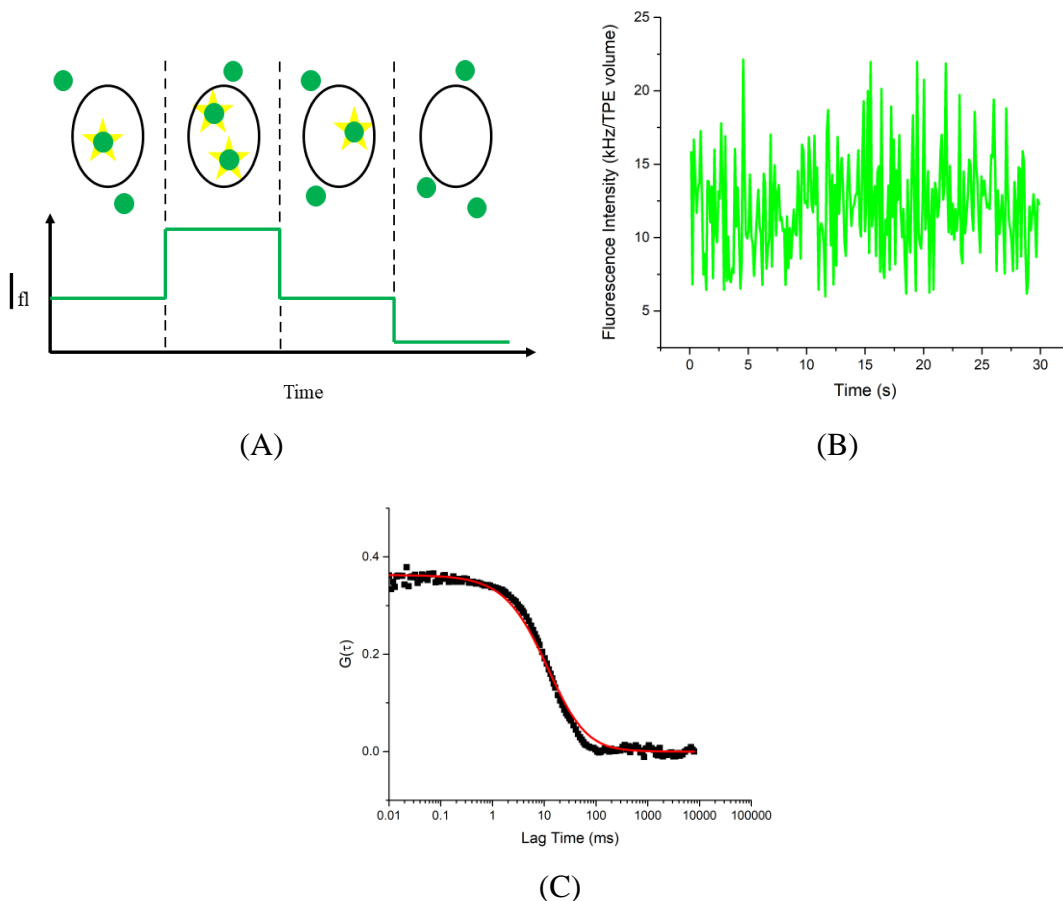


**Figure 2.3** Overview of Fluorescence Correlation Spectroscopy. (A) Fluorescent particles diffuse into and out of the excitation volume, which generate fluctuations in the detected fluorescence intensity signal. (B) The corresponding fluorescence intensity fluctuations tracked over time. (C) The resulting autocorrelation decay curve from the fluctuations in fluorescence intensity. The red line is the fitting with Equation 2.10.

The concentration of a fluorescent species can also be found from the amplitude of the autocorrelation function. Recall from Equation 2.6 that the amplitude of the autocorrelation function is equal to  $1/N$ , where  $N$  is the average number of emitters in the focal volume. Therefore, as the concentration of emitters in solution increases, the amplitude of the autocorrelation function decreases, as demonstrated in Figure 2.4.<sup>99</sup> It is important to minimize the number of molecules in the focal volume, while maintaining the fluorescence signal higher than the residual background signal.<sup>10</sup> These conditions will

result in the largest fluctuations and therefore the fastest situation to acquire a correlation decay. The temporal average of the particle number should be between 0.1 to 1000, which corresponds to concentrations in the nanomolar to micromolar range, since the focal volume is approximately one femtolitre.<sup>10</sup>

The autocorrelation function can further provide insight into the value of the diffusion coefficient. Larger molecules diffuse more slowly into and out of the focal volume, which results in shifting the autocorrelation decay curve to longer lag times, as shown in Figure 2.4.<sup>9</sup>

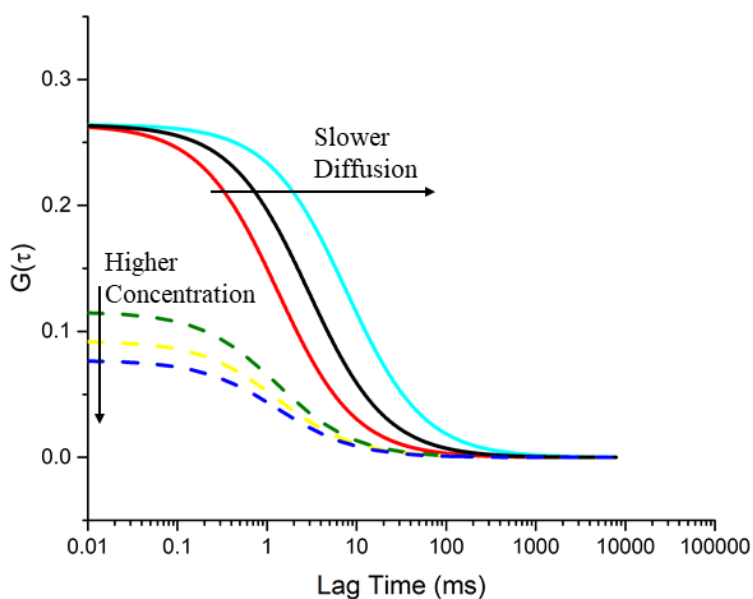


**Figure 2.4** An example of the effect of concentration and diffusion on the resulting autocorrelation decay curves. Increasing the concentration of a fluorescent particle will lower the amplitude of the autocorrelation decay curve. Larger particles that diffuse more slowly out of the focal volume will shift the autocorrelation curve to the right.

### 2.3.2.2 Cross-correlation

Fluorescence cross-correlation spectroscopy (FCCS) is performed when an experimentalist wants to track the diffusion of two fluorescently labeled, coupled species

in solution. The cross-correlation analysis allows for the detection and correlation of the fluorescence intensity signals from the two spectrally separate fluorescent molecules. The normalized cross-correlation function can be described as:<sup>92</sup>

$$G_{ij}(\tau) = \frac{\langle \delta F_i(t) \delta F_j(t + \tau) \rangle}{\langle F_i(t) \rangle \langle F_j(t) \rangle} \quad \text{Equation 2.11}$$

where the subscripts  $i$  and  $j$  refer to the two independently labeled fluorescent molecules.

A cross-correlation signal is detected when both channels are temporally correlated with each other, and this is indicative of a linkage of two spectrally distinct fluorophores. This implies that the two emitters are moving through the focal volume together, as one entity. Therefore, cross-correlation analysis has proven to be a very powerful tool to probe and study interactions between different molecules as well as chemical reactions. As an example, Figure 2.5 (A) depicts an example of a real-time fluorescence count rate trajectory for a solution of red-labeled BSA (at 2000 nM) and yellow-green-labeled FS<sub>200</sub> (at 1 nM) in PBS over a run time of 30 seconds. The corresponding cross-correlation curve is shown in Figure 2.5 (B), where the amplitude of the decay curve,  $G_{ij}(0)$  or  $G_x(0)$ , is proportional to the concentration of complexed species in solution, demonstrated in Equation 2.12.<sup>94</sup>

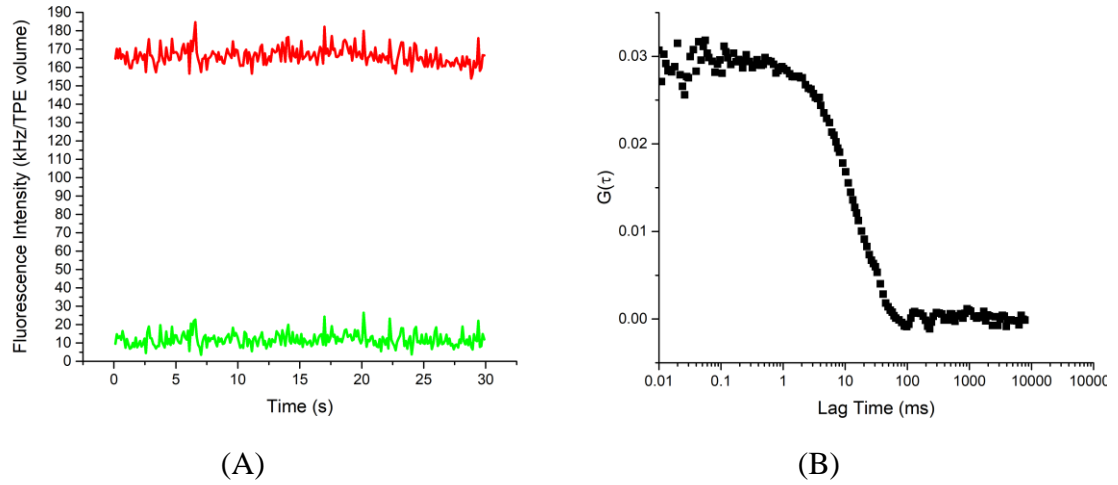


**Figure 2.5** An example of the output of Fluorescence Cross-correlation Spectroscopy. (A) Shows the fluorescent count rate trajectories of two fluorescently-labeled entities, while (B) shows the corresponding cross-correlation decay curve, indicating that the two fluorescent entities are interacting with one another in solution.

$$G_x(0) = \frac{\sum \eta_i \eta_j C_{ij}}{\sum \eta_i C_i \cdot \sum \eta_j C_j} \quad \text{Equation 2.12}$$

Assuming a Gaussian TPE volume, collected cross-correlation curves can be fitted to Equation 2.13<sup>92, 94</sup> below:

$$G_{ij}(\tau) = G_{ij}(0) \cdot \left(1 + \frac{8D_{ij}}{r_0^2}\right)^{-1} \cdot \left(1 + \frac{8D_{ij}}{z_0^2}\right)^{-1/2} \quad \text{Equation 2.13}$$

### 2.3.3 TPE-FCS/FCCS Instrumentation

For all TPE-FCS and FCCS experiments, a mode-locked Titanium:Sapphire, 100 fs pulsed laser, operating at 82 MHz and an excitation wavelength of 780 nm was used. A series of lenses first expands the excitation laser beam, then passes through the objective to optimally fill the back aperture of a 40X, 1.2 NA, 0.8 mm working distance Zeiss objective lens. The beam is then directed into the back of a Zeiss Axiovert 200 fluorescent

microscope. The fluorescence emissions of the diffusing particles in the focal volume are collected back through the objective lens, then reflected off the dichroic optic (Chroma 700DCSPXR). This dichroic optic separates the emitted light that of the excitation source. The emitted light is then separated into the two differently colored fluorescence emissions (red and green) by another dichroic optic (Chroma 565DCLP) outside of the microscope. These emissions are filtered (Chroma, D605/40m [red] and D535/50x [green]) and directed to avalanche photodiodes (APD, Perkin-Elmer, SPCQ-200) by optical fibers. The fluorescence intensity information from the APDs can then be analyzed by a PC using a correlator card (ALV-6000). Finally, the data is plotted and analyzed. The data for the experiments performed in this study were plotted and analyzed using OriginPro 7.0 and OriginPro 15.0 software.

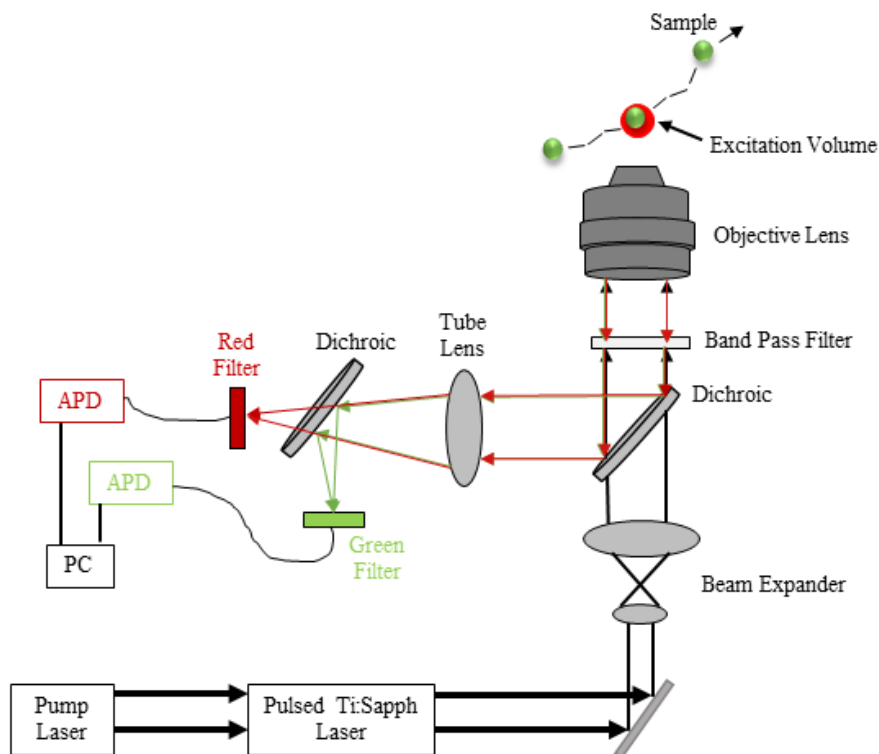


**Figure 2.6** Schematic of the setup and instrumentation involved for the TPE-FCCS experimentation. A 100 fs pulsed titanium:sapphire laser, pumped by the Nd:VO<sub>4</sub> laser, is expanded to fill the back aperture of the objective lens. The band pass filter then separates the fluorescence emission signals that arise from the excitation volume. The dichroic optics directs the beam to and from the objective lens. The tube lens guides the emission signals to another dichroic optics, which allows for the separation of the signals into red and green emissions. These emissions pass to their respective filters, then to the avalanche photodiodes, which are analyzed by PC.

## 2.3.4 TPE-FCCS Nanoparticle-Protein Binding Experiments

### 2.3.4.1 Methods

Table 2.1 shows all the tested mixtures of FS<sub>100</sub> and FS<sub>200</sub> (prepared at 1 nM each) with various concentrations of BSA. Solutions of 1 nM FS<sub>100</sub> or FS<sub>200</sub> in PBS and X nM BSA (indicated in the Table) in PBS and 250 μL of each solution was placed in separate chamber slides to assess for solution stability prior to mixing. FCS autocorrelation

measurements were taken of both solutions. Cross-correlation measurements of the FS solution were also taken to later correct for cross talk. Run times for all measurements were 30 seconds each. For the binding studies, stock BSA (volume dependent on the total final concentration being tested, shown in Table 2.1) was added into the FS solution in a chamber slide and mixed using a micropipette. The first auto- and cross-correlation measurements that were taken were denoted as time = 0. Alternating auto- and cross-correlation measurements were taken until equilibrium was detected, which was defined as the point at which there was no further change in the cross-correlation amplitude. Other mixtures using different initial BSA concentrations were performed in a similar manner. All experiments at these concentrations were performed in triplicate.

**Table 2.1** Tested mixtures and corresponding concentrations of BSA (nM) mixed with 1 nM red-labeled FS<sub>100</sub> or yellow-green-labeled FS<sub>200</sub> analyzed for the binding and kinetics studies. All mixtures were performed in triplicate.

Size and colour of FluoSphere	BSA concentrations (nM)
Red, 100 nm	400
	800
	1600
	2400
	3500
	5000
Yellow-green, 200 nm	200
	400
	800
	1600
	2000
	2400
	3500
5000	

Mixtures with higher ratios of BSA to FS concentrations were also performed for further binding and kinetics studies, where the concentration of BSA was held at 5000 nM, and the FS<sub>100</sub> concentration was dropped to 0.5 nM. Similarly, for the BSA-FS<sub>200</sub> system, the BSA concentration was held at 5000 nM, while the FS<sub>200</sub> concentration was dropped to 0.5, 0.25, 0.125, and 0.0625 nM.

### 2.3.4.2 FCCS Cross-Talk Correction

The complete separation of the yellow-green-labeled FS<sub>200</sub> and red-labeled BSA emissions is not possible. As seen in Figure 2.7, the red tail of the yellow-green-labeled FS<sub>200</sub> bleeds into the red detection channel, and this results in the observation of a false cross-correlation signal.

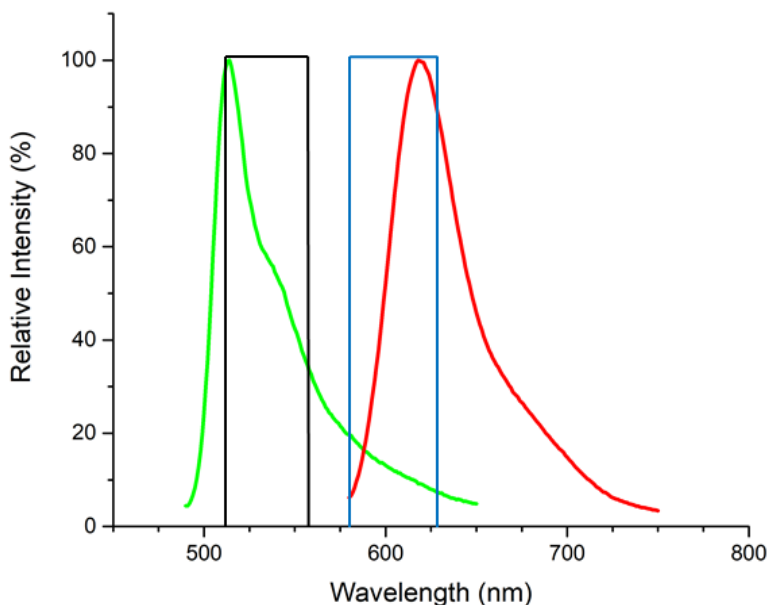


**Figure 2.7** An example of cross-talk or “bleed-through” in the emission detection filters. The spectral cut offs of the green and red emission filters are shown by the black and blue lines, respectively. The green curve corresponds to the emission spectrum of yellow-green dye labeling the FS<sub>200</sub>, where the long tail of its emission is seen to bleed into the red detection channel. The red curve corresponds to the emission spectrum of the Alexa Fluor® 594 dye labeling the BSA.

As a result, this cross-talk must be accounted for to determine the true cross-correlation amplitude for the experiments involving the yellow-green FS<sub>200</sub> and red-labeled BSA. The true cross-correlation amplitude can be calculated from  $\kappa$ , which is the bleed-through ratio of the green dye into the red detection channel, the amplitudes of the cross- and autocorrelation decays, and the measured count rates.<sup>100</sup>

$$\kappa = \frac{F_j^{cal}}{F_i^{cal}} \quad \text{Equation 2.14}$$

$$\hat{G}_x(0) = \frac{-\kappa F_i G_i + F_j G_x(0)}{F_j - \kappa F_i} \quad \text{Equation 2.15}$$

$\kappa$  is determined by calibration of a sample that contains only green-labeled particles of the experimentally relevant concentration (in this case of yellow-green FS<sub>200</sub> alone in PBS). The calibration measurement determines the fluorescence intensity in both the red and green channels ( $F_j^{cal}$  and  $F_i^{cal}$ , respectively). The true cross-correlation amplitude,  $\hat{G}_x(0)$ , can then be calculated according to Equation 2.15.<sup>100</sup>

## **CHAPTER THREE: EQUILIBRIUM BINDING RATIO DETERMINATION BETWEEN BOVINE SERUM ALBUMIN PROTEINS AND FLUOSPHERES**

### **3.1 Motivation**

The thermodynamics of the FS-BSA interactions were primarily studied using TPE-FCCS. FS's of two different sizes (100 nm and 200 nm in diameter) but the same reported surface chemistry and composition were chosen for this study. Choosing two differently sized FS allowed for the comparison of each FS's interactions with the BSA proteins, and further, to determine if these interactions were size-dependent. FS in general have not been as intensively studied as Quantum Dots for biomedical application purposes, making FS of great interest for this study. BSA was chosen as the model protein for all FS-BSA interaction experiments since serum albumin is the most abundant protein in blood serum and is well-studied itself.<sup>71, 72</sup> Previous studies, discussed in Chapter 1, that have attempted to study the interactions of FS with proteins have used rather indirect techniques such as gel electrophoresis, UV-Vis, calorimetry, and centrifugation, which could alter the equilibrium of the system. Therefore, using the techniques of FCS and FCCS will provide a more direct and quantitative analysis and understanding of the interactions and equilibrium between the BSA and FS in buffer solution. The results in this chapter are as follows: the occurrence of equilibrium interactions between FS and BSA will be confirmed through FCCS data; two mathematical models will be presented for insight into the equilibrium binding ratio between FS and BSA; Transmission Electron Microscopy (TEM) images will demonstrate support for the estimated binding ratio between the FS and BSA.

## 3.2 Results

### 3.2.1 Time Evolution and Equilibration of BSA-FS Interactions

To establish the experimental conditions to verify BSA-FS binding equilibrium was reached, the time evolution of the interaction between the FS and BSA was investigated prior to mixing and immediately after mixing the two entities in a chamber slide. This procedure was tested for both systems under study: green-labeled BSA and red-labeled, 100 nm diameter FS (FS<sub>100</sub>); and red-labeled BSA and yellow-green-labeled, 200 nm diameter FS (FS<sub>200</sub>).

For the system comprised of green-labeled BSA and red-labeled FS<sub>100</sub>, nearly complete separation between signals from the two detection channels was feasible. As shown in Figure 3.1, the count rate intensities measured in the green channel for the FS sample (0.11 kHz) and the majority of those measured in the red channel for the BSA sample (0.49 kHz) are due to laser scatter and the dark counts.<sup>92</sup> Additionally, no cross-correlation signal was detected for either sample, which confirmed the absence of cross-talk between the channels.

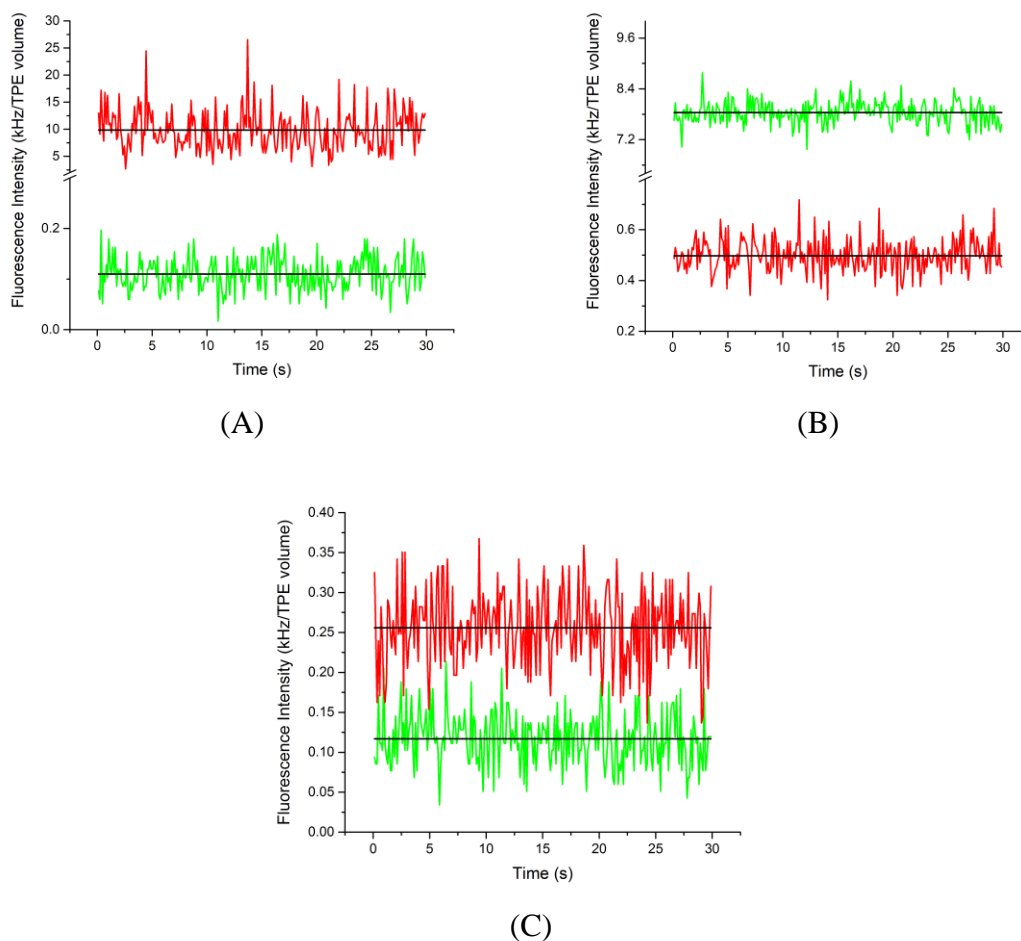


**Figure 3.1** Fluorescence count rate trajectories for (A) 1 nM red-labeled FS<sub>100</sub> and (B) 800 nM green-labeled BSA. (C) demonstrates the background signal from the PBS buffer alone. The green and red signals correspond to the signals detected in the green and red channels, respectively. The black lines represent the average fluorescence intensities.

Complete separation between signals from the two detection channels (FS and BSA) was not feasible for the experiments comprising the yellow-green-labeled FS<sub>200</sub> and red-labeled BSA. FS are known to have broad emission spectra, especially in comparison to quantum dots.<sup>101</sup> The bleed-through of the tail of the fluorescence emission spectrum for the yellow-green-labeled FS<sub>200</sub> into the spectral detection range for the red channel was shown in Figure 2.7 (from Chapter 2).

Due to the incomplete separation between signals for the two detection channels, a false cross-correlation signal was also detected from samples of the yellow-green FS<sub>200</sub> alone. This cross-correlation signal, shown in Figure 3.2 (A), was detected because of bleed-through of red fluorescence from the yellow-green FS<sub>200</sub> NPs. Figure 3.2 (B) gives an example of the relative ratio of bleed-through of red fluorescence (1.64 kHz) to green fluorescence (15.21 kHz) from a sample of yellow-green FS<sub>200</sub>. This further implied that cross-talk was present between channels. Therefore, a cross-talk correction, previously mentioned in Section 2.3.4.2 of Chapter 2, was necessary. The application of the cross-talk correction to the experimental data allowed for a proper analysis of the cross-correlation decay curves for this BSA-FS<sub>200</sub> system.

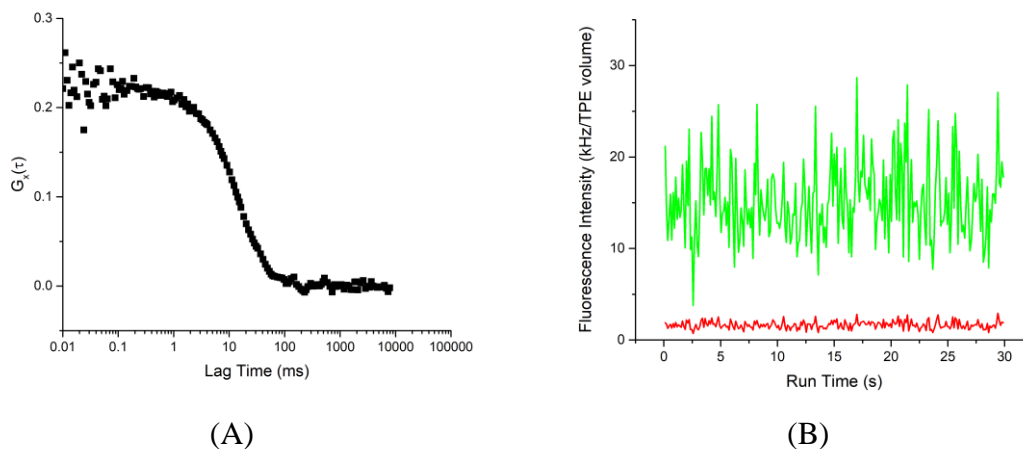


**Figure 3.2** Apparent cross-correlation decay (A) and corresponding relative cross-talk (B) of red fluorescence (shown in red) to green fluorescence (shown in green) from a 1 nM sample of yellow-green-labeled FS<sub>200</sub>.

To determine if any interactions were occurring between the BSA and FS in both systems, the cross-correlation amplitude as well as the changes in the autocorrelation amplitude for the BSA were thoroughly analyzed. The cross-correlation decay amplitude

provides direct evidence of interactions and “binding” between two spectrally different fluorescently-labeled entities. As previously mentioned, if binding did not occur between the BSA and FS, then a cross-correlation signal would not be detected, and there would not be a resulting cross-correlation decay curve. Therefore, the analysis of the cross-correlation decay curve and in particular the changes in the amplitude of the cross-correlation decay curve,  $G_x(0)$ , would allow for determination of any binding occurring between the BSA and FS in solution.

Upon mixing the BSA with the FS, an increase in the  $G_x(0)$  amplitude over time was observed for both systems under study (BSA with FS<sub>100</sub> and FS<sub>200</sub>, respectively) and all mixtures tested. Once removed of cross-talk, the corrected cross signals must truly originate from the formation of BSA-FS complexes and not cross-talk. An example of cross-correlation decay curves obtained at various time intervals for a 1 nM solution of FS<sub>200</sub> with added 2000 nM BSA is demonstrated in Figure 3.3. The individual measurements of the  $G_x(0)$  were well-defined (on the order of  $10^{-2}$ ), and thus, allowed for the retrieval of qualitative as well as quantitative information. For all tested mixtures, with varying concentrations of added BSA to the FS, the cross-signal was observed to increase over time until equilibrium was reached. At equilibrium, no further changes in the cross-correlation amplitude were observed.

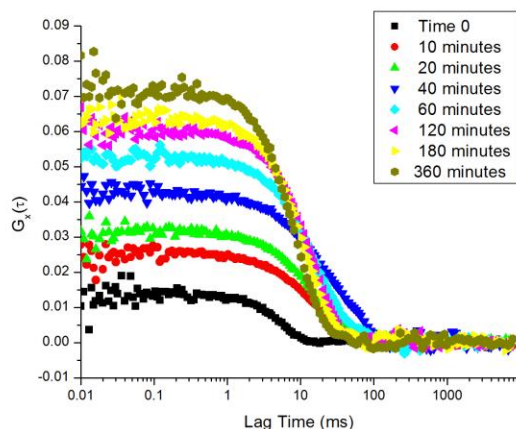


**Figure 3.3** Cross-correlation decay curves obtained at various time points upon mixing yellow-green FS<sub>200</sub> (1 nM) with red-labeled BSA (2000 nM).

To ensure that equilibrium was established for each mixture of FS and BSA, the  $G_x(0)$  data were collected and were plotted as a function of time (Figure 3.4). Initially, the  $G_x(0)$  values increase rapidly, suggesting that interactions between the BSA and FS occur as soon as the two entities are mixed in solution. After a certain amount of time (around approximately 12,500 seconds in the example below), the  $G_x(0)$  starts to plateau, signifying that the system is nearing equilibrium. Equilibrium is defined as the time at which the  $G_x(0)$  ceases to change any further. At equilibrium, the maximum number of interactions or “binding” between FS and BSA is established.

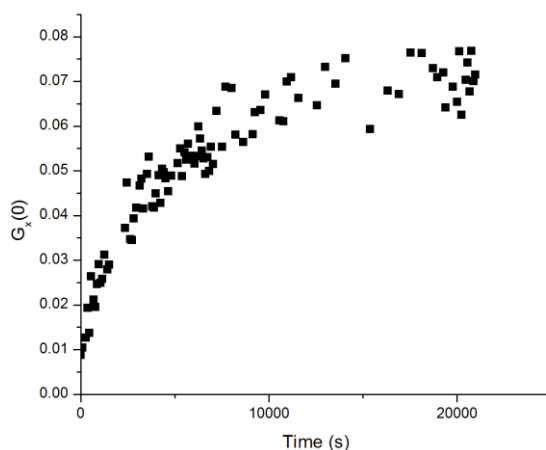


**Figure 3.4** Cross-correlation curve amplitudes over various time points for a mixture of yellow-green FS<sub>200</sub> (1 nM) and red-labeled BSA (2000 nM).

A change in the amplitude of the autocorrelation decay curves ( $G_p(0)$ ) for the BSA would also support the presence of interactions occurring between the FS and BSA; however, a definitive change in  $G_p(0)$  was observed only for the experiments involving the red-labeled BSA with the FS<sub>200</sub>. For the experiments involving the green-labeled BSA, no similar trends between mixtures of various BSA concentrations to FS<sub>100</sub> emerged from the analysis of the change in  $G_p(0)$  over time. In all cases, the scatter on the  $G_p(0)$  measurements was very high, and thus no observable nor definitive trends that emerged. This does not imply, however, that interactions were not occurring between the FS<sub>100</sub> and green-labeled BSA for this system. There was a distinctive increase in the cross-correlation amplitude for this system, which is evidence that supports interactions occurring. There are a few possible reasons that a change in  $G_p(0)$  for the green-labeled BSA may not be observed. Firstly, the Alexa Fluor 588 dye is much dimmer when compared to the Alexa Fluor 684 dye, resulting in the green-labeled proteins having lower signal-to-noise, thus the higher scatter in  $G_p(0)$ . This would become especially problematic when the tested

protein concentrations were low. Large, slow fluctuations in the  $G_p(0)$  could also be due to the intensity drift of the laser such and would contribute to the observed scatter.

The observed change in amplitude for the autocorrelation decay curves for the red-labeled BSA further supported that interactions were occurring between the FS<sub>200</sub> and BSA. Upon mixing the red-labeled BSA with the FS<sub>200</sub>, an increase in the  $G_p(0)$  signal for the red-labeled BSA for all concentrations tested was observed over the experiment time. An example of autocorrelation decay curves obtained at various time intervals for a 1 nM solution of yellow-green FS<sub>200</sub> with added 2000 nM red-labeled BSA is demonstrated in Figure 3.5. Recall from Chapter 2,  $G_p(0)$  is approximately inversely proportional to the number of particles in the focal volume. The increase in  $G_p(0)$  over time would suggest that the apparent number of protein diffusers in the focal volume is decreasing. When multiple proteins adsorb onto the surface of the FS, the apparent number of freely diffusing proteins should decrease, leading to an increase in  $G_p(0)$ . Therefore, this observation further suggests that interactions are occurring between the FS and BSA. The individual measurements of the  $G_p(0)$  were well-defined (on the order of  $10^{-2}$ ). Both qualitative and quantitative information could be obtained from the analysis of the  $G_p(0)$ . Similarly, for the change in cross-signal, the  $G_p(0)$  was observed to increase until equilibrium was reached for all tested mixtures with varying concentrations of added BSA to the FS<sub>200</sub>. At equilibrium, no further changes in  $G_p(0)$  were observed.

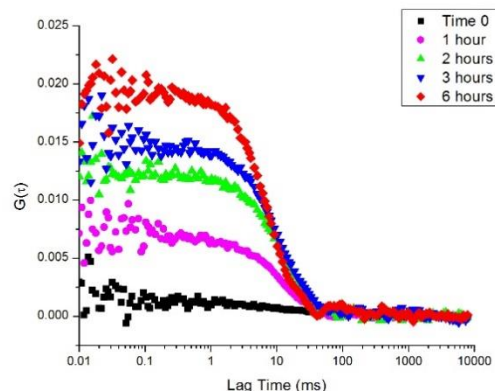


**Figure 3.5** Autocorrelation decay curves for the red-labeled BSA (2000 nM) obtained at various time points upon mixing with yellow-green-labeled FS<sub>200</sub> (1 nM).

It should also be noted that upon mixing the red-labeled BSA with the FS<sub>200</sub>, the fluorescence intensity of the BSA was observed change as a function of BSA concentration, while that of the FS<sub>200</sub> dropped slightly over time. However, a more in-depth discussion of these fluorescence changes will be found in Chapter 4.

The amount of time taken to reach equilibrium for each tested concentration ratio of BSA and FS for both systems was also determined. Equilibrium was said to be the point at which no further changes in  $G_x(0)$ ,  $G_s(0)$ , and  $G_p(0)$  were observed. Therefore, a plateau in a plot of  $G_x(0)$  over time for a particular mixture of BSA and FS<sub>100</sub> or FS<sub>200</sub> was used as an indicator that equilibrium has been reached. Tested mixtures of BSA (of 400 and 800 nM) with FS<sub>100</sub> (at 1 nM) were found to take slightly less than one hour to establish equilibrium. Higher concentrations of BSA (1600- 5000 nM) with FS<sub>100</sub> (1 nM) took approximately 1.25 hours to establish an equilibrium. For the system composed of BSA interacting with the larger FS<sub>200</sub> NPs, slightly longer times were taken to reach equilibrium. Mixtures of BSA at the lowest tested concentration (200 nM) with FS<sub>200</sub> (1 nM) were found to take the least time to equilibrium, at slightly less than 3 hours. Mixtures of higher BSA

concentrations (1600-5000 nM) with FS200 (1 nM) were found to take approximately 4 hours to equilibrium. However, the mixtures of BSA at 800 nM with FS<sub>200</sub> at 1 nM were found to take the most time to equilibrium – 4.75 hours.

Interestingly, the time taken to establish equilibrium appeared to be fairly linear in the case of the FS<sub>100</sub> interacting with BSA, but this trend was not apparent for the FS<sub>200</sub> interacting with BSA. Instead, the time to establish an equilibrium appears to depend on the concentration of BSA, where the time to equilibrium appears to decrease at BSA concentrations of 5000 nM. Such a trend was also suggested through the BSA fluorescence intensity changes, which appeared to change as a function of BSA concentration. Both results are suggestive that the kinetics of this system of FS<sub>200</sub> and red-labeled BSA are complex and could be dependent on the concentration of BSA protein as well as how many proteins are bound to the FS. The differences in trends observed between the two systems further suggest that the kinetics of the association of BSA to the FS NPs operate under different mechanisms based on the size or surface area of the FS. However, the discussions around these observations will be provided in more depth in Chapter 4.

### **3.2.2 Approaches to Estimate the Protein-NP Binding Ratio at Equilibrium**

In the following, a mathematical expression will be derived to estimate the average binding ratio of BSA to FS for various initial concentrations of BSA added to a constant concentration of FS. The approach contains assumptions that simplify the reality of the interactions between the FS and BSA. It is, however, important to start analyzing from the simplest beginnings and then increase in complexity as necessary to describe the complex nature of NP and protein interactions.

We start by assuming an equilibrium expression describing the interactions between the BSA and FS could be written in the form of Equation 3.1.



Where  $P$  represents a BSA protein,  $S$  represents a FS, and  $n$  represents an integer number. This equilibrium expression implies that a certain number of BSA proteins,  $n$ , initially free in solution, bind to FS in solution such that a single type of FS-BSA complex results. In reality, there is a distribution of FS-BSA complexes in solution. However, the assumption of a single type of FS-BSA complex helps simplify the reality of the distribution. Therefore, this single type of FS-BSA complex will describe the average BSA to FS binding ratio.

For every mixture of FS and BSA, experimental measurements for  $G_s(0)$  (autocorrelation amplitude for the FS),  $G_p(0)$ , and  $G_x(0)$  were obtained. These amplitudes provide information on the concentration of labeled species. Additionally, the  $G(0)$  depends on both the brightness of the fluorescent entity,  $\eta$ , as well as the number of fluorescent entities,  $i$ , in the focal volume,  $N$ , as described in Equation 3.2 for the FS in this case.

$$G_s(0) = \frac{\sum_i \eta_i^2 N_i}{(\sum_i \eta_i N_i)^2} \quad \text{Equation 3.2}$$

Presuming there is only one kind of FS – such that when a BSA binds, the FS does not appear to change – then there would be no change in the apparent brightness of the FS. This assumption would simplify the above expression by allowing the brightness terms to cancel. The resulting expression is given in Equation 3.3, which indicates that the  $G_s(0)$  is

inversely proportional to the number of FS,  $N_s$ , in the focal volume. This expression only holds true if there is not a change in brightness of the FS upon the binding of BSA.

$$G_s(0) = \frac{1}{N_s} \quad \text{Equation 3.3}$$

Referring to the initial equilibrium expression and presumption, the BSA is either free or has  $n$  proteins bound to the FS. Moreover, these quantities can be measured using the autocorrelation analysis to follow (Equation 3.4 and 3.5). Similar to Equation 3.2 we have:

$$G_p(0) = \frac{\sum_i \eta_i^2 N_i}{(\sum_i \eta_i N_i)^2} \quad \text{Equation 3.4}$$

Which expand to the following if all the proteins are either free ( $f$ ) or have an integer number bound to the FS ( $b$ ).

$$G_p(0) = \frac{\eta_f^2 N_f + \eta_b^2 N_b}{(\eta_f N_f + \eta_b N_b)^2} \quad \text{Equation 3.5}$$

We acknowledge that there is a high probability of a distribution of BSA bound to the FS but will not accommodate for that here. Continuing, if the brightness of the BSA was not changing as the BSA are bound, we can make the following association.

$$\eta_b = n\eta_f \quad \text{Equation 3.6}$$

Substituting Equation 3.6 into Equation 3.5, leads to a cancellation of the brightness terms and a simpler expression for  $G_p(0)$ .

$$G_p(0) = \frac{\eta_f^2 N_f + n^2 \eta_f^2 N_b}{(\eta_f N_f + n\eta_f N_b)^2} \quad \text{Equation 3.7}$$

$$G_p(0) = \frac{N_f + n^2 N_b}{(N_f + n N_b)^2} \quad \text{Equation 3.8}$$

$$G_p(0) \cong \frac{1}{N_f + n N_b} \quad \text{Equation 3.9}$$

Upon inspection, the expression in Equation 3.9 reflects the initial equilibrium expression, which is a good thing. The approximation of  $\eta^2 N_b$  being roughly equal to  $\eta N_b$  was used to arrive at Equation 3.9 from Equation 3.8.

Recall from the discussion in Chapter 2 that  $G_x(0)$  is proportional to the number of bound or complexed species in solution. Therefore, the final, equilibrated  $G_x(0)$  can be written based on the above equilibrium expression, in the form of Equation 3.10.

$$G_x(0) = \frac{\sum_i \eta_{ip} \eta_{is} N_{iPS}}{\sum_i \eta_{ip} N_{ip} \sum_i \eta_{is} N_{is}} = \frac{\eta_{bp} \eta_s N_{ps}}{(\eta_{fp} N_{fp} + \eta_{bp} N_{bp})(\eta_s N_s)} \quad \text{Equation 3.10}$$

Where  $N_{PS}$  represents the number of BSA-FS complexes in solution. Based on this expression, it can also be assumed that  $\eta_{ip} = n \eta_{if} = \eta_b$ . Substituting  $\eta_{ip}$  for  $n \eta_{if}$  and  $N_{ip}$  for  $N_f + N_b$  the denominator of Equation 3.9, the above Equation 3.10 can be re-written since the brightness terms cancel.

$$G_x(0) = \frac{n N_{PS}}{(N_f + n N_b) N_s} \quad \text{Equation 3.11}$$

If all the FS are occupied with BSA, then the  $N_{PS}$  and  $N_s$  terms will cancel out, resulting in a final, useful estimation expression that can help determine  $n$  – the average binding ratio of BSA to FS, shown in Equation 3.13.

$$G_x(0) = \frac{n}{N_f + n N_b} = n G_p(0) \quad \text{Equation 3.12}$$

$$\frac{G_x(0)}{G_p(0)} = n \quad \text{Equation 3.13}$$

The above estimation expression was applied to calculate the average number of BSA per FS at various BSA concentrations. The BSA concentrations ranged from 400 to 5000 nM for the experiments involving the red-labeled FS<sub>100</sub> and from 200 to 5000 nM for the experiments involving the yellow-green-labeled FS<sub>200</sub>. The FS concentrations in these experiments were both held at 1 nM. The values used for the  $G_x(0)$  for each mixture were the final, equilibrated  $G_x(0)$  values, determined from the plateau in the trendline of the fitted plots of  $G_x(0)$  versus time unique to every mixture (similar to Figure 3.4). The values used for the  $G_p(0)$  for each mixture were the final, equilibrated  $G_p(0)$  for the BSA. Figure 3.6 (A) shows the observed binding ratios using this estimation calculation for the system comprising the green-labeled BSA and red-labeled FS<sub>100</sub>. From this figure, the maximum average number of BSA per FS<sub>100</sub> appears to be approximately 6 proteins/sphere at the highest BSA concentration of 5000 nM. Figure 3.6 (B) shows the ratios for the system comprising the red-labeled BSA and yellow-green-labeled FS<sub>200</sub>. The maximum average number of BSA to FS<sub>200</sub> for this system appears to be approximately 7-8 proteins/sphere at the highest BSA concentration of 5000 nM.

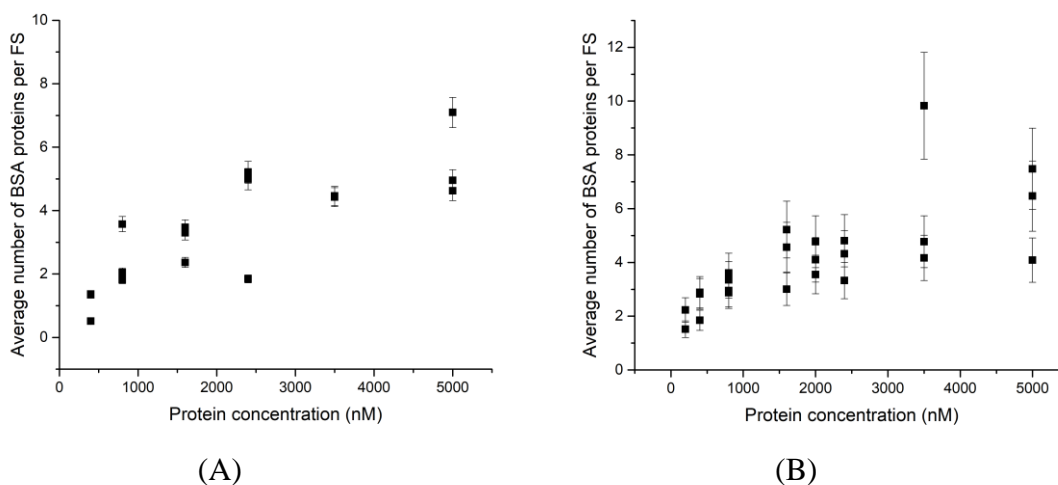


**Figure 3.6** Average number of BSA proteins per FS using Equation 3.13 for (A) the system composed of green-labeled BSA and red-labeled FS<sub>100</sub>, and (B) for the system composed of red-labeled BSA and yellow-green-labeled FS<sub>200</sub>. The concentration of FS in both systems was held at 1 nM. The errors correspond to the propagation of error calculations.

To determine whether or not FS were saturated with BSA further experiments were performed in which the concentration of FS was lowered, allowing for a larger BSA/FS ratio. This is because the maximum concentration of BSA that could be analyzed before being prone to too much BSA agglomeration was 5000 nM.

FS concentrations were lowered from 1 nM to 0.5 nM for the FS<sub>100</sub>, and from 1 nM to as low as 0.0625 nM for the FS<sub>200</sub>. For the system comprised of the FS<sub>100</sub> mixed with green-labeled BSA, a saturation point for the number of BSA-FS interactions was observed when the concentration of FS<sub>100</sub> was dropped to 0.5 nM, demonstrated in Figure 3.7 (A). Based on the estimation formula, the maximum average binding between BSA and FS<sub>100</sub> is approximately 6 BSA proteins per FS, as shown in Figure 3.7 (A). This average approximate number of BSA-FS interactions is determined by the plateau in the experimental data points, implying that a saturation point has been reached. However, when the concentration of FS<sub>200</sub> was dropped to 0.5 nM, a plateau in the experimental data

was not as apparent. A plateau was also not observed when the concentration of FS<sub>200</sub> was dropped subsequently to 0.25 nM, to 0.125 nM, nor to 0.0625 nM, as seen in Figure 3.7 (B). It was expected that the larger FS<sub>200</sub>, if following the binding regime present between the red-labeled FS<sub>100</sub> and green-labeled BSA, that a saturation point would have been reached by a factor of four times the saturation point observed for the smaller FS<sub>100</sub>, owing to the increase in surface area. This, however, was not the case, which suggests that the binding interactions between the BSA and larger FS<sub>200</sub> may be specific, and therefore, that a deeper examination into the differences between the two sizes of FS should be considered in the future.

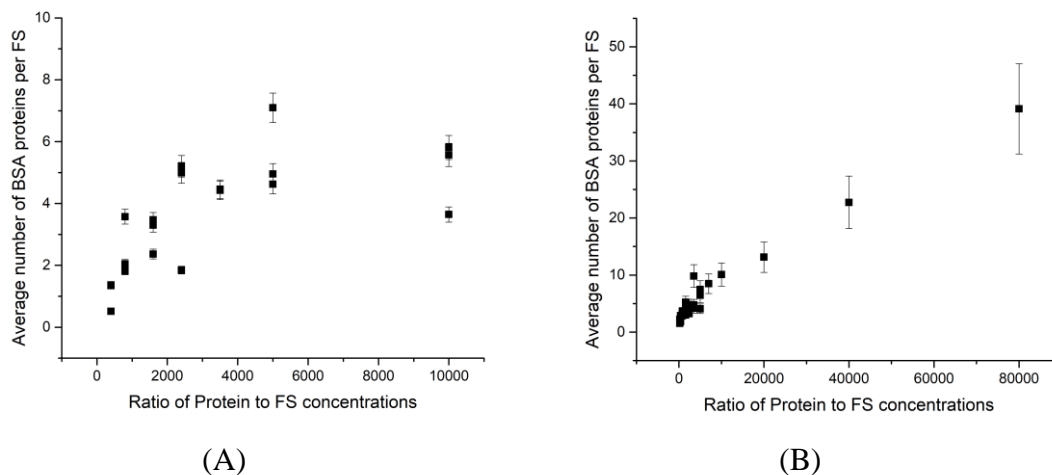


**Figure 3.7** Average number of BSA proteins per FS using Equation 3.13 employing larger concentration ratios of (A) green-labeled BSA with the red-labeled FS<sub>100</sub> and of (B) red-labeled BSA with the yellow-green-labeled FS<sub>200</sub> to determine if a saturation of BSA at the surface of the FS could be achieved. The errors correspond to the propagation of error calculations.

### 3.2.3 Further Evidence to Support the Low Binding of Protein to NPs; Introduction of the Pseudo-Explicit Model

The degree to which the binding ratios estimated by the approximation in Section 3.2.2 are valid can be examined by using them to generate hypothetical values for  $G_x(0)$  and  $G_p(0)$ . This approach may help us understand how a distribution around the average binding ratio could affect the changes in the measured values of  $G_x(0)$  and  $G_p(0)$ . The hypothetical calculations of the correlation amplitudes were performed for both systems; however, the following example calculations were performed using experimental data from a system composed of 5000 nM red-labeled BSA mixed with 1 nM yellow-green-labeled FS<sub>200</sub>.

The  $G_x(0)$  was calculated using Equation 3.10 following the equilibrium expression given in Equation 3.1. Experimentally, the brightness of a single BSA protein and a single FS can be determined from the product of the  $G_p(0)$  or  $G_s(0)$  and respective fluorescence intensity, presuming a single type of emitter. Assuming once again that the expression in Equation 3.6 holds true (that the brightness of the BSA bound to the FS is the same as that of the free BSA, multiplied by the number of BSA that are bound), then  $G_x(0)$  can be calculated using various theoretical binding ratios. The resulting  $G_x(0)$  from these calculations can be compared to the experimentally observed  $G_x(0)$  to see the expected binding ratio for that particular mixture. Again, this  $G_x(0)$  calculation contains a few assumptions that act to simplify the calculation, but can still serve as a starting point for comparison with experimental  $G_x(0)$  values. An example of theoretical calculated  $G_x(0)$  values for various combinations of free and bound protein are shown in Figure 3.8 using experimental brightness values from a mixture of 5000 nM red-labeled BSA and 1 nM yellow-green-labeled FS<sub>200</sub>.

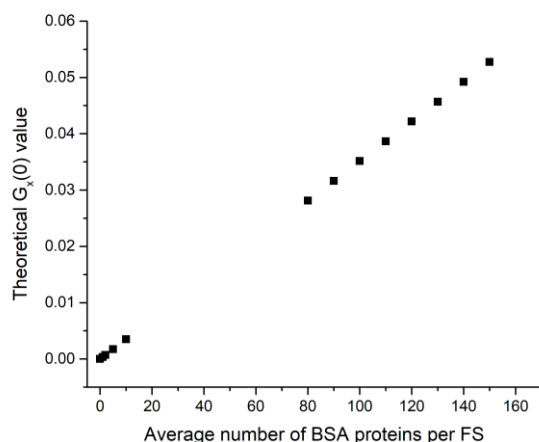


**Figure 3.8** Theoretical  $G_x(0)$  values calculated using Equation 3.10 for various combinations of bound and free BSA based on a mixture of red-labeled BSA (5000 nM) and yellow-green-labeled FS<sub>200</sub> (1 nM). The experimentally obtained  $G_x(0)$  for this system was between 0.05 and 0.06, which would theoretically correspond to an average of approximately 140 BSA proteins per FS<sub>200</sub> NP based on this estimation.

Experimentally for this particular mixture, a plateau in the kinetics plot of  $G_x(0)$  as a function of time was observed at a value of approximately 0.055 for  $G_x(0)$ . This was how we determined the equilibrium value for  $G_x(0)$ . Comparing this experimental value to the theoretical calculated values in Figure 3.8 indicates that the theoretical binding ratio should be approximately 140 BSA proteins per FS. The  $G_x(0)$  value that would have been observed at maximum binding of BSA to FS of 6-7 (as predicted by the previous model in Section 3.2.2) would have been just above a value of 0.002 using this hypothetical calculation. This result indicates an inconsistency between this hypothetical model and that discussed in the previous section in regard to the best approximate binding ratio. The inconsistency between the two proposed models was further explored through the generation of a hypothetical model for  $G_p(0)$ .

A hypothetical calculation of  $G_p(0)$ , using Equation 3.5, was also used to compare with the experimentally determined  $G_p(0)$  values for each mixture. Another reason for this

hypothetical calculation was to see if the two hypothetical calculations (for  $G_p(0)$  and for  $G_x(0)$ ) followed similar trends and would generate the same approximate binding ratios when compared with the experimental values. The values for the brightness of the free and bound BSA proteins were calculated from experimental values described previously for the hypothetical calculation of  $G_x(0)$ . Varying the theoretical binding ratio of the BSA proteins produces the hypothetical values for  $G_p(0)$  as shown in Figure 3.9. The calculated values were based on the same system of BSA and FS<sub>200</sub> that was previously described, such as so comparisons could be drawn.

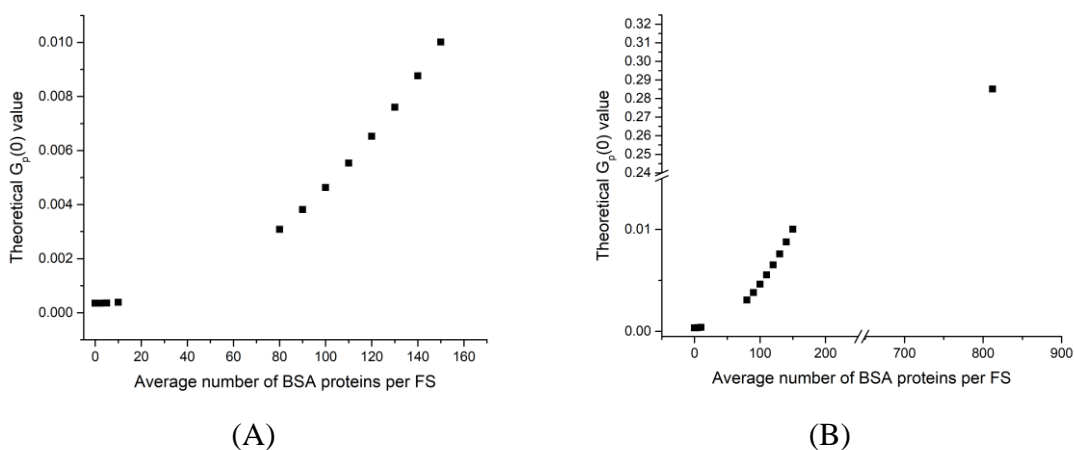


**Figure 3.9** (A) Theoretical  $G_p(0)$  values calculated using Equation 3.5 for various combinations of free and bound BSA based on a mixture of red-labeled BSA (5000 nM) and yellow-green-labeled FS<sub>200</sub> (1 nM). The experimentally obtained  $G_p(0)$  was found to be 0.008 for this system, which would theoretically correspond to an average of approximately 140 BSA proteins per FS. (B) shows the estimated value for  $G_p(0)$ , approximately 0.29, if all proteins were bound to FS.

For this mixture of BSA and FS, a final experimental value of 0.008 for  $G_p(0)$ . Based on Figure 3.9 (A), a binding ratio of approximately 140 BSA proteins per FS should be expected. Again, at maximum binding, an experimental value of roughly 0.29 for  $G_p(0)$  should have been observed, as shown in Figure 3.9 (B). Firstly, it is also noteworthy and

makes sense that there is consistency within the above hypothetical model for the estimation of the hypothetical binding ratio. However, these results, along with those determined for  $G_x(0)$  in the previous paragraph, further indicate a lack of consistency between the proposed hypothetical described here and that described in the previous section. The estimated binding ratios for each system tested were calculated using this second model (which will be called the “pseudo-explicit” model) and are shown in Figure 3.10, where the concentration of FS was held constant at 1 nM, and the BSA concentration was varied from 200 nM (for the FS<sub>200</sub>) or 400 nM (for the FS<sub>100</sub>) up to 5000 nM.

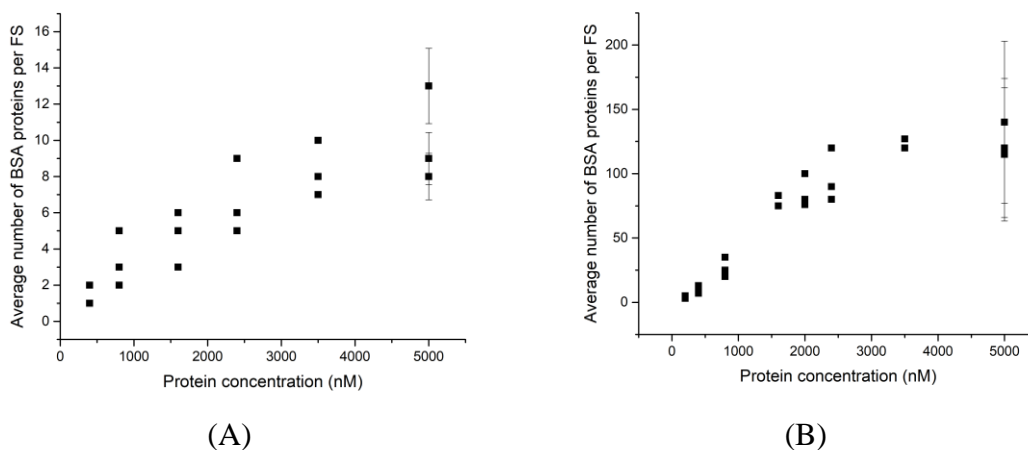


**Figure 3.10** Average number of BSA proteins per FS as calculated using the pseudo-explicit model for (A) the system composed of green-labeled BSA and red-labeled FS<sub>100</sub>, and (B) for the system composed of red-labeled BSA and yellow-green-labeled FS<sub>200</sub>. The concentration of FS in both systems was held at 1 nM. Errors on the last points correspond to propagation errors from the calculations.

From the above figures, the maximum number of BSA to FS appeared to be approximately 8-10 BSA per FS<sub>100</sub> and approximately 130 BSA per FS<sub>200</sub>. Comparing these estimated binding ratios to the model described in the previous section (which will be called the “simplified” model) clearly shows a discrepancy in the values, especially for the system composed of BSA interacting with the FS<sub>200</sub>. The simplified model in Section 3.2.2

estimated a binding ratio of approximately 7-8 BSA per FS<sub>200</sub> at the highest BSA concentration of 5000 nM. Conversely, the simplified model in the previous section estimated a binding ratio of approximately 6 BSA per FS<sub>100</sub>, which is only slightly lower than the estimated ratio given by the pseudo-explicit model.

To determine with more certainty if the FS were saturated with BSA, experiments were performed in which the concentration of FS was lowered, as described in the previous section. The FS<sub>100</sub> concentration was dropped to 0.5 nM, and the FS<sub>200</sub> concentration was dropped as low as 0.0625 nM to allow for a larger BSA/FS ratio. Using the proposed pseudo-explicit hypothetical model described in this section, the estimated binding ratios of BSA to FS were calculated, and the results are shown in Figure 3.11.

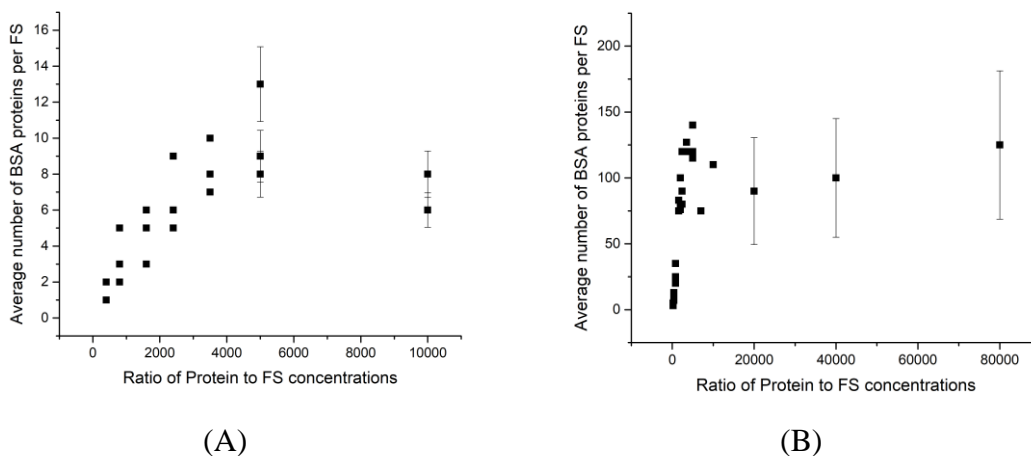


**Figure 3.11** Average number of BSA proteins per FS as calculated using the pseudo-explicit hypothetical model and employing larger concentration ratios of (A) green-labeled BSA with the red-labeled FS<sub>100</sub> and of (B) red-labeled BSA with the yellow-green-labeled FS<sub>200</sub> to determine if a saturation of BSA at the surface of the FS could be achieved. Errors on the last points correspond to propagation errors from the calculations.

The plateau in the experimental data points in Figure 3.11 implied that a saturation point had indeed been reached for both BSA-FS systems. For the BSA-FS<sub>100</sub> system, the

estimated binding ratio using the pseudo-explicit model still compared to that given by the simplified model in Section 3.2.2 (approximately 6 proteins/sphere from Figure 3.7 (A)). Interestingly, a plateau is observed in Figure 3.11 (B) for the system comprised of BSA interacting with FS<sub>200</sub>, which was not observed by the simplified model's estimations (Figure 3.7 (B)). At the highest concentration ratio between BSA and FS<sub>200</sub>, the simplified hypothetical model estimated a binding ratio of approximately 40 proteins/sphere; whereas, the pseudo-explicit model proposed in this section estimates a saturation of approximately 130 proteins/sphere. The discrepancy is clearly indicative of the simplified model's over-simplicity in its assumptions, which clearly influences the estimated binding ratio.

Analyzing the two models, it is likely that the pseudo-explicit proposed model, although making a few assumptions, gives a more accurate depiction of the binding ratio between BSA and FS. One difference between the two proposed models involves the assumption made in Equation 3.8 – which likely will not hold if the brightness of the BSA proteins is changing significantly. Although the simplified model was perhaps too simplistic in many of its assumptions, this model was a good starting point for insight into the binding ratio. This simplified model also predicted very low binding ratios, which was slightly unexpected and more questionable based on the significant changes observed experimentally in the cross-correlation amplitude upon mixing the BSA with the FS over long time periods. Further support for the greater accuracy of the pseudo-explicit hypothetical model proposed in this section was gained upon obtaining Transmission Electron Microscopy images of BSA interacting with FS.

### 3.2.4 Transmission Electron Microscopy Images give Insight into the Binding Ratio

For further insight into the interactions and binding ratio between the FS and BSA, Transmission Electron Microscopy (TEM) images were taken of FS<sub>100</sub> alone and of an equilibrated mixture of green-labeled BSA and red-labeled FS<sub>100</sub> (800 nM and 1 nM, respectively). Images of the other system with the larger FS<sub>200</sub> were not taken; the electron beam would not pass through FS of this size and would likely not result in useful images.

Images of the red-labeled FS<sub>100</sub> alone were first taken to see the appearance of the surface prior to the addition of BSA protein. That way, it would be easier to recognize any visible change at the FS surface upon addition of BSA. A drop of a 1 nM solution of FS<sub>100</sub> was imaged and is shown in Figure 3.12 (A). From the image, it is easily seen that these nanoparticles are indeed spherical and do not appear to have any observable surface defects. The particles also appear to be fairly monodisperse.

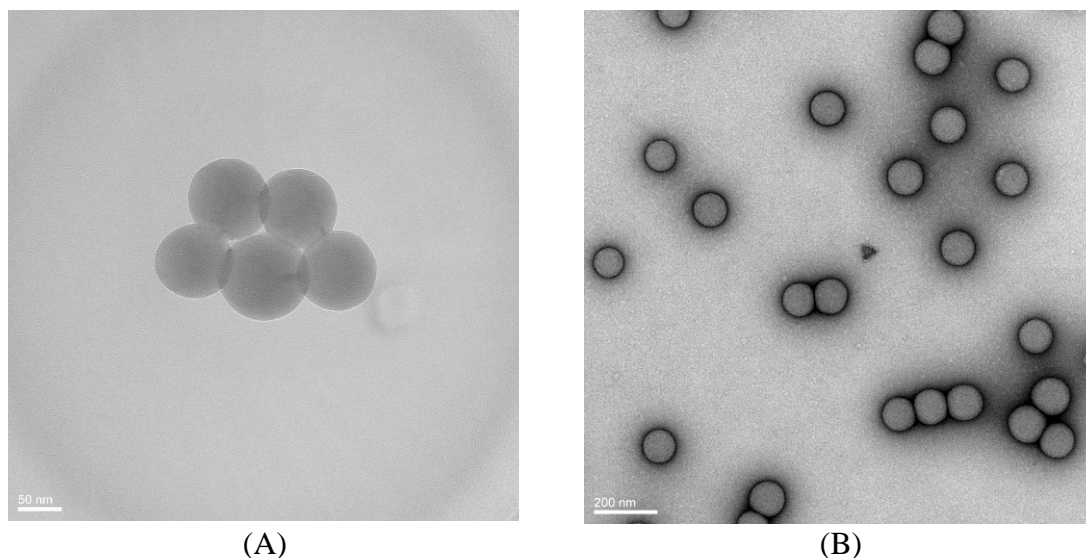


**Figure 3.12** TEM images of (A) unstained red-labeled FS<sub>100</sub> alone and of (B) red-labeled FS<sub>100</sub> stained with uranyl acetate.

To view proteins in a TEM image, the proteins must first be stained. Uranyl acetate is an extensively used negative stain used to image proteins in electron microscopy. The stain complexes with carboxylate functionalities on the protein. This causes the proteins to appear darker because the stain helps to prevent the electron beam from passing through the proteins. Because it was uncertain if the stain would affect the appearance of the FS alone and result in misinterpretation of the images for the mixture, images of the FS with added stain were taken. An example is shown in Figure 3.12 (B), where the only apparent difference is that the surfaces appear darker than previously as in Figure 3.12 (A). The FS appear darker because of the complexation formed between the stain and the carboxylate surface groups at the FS surface.

Next, images were taken of an equilibrated mixture of green-labeled BSA and red-labeled FS<sub>100</sub> (800 nM and 1 nM, respectively). A drop of uranyl acetate stain was added to the grid so that the proteins could be seen by TEM. Figure 3.13 (A) shows the resulting images from this equilibrated mixture. Looking closely, as in Figure 3.13 (B), there appear to be the presence of bumps at the surface of some of the FS. Due to their darker nature, and the fact that these bumps were not observed in previous images, it can be assumed that the bumps represent BSA proteins. It is interesting to observe that the proteins do not seem to appear on all FS surfaces and that the proteins appear as a bump as opposed to being dispersed about the FS surface.

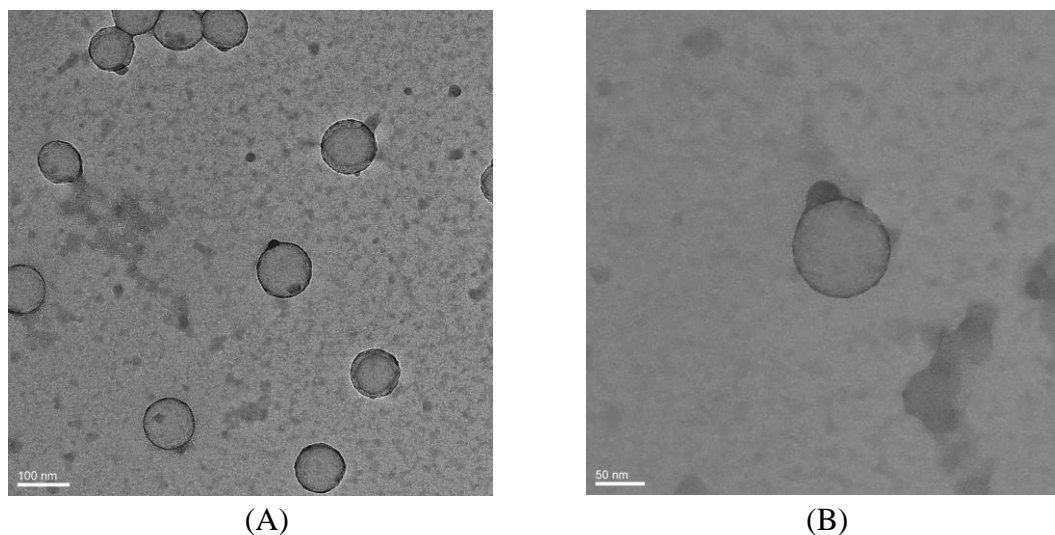


**Figure 3.13** TEM image of an equilibrated mixture of green-labeled BSA (800 nM) and red-labeled FS<sub>100</sub> (1 nM).

ImageJ Software was used to measure the height and width of the bumps to get insight into the binding ratio. Measurements were taken specifically of the bump in Figure 3.13 (B). The approximate measurements were found to be 22 nm in width and 14 nm in height for the bump. Recalling from Chapter 2 the dimensions of a single BSA protein, these measurements could indicate the possibility of 8-9 BSA proteins, stacked or clumped on top of one another. Comparing this rough estimate to the values for the calculated estimated binding ratios from both models in Sections 3.2.2 and 3.2.3 and for this particular BSA-FS mixture, the binding ratio was found to be best comparable with that estimated by second hypothetical model proposed in Section 3.2.3 (approximately 5 BSA per FS). It was also interesting to observe that the BSA appeared to stack or clump together in the TEM images, as opposed to appearing distributed about the surface of the FS.

It was of concern, however, that the drying process prior to imaging these complexes affected how the interactions appeared between the BSA and FS, essentially causing the BSA to appear as clumps at the FS surface. For a more concrete depiction of

the interactions, cryo-TEM images were attempted. Cryo-TEM imaging involves flash-freezing the sample of interest, which is thought to give a more accurate depiction of what is occurring in solution, but frozen in time. Unfortunately, it was observed that the addition of the uranyl acetate stain caused the images to become very unclear. Previous research suggests using sucrose for such applications to enhance image clarity and visibility; however, the addition of sucrose to the FS-BSA system appeared to affect the equilibrium and was deemed not comparable to the systems without added sucrose.

### **3.2.5 Unlabeled BSA Experiments for Insight into BSA-FS Binding**

It was of interest to determine if the fluorescent label on the BSA had any driving impact or force on the binding of the BSA to the surface of the FS. To address this question and explore the interactions between the FS and BSA, a competition experiment consisting of a 50:50 mixture of red-labeled and unlabeled BSA was added to the yellow-green-labeled FS<sub>200</sub> and was monitored by FCCS. Theoretically, if the label on the BSA had no influence on the binding events, then the binding ratio of labeled BSA to FS<sub>200</sub> would be approximately half as much as compared to a mixture of 100% labeled BSA with FS<sub>200</sub>.

As a control, a 50:50 mixture of 400 nM unlabeled BSA and 400 nM labeled BSA in PBS was made and analyzed by FCS to confirm solution stability. There did not appear to be any aggregation or other events to indicate that this solution was unstable. The mixture was also left, covered with parafilm in the dark room for the duration of the experiment (approximately 3 hours), and analyzed again by FCS at the end of the experiment. The solution had remained stable over this time, as there were still no visible aggregates, precipitation, or other events seemed to indicate instability.

Next, both unlabeled and labeled BSA were added to a 1 nM FS<sub>200</sub> solution in PBS. The final concentrations of unlabeled and labeled BSA were 400 nM each, respectively, similarly to the control mixture that was tested. This mixture was analyzed over time using FCS and FCCS until equilibrium was established. It was found that the estimated binding ratio, by the pseudo-explicit model from Section 3.2.3 and based on the final, equilibrated  $G_x(0)$  and final  $G_p(0)$  was found to be approximately 9 BSA per FS<sub>200</sub>. This binding ratio best compared with the binding ratio for the system of 400 nM red-labeled BSA and 1 nM yellow-green-labeled FS<sub>200</sub> (indicated by the red point on Figure 3.14) over the estimated binding ratio of approximately 35 BSA per FS for the experiments involving 800 nM labeled BSA to 1 nM FS<sub>200</sub>. These results suggested that the dye used to fluorescently label the BSA did not dictate the binding between BSA and FS.

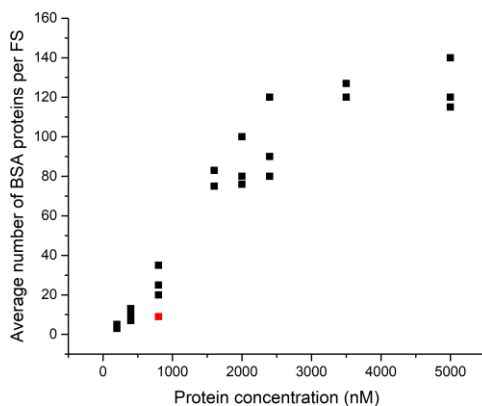


**Figure 3.14** Comparison of the estimated binding ratio of a mixture of 400 nM unlabeled and 400 nM BSA with 1 nM yellow-green FS<sub>200</sub> (red point) to a mixture of 800 nM labeled BSA with 1 nM yellow-green FS<sub>200</sub>. The red point better compares with the estimated binding ratio for a mixture of 400 nM labeled BSA with 1 nM FS, therefore suggesting the label on the BSA does not drive the interaction between the BSA and FS.

### **3.2.6 Stability of BSA-FS complexes in Culture Media**

Stability tests of FS<sub>100</sub> and FS<sub>200</sub> alone and complexed with BSA were analyzed in cell culture media for potential application in exploring cell uptake of NPs. Control experiments of the two differently-sized FS were analyzed in two types of commonly used cell culture media, EBM-2 and EGM-2, as well as equilibrated mixtures of the FS with BSA. Unfortunately, both the FS alone and the equilibrated mixtures of FS and BSA were found to be extremely unstable in both cell culture medium, to the point that precipitation of the FS<sub>200</sub> NPs was observed in under one hour upon addition to the medium, shown in Figure 3.15. These were interesting results, since many groups currently analyze the behavior and interactions of NPs with cells, and further demonstrates the importance of running control and stability tests prior to experimentation with NPs.<sup>8</sup>

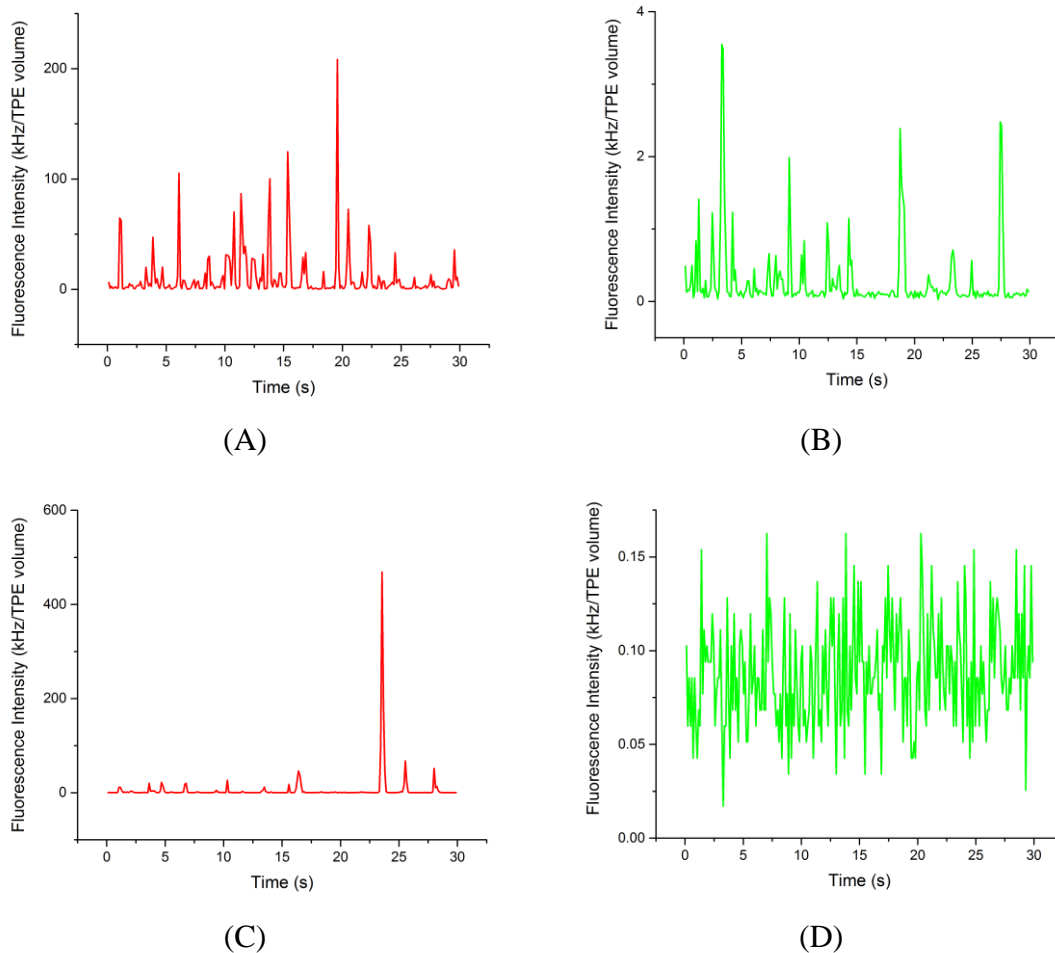


**Figure 3.15** Initial fluorescence intensity measurements of (A) red-labeled FS<sub>100</sub> in EBM-2 and (B) yellow-green-labeled FS<sub>200</sub> in EGM-2. The large peaks in these fluorescence intensity measurements are indicative of immediate agglomeration of the NPs in the media. After approximately two hours, the FS<sub>100</sub> (C) were visible in the media as large agglomerates, and the FS<sub>200</sub> (D) had completely precipitated out of the media, indicated by the absence of a fluorescence intensity signal.

### 3.3 Discussion

#### 3.3.1 Dynamics and Mechanism of the BSA-FS Interactions

From the experimental data, there are three instances that provide evidence to support that interactions are occurring between the FS and BSA: the presence of a  $G_x(0)$  signal of which the amplitude increases until an equilibrium is established; an increase in

$G_p(0)$  amplitude for the red-labeled proteins when mixed with yellow-green-labeled FS<sub>200</sub>; and TEM images that reveal the presence of protein “bumps” on the surface of red-labeled FS<sub>100</sub>. Therefore, the data collected for both systems provides support for the presence of interactions occurring between the FS and BSA; but, how exactly are the BSA proteins interacting with the FS?

The formation of any NP-protein complex is driven by several possible forces and is likely a complicated process. Examples of driving forces include electrostatic interactions, the hydrophobic effect, hydrogen bonding, and van der Waals forces. Although recent studies, discussed in Chapter 1, have suggested that electrostatic interactions play one of the most important role in the formation of these NP-protein complexes, the following will analyze various possible contributing factors to the interactions between FluoSphere NPs and proteins, with emphasis on the low observed binding ratios. The factors involved could include the surface charge of the FS or the zeta potential of the FS, the charge of the BSA proteins, the conditions in the solution environment, and physical characteristics of the FS (such as surface curvature and surface defects).

The surface charge of the FS is an important factor to consider when analyzing the interactions between the FS and BSA, keeping in mind, under the conditions of the experiments outlined in this thesis, both entities are overall negatively-charged. The charge density at the surface of an FS should give an indication of how strongly the FS interact with their surroundings and environment. ThermoFisher Scientific, the supplier of the FS, states the charge in milliequivalents per gram for their FS particles in their Certificates of Analysis. In the case of this study, both sets of FS had the same carboxy-terminated surface

functionality. Using these values of charge per gram of dry particulate, the charge per particle can be calculated. It was determined that the charge per particle for the FS<sub>100</sub> is  $7.89 \times 10^{-15}$  meq/particle and for the FS<sub>200</sub> is  $4.88 \times 10^{-14}$  meq/particle. These values suggest that there is not an exact linear relationship between the surface area and amount of charge at the surface; therefore, the number of interactions between the BSA and FS may not follow a linear pattern based on the two different sizes of FS, if the surface charge of the FS predominantly drives the interactions. However, since the binding experiments were performed in PBS, it is worthwhile to also consider the overall charge of the FS as well, by analyzing the zeta potentials of the FS.

Zeta potential measurements of the FS were taken in Millipore water and in PBS to determine the overall charge of both sets of FS. Zeta potential is an indirect measurement of a particle's overall surface charge. The zeta potential measures the charge of the aqueous layers that surround a particle's surface.<sup>102, 103</sup> These aqueous layers contain ions, which are organized around the particle based on the strength of the surface charge of the particle.<sup>102, 103</sup> Therefore, both the ionic strength and pH of the ultra-pure water (pH = 7.0) and PBS (pH = 7.4) must be considered. Furthermore, the zeta potential measurements should be taken as relative rather than absolute measurements, since the instrument does not have an absolute reference point.

The zeta potentials for the FS<sub>100</sub> and FS<sub>200</sub> in water were found to be the same, within error (FS<sub>100</sub>:  $-37.7 \pm 12.7$  mV; FS<sub>200</sub>:  $-43.9 \pm 9.5$  mV). The pKa for the deprotonation of a carboxylate functional group is approximately 4.6, and in both the ultra-pure water and PBS, is expected to be negatively charged. The zeta potentials for both sets of FS in PBS were difficult to obtain as these solutions appeared to be highly conductive. Based on

previous reports and studies, the zeta potentials of these FS in PBS should be significantly less negative and have larger margins of error when compared to those obtained in water. This is likely because of greater ion association at the surface of these particles. Not only would this change the overall charge of the particles, but it would also increase the variation of surface charges, as different ions adsorb to the surfaces in different amounts. Previously reported zeta potentials for FS<sub>100</sub> and FS<sub>200</sub> in 1X PBS were found to be  $-40.8 \pm 24.7$  mV and  $-31.2 \pm 26.2$  mV, respectively.<sup>67</sup> These values are surprisingly similar within error to those measured in water; however, in the same study, the zeta potentials measured in water were reportedly more negative (FS<sub>100</sub>:  $-59.6 \pm 11$  mV; FS<sub>200</sub>:  $-53.2 \pm 6.8$  mV).<sup>67</sup> However, based on our results, the zeta potential values from water are an unlikely justification for the observed difference in interactions between the BSA and the two sizes of FS. Moreover, these measurements do not provide much insight into the binding mechanism of the BSA to the surface of the FS.

Another factor to consider that could influence the interactions and binding mechanism between the FS and BSA is the surface charge distribution of the BSA. Under the conditions used in these experiments, the BSA has an overall net negative charge (as the pI value of BSA is 4.7). Recall, however, as described in Section 1.4, albumin has both a hydrophobic and positively charged patch in its binding sites, which could be used to interact with the surface of the FS. Recent studies, discussed in Chapter 1, also suggested that electrostatic interactions play a major role in NP-protein interactions. These studies showed that the positive patches located on the proteins, as opposed to the overall charge of the protein, are responsible for governing the interactions between proteins and negatively charged NPs. Based on these findings, the positive patch on the BSA proteins

could be governing the interactions between the albumins and FS. This could also suggest that the interactions between the two entities are mainly electrostatic, which is difficult attribute to a single driving factor without having changed other parameters and analyzed for the effect on the BSA-FS interactions.

The ionic strength of the environment could also affect the interactions and binding mechanism between the BSA and FS. A 10X PBS was used for all the BSA-FS experiments. The ionic strength of this buffer is therefore greater than the 1X PBS and was chosen to model the ionic strength of a physiological-relevant system more closely. At higher ionic strength, the high concentration of ions in solution reduces the availability of water molecules, therefore favoring hydrophobic interactions.<sup>82</sup> At higher ionic strength, it is also more common or expected to see NP and BSA individual agglomeration. This is because the hydrophobic patches at the surfaces of the proteins and FS are exposed under these conditions, which results in destabilization. It is highly possible that the observed interactions between the BSA and FS are a result of the hydrophobic effect driving the two entities together. However, the low binding ratio suggests that few proteins are interacting with the FS. This could further imply that at high ionic strength, the FS and BSA prefer to interact with themselves over each other. During the run times of the experiments, there was not any evidence to support such interactions (as no evidence of large aggregate formation was observed); however, if the mixtures were left overnight, agglomeration would occur. In terms of the difference in binding ratios for the two sets of FS, the difference could be due to the difference in surface area between the FS. The FS<sub>200</sub> has much more surface area for adsorption of BSA when compared to the FS<sub>100</sub>. Because of their larger surface area, the FS<sub>200</sub> may also have more hydrophobic patches that are

exposed under the experimental conditions than the FS<sub>100</sub>, which could lead to a higher binding ratio between the larger FS and BSA.

Physical characteristics of the FS, such as surface curvature and potential surface heterogeneity could also influence the number of BSA proteins that interact with the surface. The difference in surface curvature (if any, from the point of view of the BSA) between the two sets of FS could also potentially explain the difference in observed binding ratios. It is difficult to say if the BSA distinguishes a difference in surface curvature between the two sets of spheres since the BSA is extremely small in comparison. From the point of view of the BSA, the larger, the surface of an FS<sub>200</sub> could appear flatter over the surface of an FS<sub>100</sub>. As a result, it could be possible that there are fewer areas for adsorption of the BSA to an FS<sub>100</sub> over an FS<sub>200</sub>, which could explain the observed lower binding ratio and saturation point for the FS<sub>100</sub>.

Lastly, discontinuities or heterogeneities at the FS surface could also influence the type of interactions occurring between the FS and BSA. Although the resolution of the TEM images was not entirely clear, the particles appear spherical, and do not show any obvious defects in their surfaces (at the 1 nm resolution level). However, if the surface was uneven, this could result in the exposure of the hydrophobic dye molecules that are encapsulated within the FS. This could encourage the interactions between the BSA and FS if the hydrophobic effect was solely responsible the interactions. An uneven surface could also produce dense patches of charge that could attract the BSA, which could explain the appearance of the BSA “clumps” at the surface of the FS in the TEM images. However, it is difficult to absolutely determine the quality of the surface in terms of uniformity and charge distribution, and all that can be done is speculation. Further discussion of the

observed BSA clumping at the FS surface will be analyzed in the discussion section of Chapter 4.

Ultimately, the BSA-FS interactions are likely due to several driving forces, including electrostatic interactions, hydrophobic interactions, hydrogen bonding, and van der Waals forces. Despite the nature of the interactions between these two entities, it is of great interest to note the extremely low binding ratio observed between both sizes of FS and the BSA. This leads into the next point of discussion – to determine if there is a size-dependency that exists on the binding ratio, although being low.

### **3.3.2 Is there a Size-Dependency for the Binding Ratio between the FS and BSA?**

By the pseudo-explicit hypothetical model described in Section 3.2.3, the small and large FS were found to generate an approximate maximum average number of 8-10 proteins/FS<sub>100</sub> and 130 proteins/FS<sub>200</sub>, respectively. Analyzing specifically the smaller spheres, Figure 3.11 (A) demonstrated that, when the concentration of FS<sub>100</sub> was dropped to 0.5 nM, a saturation point of 8-10 BSA interactions per FS<sub>100</sub> was achieved, and this estimated binding ratio was found to be roughly comparable between both proposed hypothetical models. Conversely, a saturation point was not observed for the system of larger FS<sub>200</sub> when the concentration of FS was dropped and when employing the simplified hypothetical model (from Section 3.2.2), as was seen in Figure 3.7 (B). The highest average number of interactions present between a mixture of 0.0625 nM yellow-green-labeled FS<sub>200</sub> and 5000 nM red-labeled BSA was found to be approximately 40 BSA protein per FS<sub>200</sub> by the simplified proposed hypothetical model. Interestingly, a saturation point for this system was suggested to be approximately 130 BSA proteins per FS<sub>200</sub> after employing the

pseudo-explicit model (Section 3.2.3), shown in Figure 3.11 (B). It was concluded in Section 3.2.3 that the pseudo-explicit model was thought to depict a more accurate representation of the binding ratios for both systems. Therefore, this estimate of 130 BSA per FS<sub>200</sub> is much higher than the simplified expected estimate of four times that of the saturation point for the interactions between BSA and FS<sub>100</sub>, based on the differences in surface area between the two sets of FS. Based on these results, it is likely that there is a sphere-dependent trend in the number of protein interactions between the two sizes of FS; however, inclusion of another differently-sized sphere could help solidify whether this is owing to size or a different surface.

Previously in Section 3.3.1, several factors were presented that could influence the number of proteins that could interact with the surface of the FS. Among these factors, it was found that the difference in charge per particle for the FS<sub>100</sub> and FS<sub>200</sub> did not follow a linear trend based on increased surface area. Although this assumption that the surface charge linearly increases based on an increase in surface area may be simplistic, it is important to rationalize from the most basic assumptions then build up. Based on this assumption, the larger, 200 nm diameter particles are more highly charged than the expected four times linear increase, which could allow for a higher binding ratio of proteins to the surface of the sphere. Although, as previously stated, including another differently-sized sphere in the analysis could help reveal if a size dependency truly exists on the number of BSA-FS interactions.

### **3.3.3 The Significance of the Estimated Binding Ratio**

The formation of a complete protein monolayer on an NP surface has been reported by several groups.<sup>53, 54, 104, 105</sup> Knowing that albumins prefer to adsorb to NP surface with

a face-on configuration<sup>59</sup>, the loading capacity of BSA at the surface of an NP can be calculated by using the dimensions of the BSA and the surface area of the NP. In the case of the current study, the loading capacity is calculated to be approximately 1,300 BSA per FS<sub>100</sub> and 5,200 BSA per FS<sub>200</sub>. Recalling the results from the calculated using the pseudo-explicit hypothetical model (Figure 3.10) and the supporting TEM images, the binding ratio of BSA to FS was found to be much lower than the anticipated protein corona formation. Comparing these values to those calculated for a complete monolayer is interesting as the results of this study questions the idea of the protein corona. However, the groups who reported the formation of a protein corona around the NP analyzed their systems used different techniques for their analysis; many of the groups mostly basing their observations on an increase in radius of the NP due to the adsorption of proteins.<sup>55, 104</sup> These conclusions were made based on indirect evidence of the formation of a protein corona and most likely under the assumption that a protein corona would form at the NP surface, which, based on the results of this study, should not be assumed.

Another point of difference between the studies in this Chapter and those of other groups is in the concentration ratio of NP and BSA employed in the experiments. In this study, concentration ratios ranged from 1:10,000 FS<sub>100</sub> to BSA and 1:80,000 FS<sub>200</sub> to BSA. One group has reported testing concentration ratios of up to 1:250,000 NP to protein<sup>104</sup> meanwhile observing the formation of a protein corona. The increased concentration ratio could be responsible for driving the interactions between NPs and proteins. At higher concentrations, protein agglomerations are often observed, and this agglomeration could either result in the formation of strong interactions between the protein and the surface of an NP or could hinder interactions between the protein and NP surface. Although, perhaps

at higher protein concentrations, more “clumps” of proteins at the surface of an FS should be expected (suggested by the TEM images in Figure 3.13) due to the adsorption of protein agglomerates instead of the perceived notion of a protein corona.

Despite the large NPs employed in these studies, with large surfaces for protein adsorption, there ultimately appeared to be minimal interactions between the FS and BSA, which was not anticipated. These results were not anticipated because of the notion of the formation of a protein corona, which is said to form when NPs are presented into a solution containing proteins. The results of these studies question the formation of a monolayer protein corona, or possibly the dependence of protein concentration on its formation, and further suggest that more studies employing techniques that provide direct evidence of NP-protein interactions must be done.

### **3.4 Conclusions**

In the studies described in this chapter, the interactions between BSA and two differently sized polystyrene FS were investigated using TPE-FCCS thermodynamically. Both the change in  $G_x(0)$  and  $G_p(0)$  (for the system comprising the yellow-green FS<sub>200</sub>) indicated that interactions were occurring upon addition of BSA to solutions of FS. Based on the results of the  $G_x(0)$  and  $G_p(0)$  for a variety of tested BSA concentrations, two models were developed to help best estimate the average binding ratio of BSA to FS. The first model, called the “simplified model,” was deemed over-simplified in its estimation of the binding ratio, as it followed the assumption that  $\eta^2 N_{\text{protein}}$  was approximately equal to  $\eta N_{\text{protein}}$ . By the second model, called the “pseudo-explicit model,” an average binding ratio of 8-10 BSA per red-labeled FS<sub>100</sub> and 130 BSA per yellow-green-labeled FS<sub>200</sub> was determined. TEM images of a mixture of the red-labeled FS<sub>100</sub> and green-labeled BSA

appeared to demonstrate support for the low estimated binding ratio. The TEM images also showed the proteins appearing as binding as “clumps” at the surface of an FS. The results of this study question the perceived notion of the formation of a protein corona monolayer, which is said to form when NPs are introduced into solutions containing proteins. Perhaps a monolayer was not observed because the highest tested concentration ratios of protein do not compare with those in a biological system. Most importantly though, this study highlights the need to employ more direct and quantitative investigation techniques, such as FCCS, over indirect techniques when analyzing interactions between NPs and proteins, especially if the end result is for application in biological systems.

## CHAPTER FOUR: DYNAMICS AND EQUILIBIRUM EVALUATION OF THE INTERACTIONS BETWEEN BOVINE SERUM ALBUMIN PROTEINS AND FLUOSPHERES

### 4.1 Motivation

The kinetics of the BSA-FS interactions were primarily studied using TPE-FCCS. As mentioned in the previous chapter, the interactions between FS and proteins – in particular, the kinetics of the interactions between polystyrene, carboxy-terminated NPs with BSA proteins – have not been deeply investigated by many groups. Only two studies reported in literature have analyzed a similar NP-protein system to that studied in this thesis; however, those reports used the techniques of isothermal titration calorimetry (ITC) and tryptophan quenching to determine the association constant of the NP-protein interaction. This emphasizes the importance of analyzing the kinetics of the BSA-FS interactions presented in this thesis. Kinetics analyses are important for determining the rate and mechanism of NP-protein interactions and potential formation of the initial steps of the protein corona.<sup>8</sup> In comparison to the techniques of ITC and tryptophan quenching, FCS and FCCS provide a direct approach to accessing and determining many kinetic parameters, such as the on- and off-rate constants ( $k_{on}$  and  $k_{off}$ ) as well as the association and dissociation equilibrium constants ( $K_A$  and  $K_D$ ). In the studies reported in this chapter: the on-rate constant and association constant for the interactions between BSA with both sizes of FS were determined using FCS and FCCS. Other changing parameters, such as average fluorescence intensity of the FS and BSA will be explored as a means of gaining insight into the mechanism of the interaction. The insight gleaned in this thesis study will be discussed in relation to those reported from two previous studies.

## 4.2 Results and Discussion

### 4.2.1 FS-BSA Interaction Kinetics

#### 4.2.1.1 On-Rate Constant ( $k_{on}$ ) Determination

The kinetics studies of the BSA-FS interactions were performed using BSA in a concentration range of 200-5000 nM with red-labeled FS<sub>100</sub> (100 nm diameter) ranging from 0.05-1 nM and yellow-green-labeled FS<sub>200</sub> (200 nm diameter) ranging from 0.0625-1 nM. This was done to examine the possible dependence of protein/FS mixing ratio on the kinetics, which provides mechanistic insight. Previously in Chapter 3, it was demonstrated that there was an observed increase in  $G_x(0)$  signal over time for all of the mixtures of BSA with the two sets of FS, indicating binding. These changes in  $G_x(0)$  signal were plotted as a function of time (example in Figure 4.1) for each mixture tested and then were fitted to an exponential equation (Equation 4.1) represented by the red line. Further examples of the resulting fittings of  $G_x(0)$  for various tested concentration ratios of BSA with FS<sub>100</sub> or FS<sub>200</sub> are shown in Appendix A.

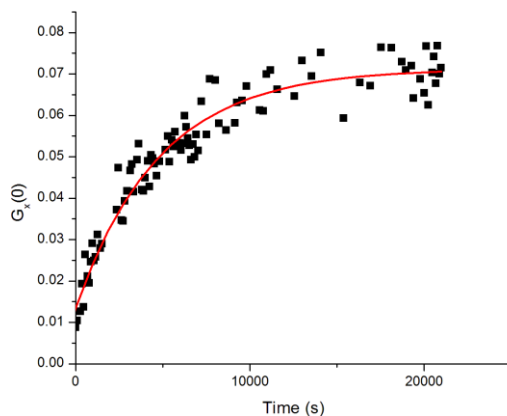


**Figure 4.1** Cross-correlation curve amplitudes over various time points for a mixture of yellow-green FS<sub>200</sub> (1 nM) and red-labeled BSA (2000 nM). The red line corresponds to fitting with Equation 4.1.

$$y(t) = A(1 - e^{-kt}) + C \quad \text{Equation 4.1}$$

In Equation 4.1,  $A$  represented  $G_x(0)_{\max}$ ,  $k$  represents  $k_{\text{on}}$ , and  $C$  represented the first measurement of  $G_x(0)$  taken as  $t = 0$ . From this exponential fit, the  $k_{\text{on}}$  rate constant was accessed, since the  $G_x(0)$  function directly measures the linking of two differently-labeled fluorescent entities. Therefore, for each concentration ratio tested for both sets of spheres,  $k_{\text{on}}$  values were obtained and were compared to each other within each set of FS, as shown in Figure 4.2.

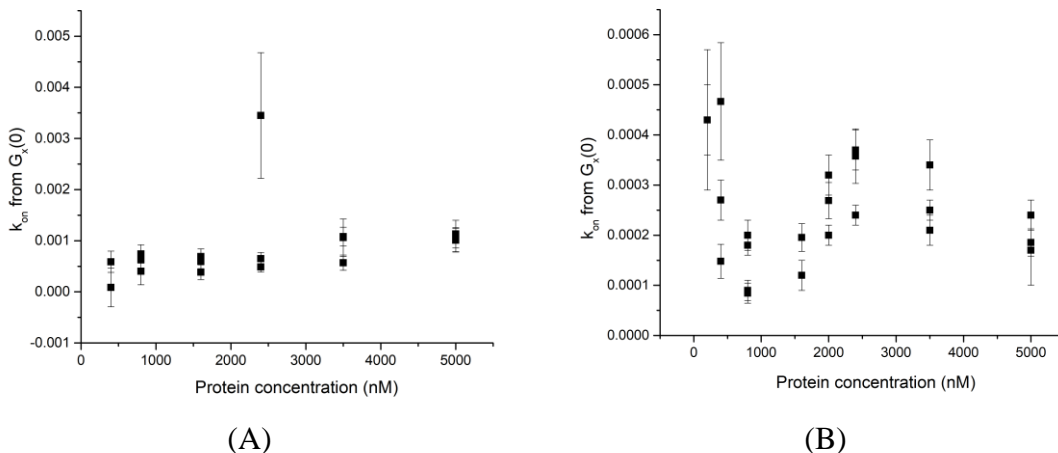


**Figure 4.2**  $k_{\text{on}}$  rate constants determined for various initial concentrations of labeled BSA mixed with (A) red-labeled FS<sub>100</sub> (1 nM) and (B) yellow-green-labeled FS<sub>200</sub> (1 nM) in PBS. The errors were obtained from the fittings.

Figure 4.2 (A) shows that for a variety of initial BSA concentrations, the  $k_{\text{on}}$  values for the system composed of the FS<sub>100</sub> and BSA are consistent within error. The average  $k_{\text{on}}$  value for the interaction between the BSA and FS<sub>100</sub> was calculated to be  $(7 \pm 0.7) \times 10^{-4} \text{ s}^{-1}$ , excluding the one outlier seen in Figure 4.2 (A), with the error corresponding to the standard error. Conversely, for the system composed of the larger FS<sub>200</sub>, the  $k_{\text{on}}$  values appear much more scattered within each tested protein concentration in Figure 4.2 (B), although the overall range of the scatter is less than that for the system of BSA interacting

with the FS<sub>100</sub>. The overall range for the  $k_{on}$  for the interaction between the BSA and FS<sub>200</sub> was calculated to be  $(1.6-4.3 \pm 0.2) \times 10^{-4} \text{ s}^{-1}$ , with the error corresponding to the standard error.

For comparison sake, the  $k_{on}$  values were also plotted (Figure 4.3) for the experiments involving the higher ratios of BSA to FS. These plots include values of different FS concentrations. For the system composed of the BSA interacting with FS<sub>100</sub>, the concentration of FS<sub>100</sub> was dropped to 0.5 nM, while the BSA concentration was kept at 5000 nM. Figure 4.3 (A) indicates that at this higher ratio of BSA to FS<sub>100</sub>, the  $k_{on}$  for this system remains the same within error in comparison to the  $k_{on}$  values found from the previous concentration ratios. Conversely, for the system composed of BSA interacting with the FS<sub>200</sub>, at higher concentration ratios, the  $k_{on}$  values were observed to increase until seemingly plateauing at the highest concentration ratio tested. This trend seems to indicate that the higher BSA concentrations show a faster association of BSA to FS<sub>200</sub> than at lower BSA concentrations.

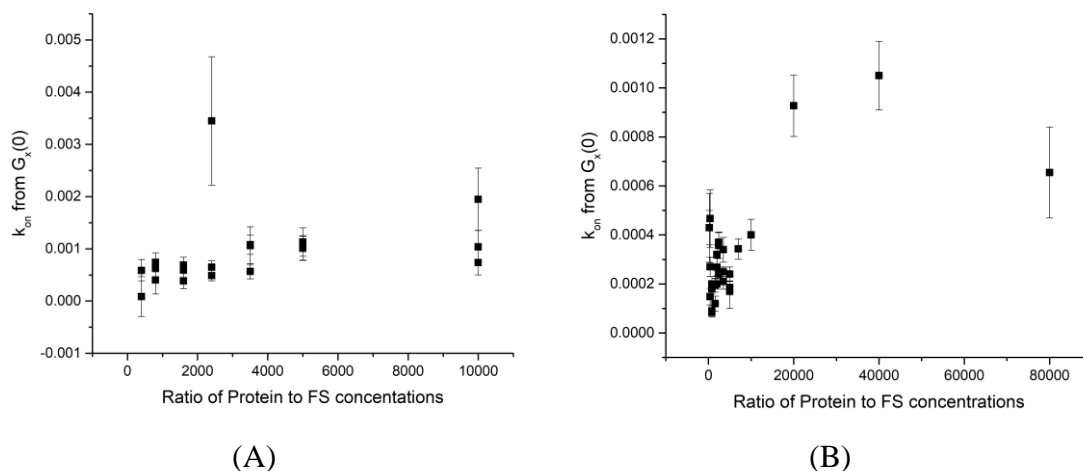


**Figure 4.3**  $k_{on}$  rate constants across all concentration ratios tested of BSA interacting with (A) red-labeled FS<sub>100</sub> and (B) yellow-green-labeled FS<sub>200</sub> in PBS. At the highest ratio, the concentration of FS<sub>100</sub> was dropped to 0.5 nM, while the concentration of FS<sub>200</sub> was dropped as low as 0.0625 nM. The errors were obtained from the fittings.

Another analysis, using collected autocorrelation data from the proteins, also gave insight into another way of accessing the  $k_{on}$  value. As mentioned in Section 3.2.1 and demonstrated in Figure 3.5, there was an observed increase in the  $G_p(0)$  signal for the red-labeled proteins over the experimental time period upon mixing with the yellow-green-labeled FS<sub>200</sub>. Recalling from Chapter 2 that  $N$  (the number of fluorescently-labeled entities in the focal volume) is approximately inversely proportional to the  $G_p(0)$  signal led to the analysis of the change in  $N_{protein}$  (or  $1/G_p(0)$ ) over the experiment time for the tested concentration ratios. Plots of  $1/G_p(0)$  as a function of time were generated for each concentration ratio of BSA to FS tested, an example of which is given in Figure 4.4. The data from each plot was fit with a first-order exponential decay function (Equation 4.2), and the  $k_{on}$  rate constant was accessed from each fitting. We chose to fit using a mono-exponential decay for simplicity's sake; however, we recognize that there could be some bi-exponential behavior in these data sets.

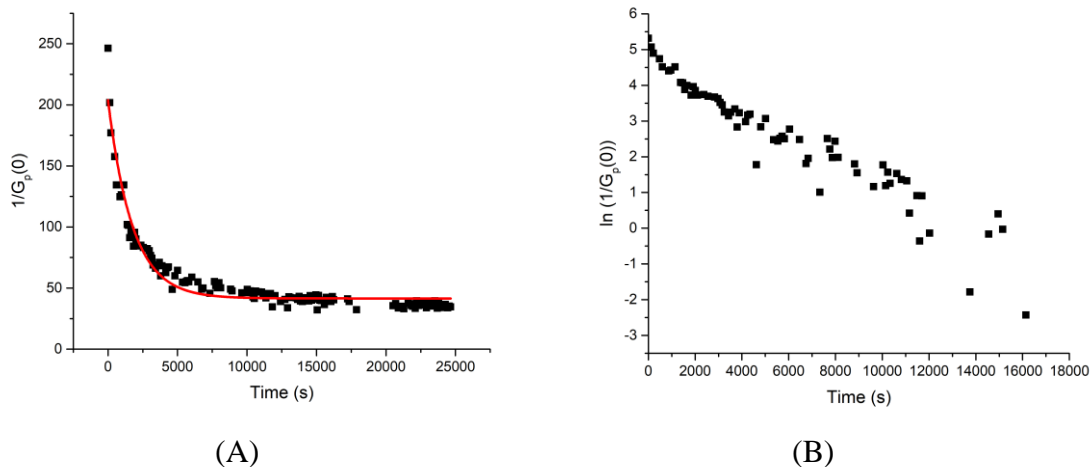


**Figure 4.4** (A)  $1/G_p(0)$  values tracked over the course of the experimental time, in seconds, for a mixture of 800 nM red-labeled BSA and 1 nM FS<sub>200</sub> in PBS. The red line represents the fitting of the data with Equation 4.2. (B) Linearized form of the data is displayed in panel (A).

$$y(t) = y_0 e^{-kt} + C \quad \text{Equation 4.2}$$

In the Equation 4.2,  $y_0$  represented the initial  $N_{\text{protein}}$  value, and  $C$  was the value of free  $N_{\text{protein}}$  after all the binding has taken place and equilibrium has been established.

The  $k_{\text{on}}$  rate constants were collected for each mixture of BSA and FS using this analysis. The  $k_{\text{on}}$  values were then analyzed as a function of BSA concentration (ranging from 200-5000 nM), while keeping the FS<sub>200</sub> concentration at 1 nM, as shown in Figure 4.5.

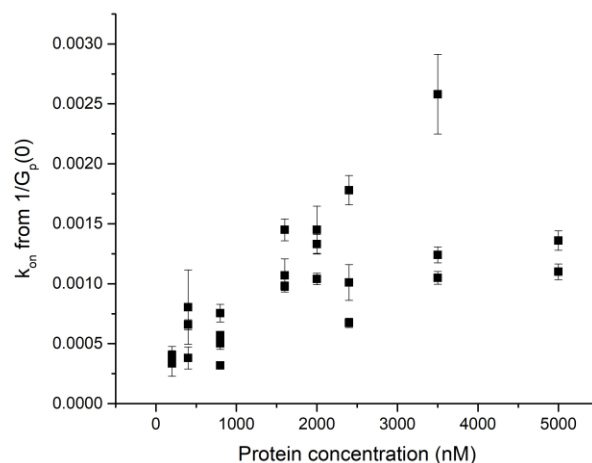


**Figure 4.5**  $k_{on}$  rate constant values obtained from the decay curves of  $1/G_p(0)$  as a function of time for various mixtures of red-labeled BSA (200-5000 nM) and yellow-green-labeled FS<sub>200</sub> (1 nM) in PBS. The errors were obtained from the fittings.

Again, for comparison sake, the  $k_{on}$  values were also found and plotted (Figure 4.6) for the experiments involving the higher ratios of BSA to FS<sub>200</sub>, where the concentration of FS<sub>200</sub> was dropped from 1 nM to as low as 0.0625 nM. Similarly to the  $k_{on}$  values determined at higher concentration ratios using the  $G_x(0)$  data, the  $k_{on}$  values found from  $1/G_p(0)$  were observed to plateau at the higher concentration ratios of BSA to FS<sub>200</sub>.

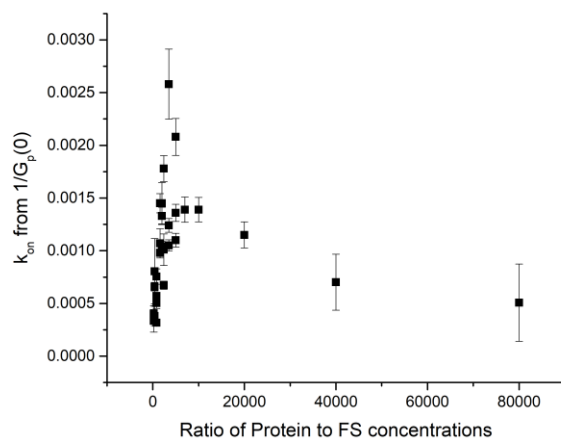


**Figure 4.6**  $k_{on}$  rate constant values obtained from the decay curves of  $1/G_p(0)$  as a function of time for all tested mixtures of red-labeled BSA (200-5000 nM) and yellow-green-labeled FS<sub>200</sub> (ranging as low as 0.0625 nM and up to 1 nM) in PBS. The errors were obtained from the fittings.

In comparison to the values obtained for  $k_{on}$  from the  $G_x(0)$  data in Figure 4.2 (B), the  $k_{on}$  values determined in Figure 4.5 are an order of magnitude higher. It is uncertain and unclear if the “ $k_{on}$ ” values determined through analysis of the  $1/G_p(0)$  or  $N_{protein}$  as a function of time are exactly comparable with those from the  $G_x(0)$  data. Because the  $N_{protein}$  values are calculated simply from the inverse of  $G_p(0)$  for the BSA (Equation 2.6 from Chapter 2), this implies that the  $G_p(0)$  is not solely measuring the interactions between the BSA and FS, but also tracking the changes in fluorescence intensity and the changes of BSA proteins alone and protein-protein interactions. Although this study refers to these constants as “ $k_{on}$ ,” these values may not be an accurate reflection of the true  $k_{on}$  value for these interactions. This will be further discussed in Section 4.2.1.4.

#### 4.2.1.2 Association and Dissociation Constant ( $K_A$ and $K_D$ ) Determination

The values for  $K_D$  were determined through two methods. First, the  $K_D$  values for both systems were calculated from the x-intercept of the linearized Hill plots in Figure 4.7.

The Hill-Langmuir theory describes the simplest binding regime is composed of a certain number (n) of ligands (L) bound to a receptor (R). This theory emerged after Hill, in 1910, discovered that it was possible to quantify the binding of oxygen to hemoglobin using a specific equilibrium expression. In the case of the experiments in this thesis, the serum albumin proteins (P) are considered to be the ligands and the fluospheres (S) are considered to be the receptors. The general equilibrium expression is given in Equation 4.3.



The fractional occupancy ( $P_A$ ) is defined as the molar ratio of occupied receptors ( $C_{PS}$ ) to the total concentration of receptors ( $C_S + C_{PS}$ ). Plotting the fractional occupancy as a function of ligand (in this case, protein) concentration can be used to find the dissociation constant ( $K_D$ ) for the case when  $n = 1$ , as shown in Equation 4.4. The dissociation constant reflects the affinity of the interaction between the protein and the spheres, where a small  $K_D$  value indicates a strong affinity between the two entities.

$$P_A = \frac{nC_P}{K_D + nC_P} \quad \text{Equation 4.4}$$

Linearizing the above formula gives rise to Equation 4.5, in which the  $K_D'$  represents the dissociation constant when  $n \neq 1$ . When  $n = 1$ ,  $K_D = K_D'$ , and in the absence of binding cooperatively,  $K_D$  can be found by taking the  $n^{\text{th}}$  root of  $K_D'$ , as shown in Equation 4.6.

$$\log\left(\frac{P_A}{1 - P_A}\right) = n \log(C_P) - \log(K_D') \quad \text{Equation 4.5}$$

$$K_D = \sqrt[n]{e^{-incpt}} \quad \text{Equation 4.6}$$

The resulting linearized Hill plots for BSA interacting with FS<sub>100</sub> and FS<sub>200</sub> are shown in Figure 4.7.

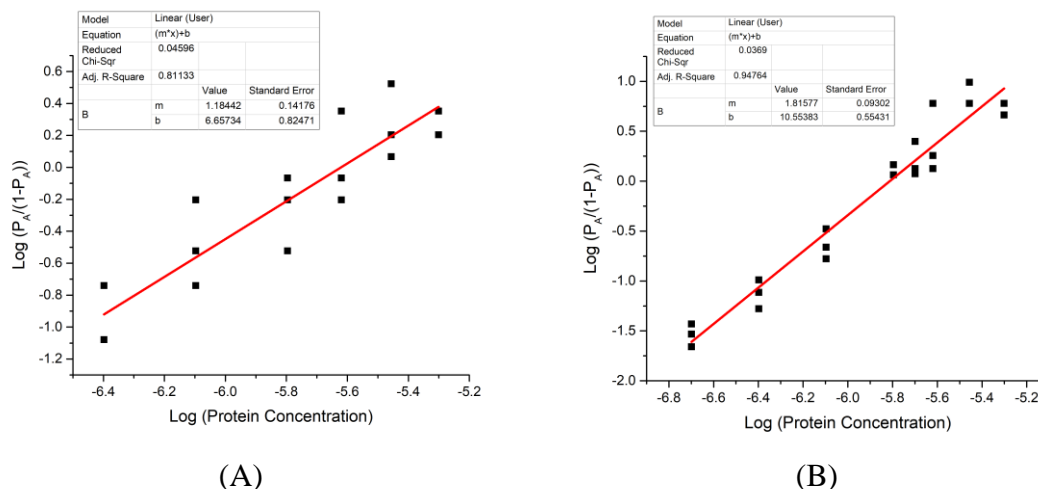


**Figure 4.7** The linearized Hill plot for the equilibrated system composed of the (A) red-labeled FS<sub>100</sub> (1 nM) and green-labeled BSA and (B) yellow-green-labeled FS<sub>200</sub> (1 nM) and red-labeled BSA. The x-intercepts of these plots allowed for the determination of the approximate  $K_D$  value for the system.

The  $K_D$  values were calculated from the linearized Hill plots and found to be  $(2.3 \pm 1.3) \times 10^{-6}$  and  $(1.6 \pm 0.9) \times 10^{-6}$  for BSA interacting with FS<sub>100</sub> and FS<sub>200</sub>, respectively, with the error corresponding to error propagation for the calculations. These values correspond to  $K_A$  values (for comparison purposes in the discussion) of  $(4.4 \pm 2.5) \times 10^5$  and  $(6.3 \pm 3.5) \times 10^5$  for BSA interacting with FS<sub>100</sub> and FS<sub>200</sub>, respectively. However, the Hill model is most likely only an approximation of the binding interactions between the BSA and FS. We believe the Hill model to be an approximation because it does not explicitly represent the number of FS binding sites. Therefore, we attempted to develop a more representative model that could provide better estimations for the kinetic parameters by accounting for both entities involved in the equilibrium binding process, and furthermore, a model that used some of the experimental measurements that had been taken.

Another approach to consider for access to kinetics association and dissociation rate constants ( $K_A$  and  $K_D$ ) involved thinking instead in terms of the number of FS receptor sites available and bound by protein once equilibrium had been established for every concentration ratio tested. By this approach, we re-defined the  $K_A$  or  $K_D$  in terms of the concentration of occupied and available receptor sites on the FS ( $[sites\ bound]$  and  $[free\ sites]$ , respectively) and the concentration of free protein in solution ( $[P_{free}]$ ) after the establishment of an equilibrium. This definition of  $K_A$  and  $K_D$  following this approach is demonstrated in Equation 4.7.

$$K_A = \frac{[sites\ bound]}{[P_{free}][free\ sites]} \text{ or } K_D = \frac{[P_{free}][free\ sites]}{[sites\ bound]} \quad \text{Equation 4.7}$$

The concentration of free FS sites available for binding was determined by taking the difference between the highest binding ratio given by the pseudo-explicit model from Section 3.2.3 ( $[\frac{n_{max}}{sphere}]$ ) for each BSA-FS and the corresponding equilibrium binding ratio  $[n / sphere]$  for a particular concentration ratio of FS and BSA being tested, per TPE volume. This definition is demonstrated in Equation 4.8.

$$[free\ sites] = \left[ \frac{\frac{n_{max}}{sphere} - \frac{n}{sphere}}{TPE\ volume} \right] \quad \text{Equation 4.8}$$

The concentration of occupied FS sites at equilibrium was determined by using the estimated binding ratio given by the pseudo-explicit model per TPE volume. This definition is shown in Equation 4.9.

$$[sites\ bound] = \left[ \frac{\frac{n}{sphere}}{TPE\ volume} \right] \quad \text{Equation 4.9}$$

The concentration of free protein in solution upon reaching the equilibrium binding was determined by taking the difference in the total initial amount of protein available [ $P_{tot}$ ] minus the protein bound to FS at equilibrium, which could be found by multiplying the equilibrium binding ratio by the concentration of FS in solution,  $[S]$ .

$$[P_{free}] = [P_{tot}] - ([n/sphere] \cdot [S]) \quad \text{Equation 4.10}$$

Following this approach, values for  $K_A$  and  $K_D$  were calculated using this “sites bound” approach, and the results are demonstrated in Figure 4.8 for BSA (200 nM to 5000 nM) interacting with FS<sub>100</sub> and FS<sub>200</sub> (both at 1 nM).

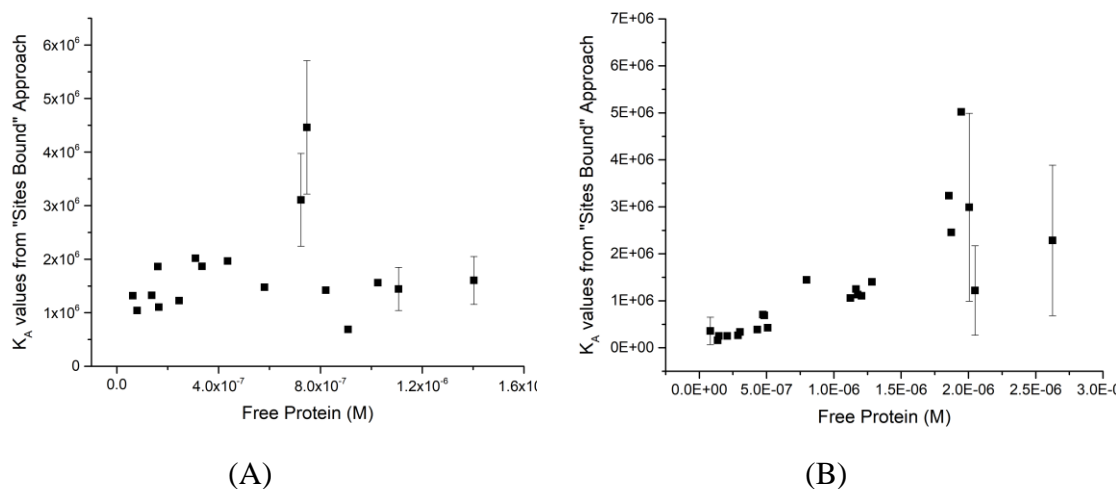


**Figure 4.8**  $K_A$  values determined using the “sites bound” approach for BSA (ranging 200 nM to 5000 nM) interacting with (A) red-labeled FS<sub>100</sub> (1 nM) and (B) yellow-green-labeled FS<sub>200</sub> (1 nM). The errors shown on a few points correspond to the propagation of errors from the calculations.

The  $K_A$  values were also calculated for the higher concentration ratios tested between BSA and FS, where the concentration of FS<sub>100</sub> was dropped from 1 nM to 0.5 nM, and the concentration of FS<sub>200</sub> was dropped from 1 nM to as low as 0.0625 nM. The

comparison of these  $K_A$  values with those found previously (Figure 4.8) are shown in Figure 4.9.

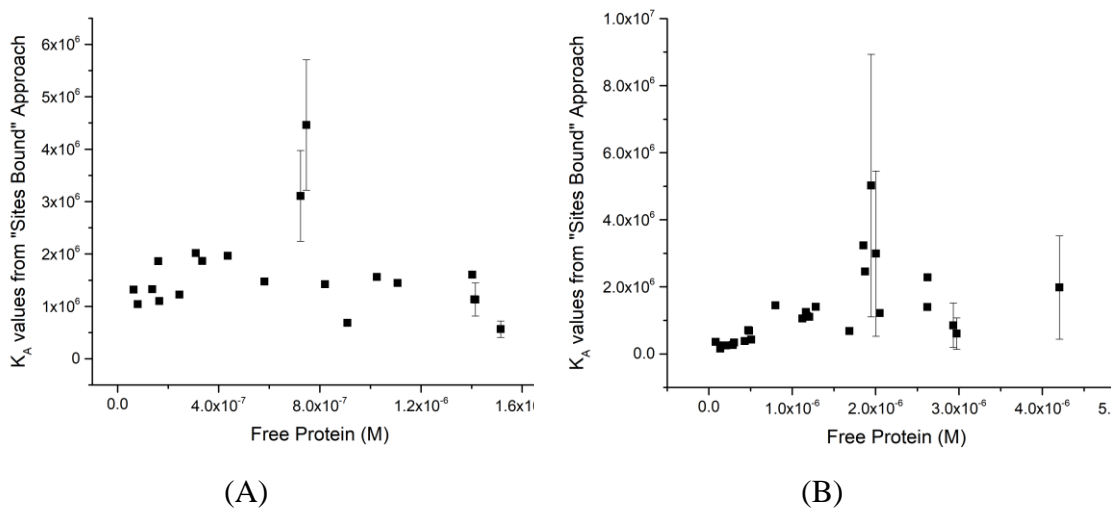


**Figure 4.9**  $K_A$  values determined for the higher concentration ratios of BSA to FS using the “sites bound” approach for BSA (200 to 5000 nM) interacting with (A) red-labeled FS<sub>100</sub> (0.5 to 1 nM) and (B) yellow-green-labeled FS<sub>200</sub> (0.0625 to 1 nM). The errors shown on a few points correspond to the propagation of errors from the calculations.

From Figures 4.8 and 4.9, the  $K_A$  values for both BSA-FS systems appear to be of a magnitude of  $10^6$ . In comparison to the  $K_A$  values determined using the linearized Hill model for both systems (on the order of  $10^5$ ), the values calculated by the “sites bound” approach are an order of magnitude larger. This discrepancy could be speaking to the simplicity of using the Hill model to describe the binding between the BSA and FS; however, both models indicate that medium-strong binding occurs between the BSA and FS. The  $K_A$  values determined using the “sites bound” approach for the BSA-FS<sub>100</sub> system appeared fairly similar, even at the higher ratios of BSA to FS that were tested (Figure 4.9 (A)). This trend in  $K_A$  values suggests that the binding of BSA to FS<sub>100</sub> was not influenced by the protein concentration and that the binding at each concentration ratio tested likely

followed a similar mechanism. As a result, an average  $K_A$  was calculated for the BSA-FS<sub>100</sub> system based on the “sites bound” approach and was determined to be  $(1.7 \pm 0.25) \times 10^6$ , with the error corresponding to the standard deviation of the errors obtained through error propagation.

Conversely, for the BSA-FS<sub>200</sub> system, there was quite a different trend in  $K_A$  values observed, depending on the concentration of the two entities in solution. Prior to testing the higher concentration ratios, Figure 4.8 (B) suggested either a possible linear trend or even exponential increase of  $K_A$  with protein concentration for this system. However, after testing the higher concentration ratios, the  $K_A$  value seemed to plateau, as seen in Figure 4.9 (B). Recalling for comparison’s sake from Figure 4.3 (B), where a similar trend and plateau was observed in the  $k_{on}$  values obtained across all concentration ratios tested for this system. As a result, a  $K_A$  value could only be drawn for the mixtures of BSA and FS<sub>200</sub> at high concentrations (BSA concentrations of 3500 to 5000 nM and FS<sub>200</sub> concentration at 1 nM), which was found to be  $(3.2 \pm 1) \times 10^6$ . The error corresponds to the standard deviation of the errors obtained through error propagation. Again, the discrepancy in  $K_A$  values using this approach versus that obtained from the linearized Hill model could be a result of the over-simplification of the binding representation occurring between the BSA and FS<sub>200</sub>. The Hill coefficient being greater than one (Figure 4.7 (B),  $n = 1.8 \pm 0.1$ ) is perhaps indicative of positively cooperative binding between the two entities, which further implies that a single, collective  $K_A$  value cannot describe the binding occurring at every concentration ratio. Furthermore, the trend in  $K_A$  values determined through the “sites bound” approach in Figure 4.8 seemed to also suggest that positively cooperative binding occurs as the protein concentration is increased up to 5000 nM.

Therefore, because of the suggested dependency of  $K_A$  on protein concentration, a log log plot was generated to provide insight into the protein dependency. The resulting plot is demonstrated in Figure 4.10 and indicates a clear linear trend, suggesting that there is a dependency on the protein concentration to the power of 1. We believe this would imply that, for this BSA-FS<sub>200</sub> system, the  $K_A$  values demonstrated in Figure 4.8 (B) would be reflective of  $K_A'$  over the actual  $K_A$  values.

$$K_A' = \frac{[sites\ bound]}{[P_{free}]^n [free\ sites]} \quad \text{Equation 4.11}$$

where

$$K_A = \frac{[sites\ bound]}{[P_{free}]^2 [free\ sites]} \quad \text{Equation 4.12}$$

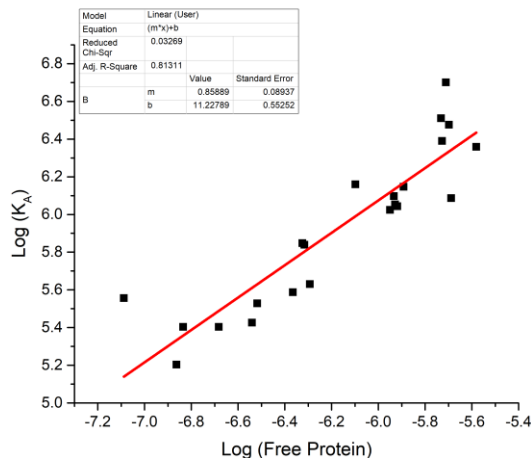


**Figure 4.10** Plot of the  $\log(K_A)$  from the values determined through the “sites bound” approach as a function of the  $\log(\text{Protein concentration})$  ranging from 200 to 5000 nM, for the system composed of BSA interacting with FS<sub>200</sub> (1 nM).

Acquiring values for the  $K_A$  for both BSA-FS systems allowed for the calculation of Gibbs free energy and comparison of those energies to that of a hydrogen bond. The

Gibbs free energy values were calculated to be approximately -35 kJ/mol for the BSA-FS<sub>100</sub> system and -18 kJ/mol for the BSA-FS<sub>200</sub> system. These values fell within the range of the strength of a hydrogen bond (approximately 4-50 kJ/mol). These results could suggest that hydrogen bonding is at least one component of the BSA-FS interactions for both systems.

If hydrogen bonding was a predominant contribution to the overall binding of the BSA to the surface of the FS, then we could speculate that this interaction could be between the negatively charged carboxylate group of the FS with the lysine amino acids of the BSA. It has been reported that the carboxyl groups of fatty acids primarily associate with three lysine residues of serum albumins (Lys-116, Lys-349, and Lys-473),<sup>72</sup> therefore supporting that this interaction could be driving the association of BSA to the FS surface. In terms of the apparent stacking of the BSA onto adsorbed BSA at the surface, we speculate that these interactions are hydrophobic in nature. Perhaps because of the locally increased concentration of the BSA at the FS surface, this allows for the stacking of BSA to take place.

#### 4.2.1.3 Off-Rate Constant ( $k_{off}$ ) Determination

The off-rate constant ( $k_{off}$ ) can be estimated through division of the on-rate constant ( $k_{on}$ ) and the association constant ( $K_A$ ), through manipulation of the expression for  $K_A$  in Equation 4.13.

$$K_A = \frac{k_{on}}{k_{off}} \Rightarrow k_{off} = \frac{k_{on}}{K_A} \quad \text{Equation 4.13}$$

The resulting  $k_{off}$  values for both BSA-FS systems were calculated using the  $k_{on}$  values determined from the  $G_x(0)$  amplitudes (Section 4.2.1.1) and from the values for  $K_A$  found

using both the linearized Hill method and from the “sites bound” approach, for comparison sake.

Using the  $K_A$  values from the linearized Hill model, the resulting  $k_{off}$  values were determined to be  $(1.6 \pm 0.9) \times 10^{-9} \text{ s}^{-1}$  and  $(2.5 \pm 1.4 \text{ to } 6.8 \pm 3.8) \times 10^{-10} \text{ s}^{-1}$  for BSA interacting with FS<sub>100</sub> and FS<sub>200</sub>, respectively. The errors correspond to the propagation of error calculations. Recall that there was a range for the  $k_{on}$  values for the BSA-FS<sub>200</sub> system, hence the range in  $k_{off}$  values. The  $K_A$  value used for this calculation for the BSA-FS<sub>200</sub> system was that determined for the higher protein concentrations, from Section 4.2.1.2. These  $k_{off}$  values are extremely small and thus suggests that these values would be too small to measure experimentally.

From the “sites bound” approach, the  $k_{off}$  values was calculated to be  $(4.1 \pm 0.7) \times 10^{-10} \text{ s}^{-1}$  for BSA interacting with FS<sub>100</sub> and  $(5 \pm 1.7) \times 10^{-11} \text{ s}^{-1}$  to  $(1.3 \pm 0.4) \times 10^{-10} \text{ s}^{-1}$  for the higher concentrations of BSA (2000-5000 nM) interacting with FS<sub>200</sub>. Similarly to the  $k_{off}$  values calculated by the Hill model, these values are also very small, indicating that the binding of BSA to either FS<sub>100</sub> or FS<sub>200</sub> is essentially irreversible.

#### **4.2.1.4 Insight into the BSA-FS Reaction Kinetics and Binding Mechanism**

The binding of both BSA-FS systems was found to follow slightly different kinetics, seemingly dependent on the size of the FS. For the system composed of BSA interacting with FS<sub>100</sub>, the binding is suggested to follow first order kinetics, or at least pseudo-first order kinetics. This was determined through the analysis of the on-rate constants,  $k_{on}$ . Figure 4.2 (A) suggested that the  $k_{on}$  value was not affected by the concentrations of protein or FS, even after the concentration ratio between BSA and FS

was increased, as shown in Figure 4.3 (A). A similar trend was observed in the values for  $K_A$  determined by the “sites bound” approach for this system. When examining  $k_{on}$  from the point of view of loss of free BSA to binding, the data for the green-labeled proteins was extremely scattered and did not produce any obvious trend in the  $G_p(0)$  over time upon analysis (unlike the changes observed for the BSA-FS<sub>200</sub> system). This can perhaps be made sense of because of the lower binding ratios estimated for this BSA-FS<sub>100</sub> system and the fact that the autocorrelation takes into account all BSA, not solely free BSA. This suggests that there was no large change in BSA concentration over the duration of the experiment, which is also consistent with a pseudo-first order situation with respect to BSA. Therefore, the conclusions for the kinetics of interaction could only be drawn from analysis of the trends in  $k_{on}$  rate constants and  $K_A$  association constants for this BSA-FS<sub>100</sub> system.

The rate limiting step for the association of BSA to the FS<sub>100</sub> surface was thought to likely be the binding of the first BSA protein, as there were immediate changes in the  $G_x(0)$  amplitude as soon as the two entities were mixed. Although this change was not as apparent in the  $G_p(0)$  measurements for this system, we attribute this to low binding and the extreme excess of free protein in solution being the main contributor to the  $G_p(0)$  values.

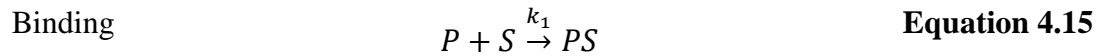
For the other system composed of BSA interacting with FS<sub>200</sub>, the binding was suggested to follow pseudo-first order kinetics. This was determined through analysis of the changes in  $G_p(0)$  as well as from the results of the log-log plot in Figure 4.10. The analysis of the change in the number of BSA proteins in the focal volume ( $N_{protein}$  or  $1/G_p(0)$ ) over time suggested that this system followed an exponential decay. However, the rate constant for this measurement increased initially with increasing protein concentration

(Figure 4.5), suggesting a pseudo-first order process with respect to protein concentration. The slope of the log log plot in Figure 4.10 also suggested that the kinetics of the interaction between BSA and FS<sub>200</sub> was dependent on the concentration of BSA to the power of 1.

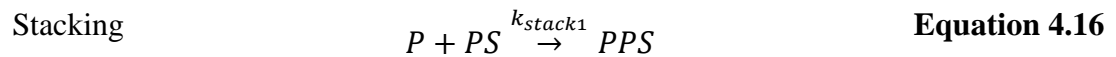
Looking even deeper into the analyses of the changes in  $G_x(0)$  and  $G_p(0)$  interestingly seemed to suggest that these two measurements were reporting on different parts of the binding process between BSA and FS<sub>200</sub>, given that they report different values for the rate constants. We thought that these differences, explored in the following paragraphs, could lead to a deeper understanding of the mechanism of binding between the BSA and FS<sub>200</sub> NPs.

Recall that  $G_x(0)$  only measures bound entities – in this case, BSA-FS<sub>200</sub> complexes, such as those formed as represented in Equation 4.14. From the TEM images in Figure 3.13, it is suggested that two possible binding processes were occurring at the surface of the FS. The first process would likely be the direct binding of a BSA protein to the FS NP surface. Since there may be many direct binding sites, these would become occupied sequentially (Equation 4.15). In this process, each protein is thought to bind to a different receptor on the FS. The second process suggested by the TEM images was the stacking of a BSA protein on top of another BSA protein already bound to an FS (Equation 4.16). Therefore, a  $G_x(0)$  signal would result from the products formed by each of these processes, but would most likely be dominated by the slower of the binding processes. We further suggest that the rate-determining step for the formation of these complexes would be the stacking of BSA onto BSA on the FS<sub>200</sub> (Equation 4.16).





*...and so on*



*...and so on*

Further recall that  $G_p(0)$  measures the change in number of BSA proteins in the focal volume, and that the analysis of  $1/G_p(0)$  over time indicated an exponential decay in protein (Figure 4.4). It is thought that the  $G_p(0)$  would pick up on the apparent loss of protein in the focal volume as a result of both of the binding processes occurring in Equations 4.15 and 4.16; however, the  $G_p(0)$  measurement is likely dominated by the fastest mechanism of the loss, which could be the binding process. This is born out by the relative values of  $k_{on}$  measured from loss of protein (on the order of magnitude of  $10^{-3}$ ) and from the formation of product (on the order of magnitude of  $10^{-4}$ ).

Interestingly, a deeper look into the kinetics on-rate constants from  $G_x(0)$  (Figure 4.2 (B), “ $k_{on-cross}$ ”) and  $G_p(0)$  (Figure 4.5, “ $k_{on-auto}$ ”) indicate that  $k_{on-auto} > k_{on-cross}$  by an order of magnitude, which seems to support the stacking of the first BSA protein onto another surface-bound BSA as the rate limiting step. The discrepancy between these two measurements of  $k_{on}$  further suggested that the  $k_{on-cross}$  and  $k_{on-auto}$  were reporting on different binding kinetics. The trends observed in the  $k_{on}$  values determined by both

methods also differed. At concentrations of BSA less than 5000 nM (FS<sub>200</sub> concentration kept constant at 1 nM), the  $k_{\text{on-cross}}$  appeared relatively consistent across the various concentrations of BSA tested, while the  $k_{\text{on-auto}}$  values appeared to have a linear, then saturating dependence on the BSA concentration. While at the higher concentration ratios (FS concentration dropped as low as 0.0625 nM and BSA concentration at 5000 nM), both the  $k_{\text{on-cross}}$  and  $k_{\text{on-auto}}$  appear to converge.

Based on these results, it appears that the binding of BSA to FS<sub>100</sub> and FS<sub>200</sub> follow slightly different kinetics and mechanism. This could be due to the difference in size or surface chemistry between the two spheres, which could further affect the number of receptor sites at the surface in a non-linear way. However, there is a possibility that the two systems are interacting by the same kinetics – but we simply cannot measure any lower concentration ratios of BSA with FS<sub>100</sub> to observe any change on the kinetics of association. There is the possibility that the  $k_{\text{on}}$  values we are measuring for this BSA-FS<sub>100</sub> system are those at which we also observe convergence of the  $k_{\text{on-cross}}$  and  $k_{\text{on-auto}}$  values for the BSA-FS<sub>200</sub> system. To analyze for this, the estimated binding ratios using the pseudo-explicit model were normalized across both BSA-FS systems and plotted as a function of their corresponding  $k_{\text{on}}$  values. These plots suggested support for our reasoning that we are perhaps only measuring the point at which the  $k_{\text{on-cross}}$  and  $k_{\text{on-auto}}$  converge for the BSA-FS<sub>100</sub> system, if that system was following similar kinetics to the BSA-FS<sub>200</sub> system.

#### **4.2.2 Fluorescence Changes in FS and BSA upon Mixing**

The fluorescence intensity changes of the FS and BSA were monitored as a function of time upon mixing for both systems under study. The count rate trajectories of both fluorescently-labeled entities over the experimental time allowed for the observation of any

sudden or slowly evolving changes in the overall fluorescence intensities, likely due to the binding events.

For the system composed of the BSA interacting with the FS<sub>100</sub>, there were no obvious changes observed in fluorescence intensities for either entity over the experimental time upon mixing. Two examples of the average fluorescence intensities for two BSA-FS<sub>100</sub> mixtures measured over time are shown in Figure 4.11, where (A) is a mixture of 400 nM BSA and 1 nM FS<sub>100</sub> and (B) is a mixture of 3500 nM BSA and 1 nM FS<sub>100</sub>. The average fluorescence intensities of both entities, as seen from the example plots, remained relatively constant over the duration of the experimental time, and remained constant despite changes in the concentration ratios of both BSA and FS<sub>100</sub>.

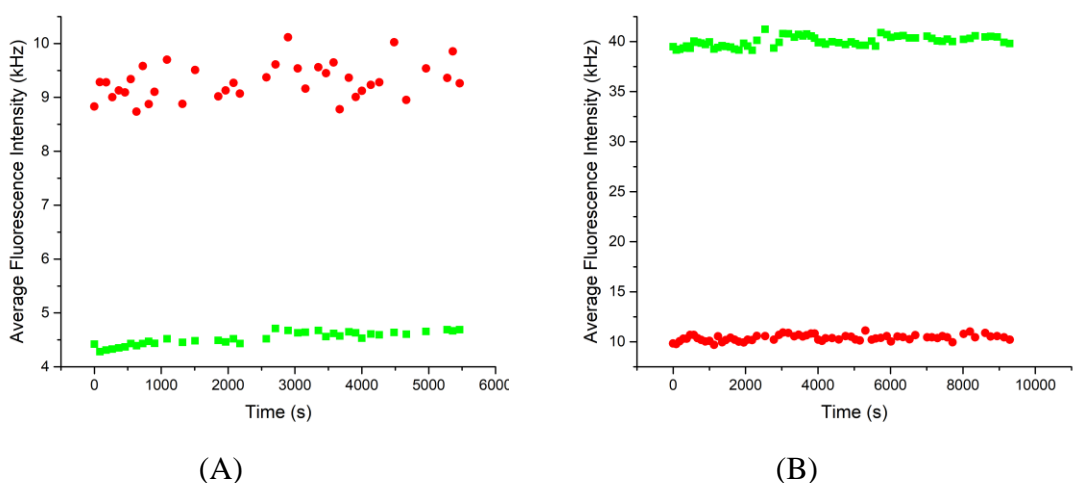


**Figure 4.11** Examples of the average fluorescence intensity changes over the total experiment time for a mixture of (A) 400 nM green-labeled BSA interacting with 1 nM red-labeled FS<sub>100</sub> and (B) 3500 nM green-labeled BSA interacting with 1 nM red-labeled FS<sub>100</sub>. The BSA proteins are denoted by the green squares, and the FS<sub>100</sub> are denoted by the red circles. As seen in both examples, the average fluorescence intensities of both entities remain relatively constant over the total experimental time.

Conversely, for the system composed of the red-labeled BSA interacting with the larger FS<sub>200</sub>, changes in fluorescence intensities were observed for both entities over the experimental time periods. A slight decrease in fluorescence intensity was observed for the FS<sub>200</sub> for every tested mixture of BSA and FS; however, the BSA fluorescence intensities either increased or decreased depending on the concentration ratio of BSA to FS<sub>200</sub> being tested. At tested BSA concentrations lower than 2000 nM with 1 nM FS<sub>200</sub>, the fluorescence intensity of the BSA was observed to increase over the experimental time. At BSA concentrations higher than 2000 nM with 1 nM FS<sub>200</sub>, the fluorescence intensity of BSA was observed to decrease over the experimental time. Examples of these trends are demonstrated in Figure 4.12 for a mixture of (A) 800 nM BSA with 1 nM FS<sub>200</sub> and (B) 5000 nM BSA with 1 nM FS<sub>200</sub> over the experimental time. Interestingly, a dependence of BSA concentration on the time to reach equilibrium between the BSA and FS was also observed in Chapter 3, which could provide insight into the mechanism of the interaction between the two entities.

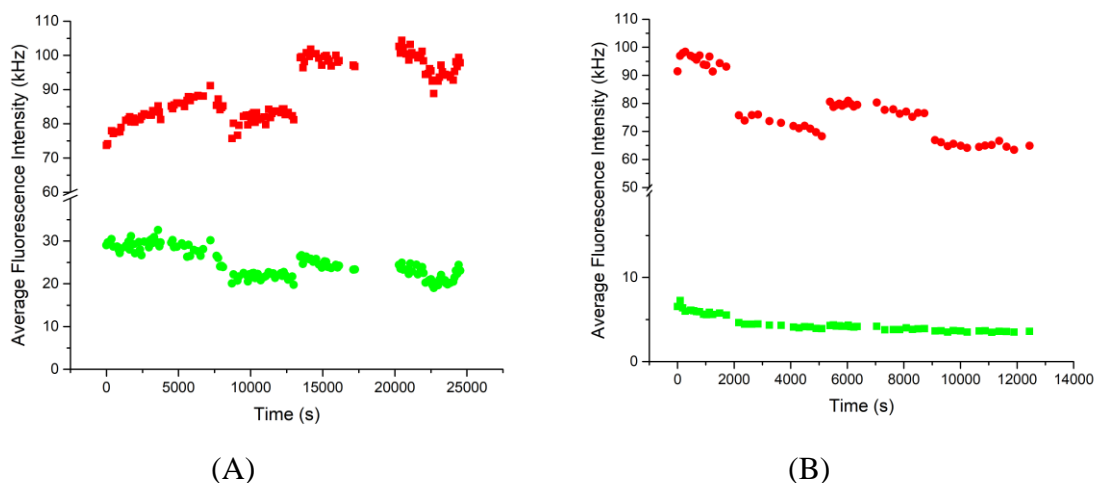


**Figure 4.12** Examples of the average fluorescence intensity changes over the total experiment time for a mixture of (A) 800 nM red-labeled BSA interacting with 1 nM yellow-green-labeled FS<sub>200</sub> and (B) 5000 nM red-labeled BSA interacting with 1 nM yellow-green-labeled FS<sub>200</sub>. The BSA proteins are denoted in red, and the FS<sub>200</sub> are denoted in green. As seen in these examples, the average fluorescence intensities of the BSA changes depending on its concentration, while the fluorescence intensity of the FS<sub>200</sub> drops slightly in both cases.

One possible explanation for the observed changes in fluorescence intensities between the FS<sub>200</sub> and BSA could be that an energy transfer is occurring between the two entities due to the binding events. For an energy transfer to occur between these two entities, there must be a spectral overlap of the emission spectrum of the donor with absorption spectrum of the acceptor. The overlap in the emission spectrum of the yellow-green-labeled FS<sub>200</sub> and absorption spectrum of the red-labeled BSA with Alexa Fluor® 594 dye does provide support for an energy transfer from the FS<sub>200</sub> to the BSA. This reasoning could, therefore, explain the observed decreasing fluorescence intensity trend for the FS<sub>200</sub> and increasing fluorescence intensity trend for the BSA. However, for the observed opposite trend – the decreasing fluorescence intensities of both entities – this reasoning does not entirely hold. An energy transfer between the FS<sub>200</sub> and BSA is likely

still occurring, as the trend fluorescence intensity of the FS<sub>200</sub> continues to decrease at higher BSA concentrations. As for the observed trend for the BSA, perhaps at higher concentrations of BSA quenching occurs due to the increased likelihood of protein-protein interactions either at the FS surface or in the surrounding solution. As a result, such interactions could result in quenching at the surface and/or in the surrounding solution and could explain the observed decrease in fluorescence intensity for the BSA at higher BSA concentrations.

Further analysis into the fluorescence intensity changes for the FS<sub>200</sub> provided insight into the possible binding mechanism and happenings at the surface of the sphere upon protein binding. The normalized changes in initial and final fluorescence intensity of the FS<sub>200</sub> were determined for each tested mixture of FS<sub>200</sub> mixed with BSA. These changes were then plotted as a function of the concentration ratio of BSA to FS<sub>200</sub> and were further compared to the binding ratio from the pseudo-explicit model (Section 3.2.3), displayed in Figure 4.13.

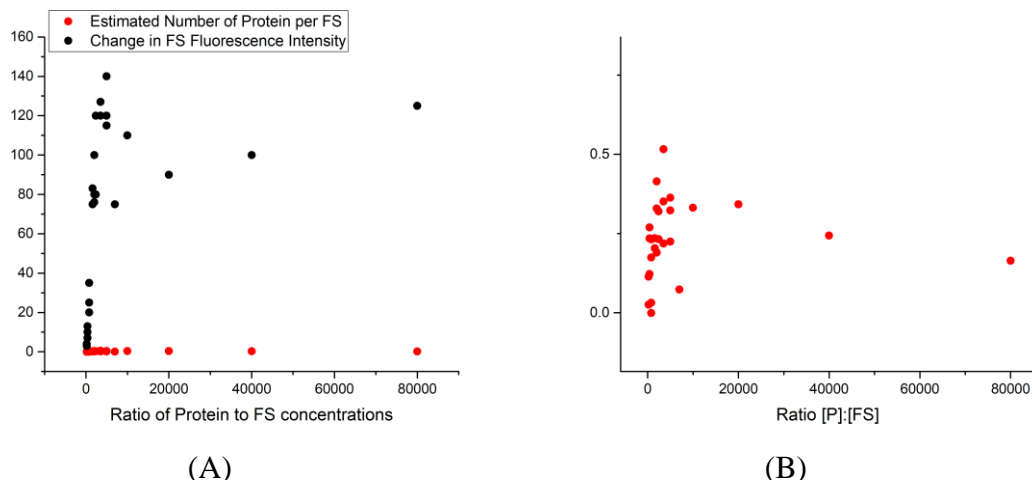


**Figure 4.13** (A) Normalized fluorescence intensity changes for the yellow-green-labeled FS<sub>200</sub> upon being mixed with red-labeled BSA (red circles) and pseudo-explicit binding ratio for this FS-BSA system (black circles). (B) shows a blow-up of the observed change in fluorescence intensity for the FS as the ratio of protein to FS increases. Interestingly, there appears to be a re-generation of fluorescence intensity after a ratio of approximately 10,000 : 1.

As the concentration of BSA increases and the FS<sub>200</sub> concentration is held constant at 1 nM, the normalized change in fluorescence intensity of the FS<sub>200</sub> increases, likely due to the increasing binding ratio of the BSA to the FS surface and energy transfer from the FS<sub>200</sub> to the BSA. However, after approximately a ratio of 10,000 BSA to 1 FS, the change in the FS<sub>200</sub> fluorescence intensity starts to become less than previously, although the estimated binding ratio continues to increase. This suggests that the change in fluorescence intensity for the FS<sub>200</sub> is not linearly related to the binding ratio of the BSA, and furthermore, that a change must be happening at the surface of the FS<sub>200</sub> for a re-generation of fluorescence intensity.

One explanation for the difference in fluorescence intensity observation between the two sizes of spheres could be that the distribution or ratio of fluorophores at the surface of the spheres could be different between the two sizes. Another explanation could be that

the proximity of the fluorophores at the surface is different between the two sizes as well. Both explanations would suggest that there is more than just a size difference between the 100 nm and 200 nm carboxy-terminated FS, which in turn, could affect the binding ratio of proteins to spheres and whether or not an energy transfer occurs as a result of binding.

#### **4.2.3 Unlabeled FS Experiments for Insight into Energy Transfer to Labeled**

##### **BSA**

A control experiment using unlabeled, 200 nm diameter, carboxy-coated polystyrene spheres was performed for insight into the possibility of energy transfer occurring between the FS<sub>200</sub> and red-labeled BSA in PBS. However, the unlabeled spheres tended to agglomerate upon being mixed with the BSA. Within minutes, the BSA noticeably precipitated out of the mixture. Mixtures of unlabeled spheres and BSA were also attempted in Millipore water and in a borate buffer, but unfortunately gave similar results to those tried in PBS. These experiments, although not entirely helpful with answering the initial question of energy transfer, provided insight into the composition of the spheres. These experiments indicated that although the unlabeled spheres were the same size and same apparent composition, they did not behave similarly to the fluorescently-labeled spheres. This could be due to the composition of the labeled and non-labeled spheres not being completely identical, or perhaps the labeling on the fluorescently-labeled sphere having some impact on solubility and stabilizing effects.

#### **4.3 Global Discussion**

##### **4.3.1 Dynamics of the BSA-FS Interactions**

According to literature sources, serum albumin proteins prefer to interact face-on as opposed to side- or end-on<sup>59</sup> with NPs, as was mentioned in Chapter 1 (Section 1.2.5).

Support for this was suggested from Figure 3.13 from the TEM images, which suggested that the BSA stack or clump to the surface of the FS by face-on interactions. These results further suggested that there must not be a uniform distribution of charge at the surfaces of the FS NPs. The BSA and FS NPs are likely interacting due to a combination of different forces; however, analysis of the  $K_A$  values from Section 4.2.1.2 indicated that perhaps hydrogen bonding could be occurring between these two entities.

Because of this face-on interaction of the BSA with the FS, changes in fluorescence intensities were could be explained, at least for the system composed of yellow-green-labeled FS<sub>200</sub> and red-labeled BSA. These changes in fluorescence are most likely indicative of an energy transfer that is occurring from the FS<sub>200</sub> to the BSA upon interaction of the BSA with the FS<sub>200</sub> surface. As previously described and shown in Figure 4.12, there was an observed consistent decrease in the fluorescence intensity for the FS<sub>200</sub> within each experiment as well as a change in BSA fluorescence that appeared to be concentration-dependent. Recall from Figure 4.13, the change in fluorescence intensity for the FS did not appear to be linearly related to the binding ratio of the BSA. Instead, after a downward trend in fluorescence with increasing BSA concentration, a subsequent increase in FS<sub>200</sub> fluorescence was observed at BSA:FS<sub>200</sub> ratios higher than 10,000. These results suggested that a change in protein environment at the FS<sub>200</sub> surface as a function of proteins bound. This could imply that the BSA may be unfolding or rearranging at the surface and altering energy transfer. This could explain the localization of BSA bound to FS<sub>200</sub> in the TEM images.

The stacking of BSA at the FS surface, as suggested by the TEM images, was not entirely anticipated. It was thought that the BSA would prefer and would be more

energetically-favorable (entropically) to spread out and bind to different binding sites around the FS surface. Recall from Chapter 3, it was of concern that the drying process for the TEM imaging was causing the BSA to appear as clumping at the surface. However, upon analysis of the Figure 4.13, the TEM image results may be supported by the fluorescence changes discussed in this chapter.

### **4.3.2 Binding affinity of the BSA-FS Interactions**

The average  $k_{on}$  value for the system composed of the green-labeled BSA interacting with the smaller, red-labeled FS<sub>100</sub> was found to be  $(7 \pm 0.7) \times 10^{-4} \text{ s}^{-1}$  using the  $G_x(0)$  data, which had the same order of magnitude as the  $k_{on}$  for the system of larger FS. The  $k_{on}$  values for the BSA-FS<sub>200</sub> system were determined to be:  $(1.6 \text{ to } 4.3 \pm 0.2) \times 10^{-4} \text{ s}^{-1}$ . Further comparing these two values shows that the  $k_{on}$  for the association of BSA to a smaller sphere is slightly faster than for the association with a larger sphere. A ratio of these  $k_{on}$  values was calculated and found to be approximately 3-4, which was not reflective of the ratio of the estimated binding ratios. This suggests that the difference in  $k_{on}$  values between the two FS NPs may not simply be related to the diffusion of the protein or to the surface area of the FS NPs. Instead, the difference in  $k_{on}$  values could be related to a difference in surface chemistries between the two differently-sized spheres, resulting in there being more “hot spots” for binding to take place on the smaller FS. Since the smaller spheres have less surface area, there may be a greater probability that the BSA would diffuse and collide more quickly into these “hot spots” for binding either an area on the sphere where the BSA would preferably interact.

The association constant,  $K_A$ , for each system was found by two methods – through the linearized Hill model and through the developed “sites bound” model. The  $K_A$  values

were found to be similar between the two systems ( $4.4 \pm 2.5 \times 10^5$  and  $6.3 \pm 3.5 \times 10^5$  for BSA interacting with FS<sub>100</sub> and FS<sub>200</sub>, respectively) by the linearized Hill model. Compared to the  $K_A$  values found using the “sites bound” method ( $1.7 \pm 0.25 \times 10^6$  and  $3.2 \pm 1 \times 10^6$  for BSA interacting with FS<sub>100</sub> and FS<sub>200</sub>, respectively), those determined through the linearized Hill model were an order of magnitude smaller. Although, the same trend in a slightly increased affinity of BSA for the larger FS<sub>200</sub> was suggested through both models. The “sites bound” model was developed in attempts to provide a more representative model to describe the binding between the BSA and FS; the model serves to provide a more explicit representation of the number of FS binding sites determined from experimental measurements. The difference in  $K_A$  values between the two models could suggest that the “sites bound” approach does, in fact, provide a more accurate measurement of the association constant – especially after comparison to a study performed on a similar system in literature, discussed in the next paragraphs. However, recall that upon analysis of the log-log plot (Figure 4.10), there appeared to be a dependency on the protein concentration, which could suggest that the values of  $K_A$  previously calculated were  $K_A'$  values instead (Equations 4.11 and 4.12). Reports in literature have not explicitly determined or whether their studies are measuring  $K_A$  or  $K_A'$  values, and we will compare the  $K_A'$  values to those reported in literature.

Comparison of the determined  $K_A$  values to reported values in literature was somewhat difficult as very few studies have performed in-depth kinetic analyses on this particular system of NPs with BSA nor on similar NPs with BSA or other proteins. Only two studies were found to provide  $K_A$  values for the association of BSA with carboxy-terminated polystyrene NPs.

The first study performed by Landfester *et al.* in 2011 determined the  $K_A$  for the interaction of BSA with 200 nm diameter carboxy-terminated polystyrene NPs under two different pH conditions.<sup>60</sup> The  $K_A$  was determined as  $(1.29 \pm 0.01) \times 10^6$  (under pH = 3) and as  $(2.97 \pm 0.13) \times 10^6$  (under pH = 6). Landfester *et al.* determined these values using isothermal titration calorimetry with the intent on analyzing the change in interactions between the BSA and NPs above and below the isoelectric point of the BSA, since the structure, size, and conformation of BSA is said to be different with pH.<sup>60, 106</sup> At pH = 3, the BSA protein will be protonated, while at pH = 6, the BSA will be slightly deprotonated. Landfester *et al.* did not directly discuss the difference in  $K_A$  values between the two pH conditions tested. Rather, their discussion focused on their calculation of the number of BSA proteins interacting with a single NP under each pH condition. Based on their calculation, Landfester *et al.* observed an increased number of BSA ( $1,210.4 \pm 0.5$ ) interacting with the NPs under pH = 3 as compared to under pH = 6 ( $616.4 \pm 11.0$ ). They attributed the increased interaction under the more acidic conditions, of which they also claimed was the stronger interaction, to the positive charges of the BSA being attracted to the anionic NP surface. Although, under the more acidic conditions, the carboxy-terminated functionalities of the NPs would be protonated as well, and this does not entirely support Landfester *et al.* explanation and statement that the ionic interactions may influence the coverage of the surface with BSA.

The values for  $K_A$  determined using the “sites bound” approach in this thesis study for the interaction of BSA with FS<sub>200</sub> compared best to those determined by Landfester *et al.*, as they were of the same order of magnitude. Aside from the technique chosen by the authors, the pH conditions and the type of buffer used for both studies were different from

those employed in this thesis study and could be reasons for the slight discrepancy in reported  $K_A$  values. Interestingly, the ratios of BSA to NP tested using the ITC technique were lower than the ratios used in this thesis study but could possibly fall on the lower end of the plot in Figure 4.8 (B), had we been able to reach such low concentrations. However, according to the estimated binding ratios calculated by the pseudo-explicit model discussed in Chapter 3 (Section 3.2.3), the results suggest that very little, if any, binding of BSA to the NP surface would occur under the conditions of the PBS buffer employed in this thesis study. Landfester *et al.* did not clearly state the buffer or solution they used for the ITC measurements, but since their control experiments were performed in water, it is believed that water was medium employed in their studies. This difference in medium, along with the different pH values tested, are most likely the reasons behind the slight differences in  $K_A$  values.

The second study, performed by Fleisher and Payne, determined the  $K_A$  for the association of BSA with a 60 nm diameter carboxy-terminated polystyrene NP using two different techniques.<sup>57</sup> Fleisher and Payne employed the techniques of ITC and fluorescence spectroscopy by monitoring the quenching of tryptophan on the BSA proteins. The  $K_A$  for the association of BSA to the carboxylate-modified NPs using ITC was determined to be  $(2.4 \pm 0.9) \times 10^5 \text{ M}^{-1}$ . Employing fluorescence spectroscopy and monitoring the quenching of tryptophan residues of the BSA as the NP concentration was increased gave a  $K_A$  value of  $(1.8 \pm 0.1) \times 10^9 \text{ M}^{-1}$ . Directly comparing these two values for  $K_A$  shows that they are off by a several orders of magnitude. Fleisher and Payne recognized this, and attributed part of the discrepancy to the buffers employed in both techniques not being identical. (A 20 mM HEPES buffer [pH = 7.4] was employed for the

ITC measurements and a 10% v/v PBS buffer without calcium and magnesium was employed for the fluorescence quenching measurements.) Fleisher and Payne emphasized in their publication that thermodynamic parameters (from ITC) are very sensitive to experimental conditions. Furthermore, they openly expressed their opinions on ITC providing better quantitative measurements of the association constant, as it is a direct and label-free measurement; but, they admit the importance of using multiple techniques to confirm the thermodynamic parameters. Based on results obtained and compared across literature, there is high variability in the determined equilibrium binding constants, of which Fleisher and Payne stated could be due to the fluorescence quenching method itself, or that the binding strength is very sensitive to the type, size, and surface modification of the NP under study.

In comparison to the results obtained in this thesis study, the  $K_A$  determined by the linearized Hill model for both systems of FS and BSA studied was found to compare best with the  $K_A$  determined by ITC from Fleisher and Payne's study. Not only were the techniques used to access the  $K_A$  different, but the NPs being compared were of largely different diameters, and the experiments were performed using different buffers. Fleisher and Payne seemed to highly emphasize the reliability of measurements performed using ITC in their publication. They further stated the technique of FCS could only be used to measure the hydrodynamic diameter of NPs with and without a protein corona – which is not entirely true. One major issue with ITC is the assumption that the measured change in heat given off or taken in is a result of protein-NP interactions, as opposed to protein-protein interactions or NP-NP interactions. Furthermore, the ratios of BSA to NPs used for the ITC measurements were so much higher (up to  $4.5 \times 10^6$ ) than the ratios employed in

this thesis study. It was found in this thesis study that above a concentration of 5  $\mu\text{M}$  BSA that agglomeration of the BSA would occur and made it too difficult to draw any reasonable conclusions. Therefore, it is interesting that Fleisher and Payne worked with such high concentration ratios, and perhaps instead they were observing more protein-protein interactions than they originally thought. Aside from this however, the magnitudes of the  $K_A$  values determined by the linearized Hill model in this thesis study were best comparable to the  $K_A$  values determined using their ITC method, although the NPs employed in Fleisher and Payne's study were much smaller than the NPs used in this thesis study.

Unfortunately, there have not been any reports specifically discussing determined  $k_{\text{off}}$  values for the interaction between BSA and FS or carboxy-terminated polystyrene NPs. However, it is important to recognize the magnitude of the  $k_{\text{off}}$  value to analyze the strength of the interaction between the protein and NP – in this case, between BSA and FS. The  $k_{\text{off}}$  was estimated in two ways, based on the values of  $K_A$  determined from the linearized Hill model and “sites bound” approach. The  $k_{\text{off}}$  values were found to be, by the linearized Hill  $(1.6 \pm 0.9) \times 10^{-9} \text{ s}^{-1}$  and  $(2.5 \pm 1.4 \text{ to } 6.8 \pm 3.8) \times 10^{-10} \text{ s}^{-1}$ , and by the “sites bound” approach to be  $(4.1 \pm 0.7) \times 10^{-10} \text{ s}^{-1}$  and  $(5 \pm 1.7) \times 10^{-11}$  to  $(1.3 \pm 0.4) \times 10^{-10} \text{ s}^{-1}$  for BSA interacting with FS<sub>100</sub> and FS<sub>200</sub>, respectively, in both cases. These values of  $k_{\text{off}}$  are quite low, implying that the backwards reaction of the dissociation of BSA from either FS surface is slow, or even negligible. Furthermore, a very low  $k_{\text{off}}$  is indicative of the great stability of the BSA-FS interaction and of the formation of the “hard” corona.

#### **4.4 Conclusions**

In the studies described in this chapter, the kinetics of the interactions between BSA and two differently sized polystyrene FS were investigated using TPE-FCCS. For both

systems under study,  $k_{on}$ ,  $k_{off}$ , and  $K_A$  values were determined. The  $k_{on}$  value was determined in two ways – by use of the  $G_x(0)$  for both systems and use of the  $G_p(0)$  data (for the system comprised of BSA interacting with FS<sub>200</sub>). However, it was determined that the results using the  $G_x(0)$  were most reliable for determination of the  $k_{on}$ . The  $k_{on}$  value was found to be  $(7 \pm 0.7) \times 10^{-4} \text{ s}^{-1}$  for the system composed of green-labeled BSA and red-labeled FS<sub>100</sub>. The  $k_{on}$  values for the BSA-FS<sub>200</sub> system were determined to be  $(1.6 \text{ to } 4.3 \pm 0.2) \times 10^{-4} \text{ s}^{-1}$ .

Two models were used to find values for  $K_A$  – the linearized Hill model and an approach we developed called the “sites bound” approach. The values were found to be slightly different between the two models, perhaps because of the Hill model being overly simplistic, or that the “sites bound” model generated more representative values because of explicit consideration of the receptor sites on the FS. By the linearized Hill model, the  $K_A$  values were found to be  $(4.4 \pm 2.5) \times 10^5$  and  $(6.3 \pm 3.5) \times 10^5$  for BSA interacting with FS<sub>100</sub> and FS<sub>200</sub>, respectively. Using the “sites bound” method, the  $K_A$  values were determined to be  $(1.7 \pm 0.25) \times 10^6$  and  $(3.2 \pm 1) \times 10^6$  for BSA interacting with FS<sub>100</sub> and FS<sub>200</sub>, respectively. For the BSA-FS<sub>200</sub> system, there appeared to be a dependency of protein concentration on the  $K_A$  values, which lead us to believe that we were measuring  $K_A'$  values instead. However, we compared these  $K_A$  and  $K_A'$  values with those from two other similar studies; the  $K_A$  values from the linearized Hill were similar to those reported in one study, while those from the “sites bound” approach were similar to the  $K_A$  values in the other study. Interestingly, there have not been many reports on in-depth kinetic analyses for the interactions of BSA with FS. This demonstrates the need to start exploring more

kinetics analyses to better understand the rate and details of the interactions between proteins and NPs.

Values for  $k_{\text{off}}$  were also determined, based on these two models for  $K_A$ . The  $k_{\text{off}}$  values were found to be, by the linearized Hill be  $(1.6 \pm 0.9) \times 10^{-9} \text{ s}^{-1}$  and  $(2.5 \pm 1.4 \text{ to } 6.8 \pm 3.8) \times 10^{-10} \text{ s}^{-1}$  for BSA interacting with FS<sub>100</sub> and FS<sub>200</sub>, respectively. By the “sites bound” approach, the  $k_{\text{off}}$  values were found to be  $(4.1 \pm 0.7) \times 10^{-10} \text{ s}^{-1}$  and  $(5 \pm 1.7) \times 10^{-11}$  to  $(1.3 \pm 0.4) \times 10^{-10} \text{ s}^{-1}$  for the BSA-FS<sub>100</sub> and BSA-FS<sub>200</sub> systems, respectively. These values for  $k_{\text{off}}$  suggested that the interaction between the BSA and both FS NPs was strong and essentially irreversible.

The kinetics for the binding of BSA to the surface of an FS<sub>100</sub> were found to best follow first order kinetics, with the binding of the first BSA protein likely being the rate-determining step. However, for the kinetics of association were thought to best follow pseudo-first order for the binding of BSA to FS<sub>200</sub>, with the rate-limiting step likely being the stacking of BSA onto a surface-bound BSA protein.

The changes in fluorescence intensity for the yellow-green FS<sub>200</sub> suggested insight on the association of subsequent BSA at the surface of the FS and further suggested support for the stacking of BSA at the surface of the FS<sub>100</sub>, as observed in the TEM images from Chapter 3. These results also question the idea of the protein corona monolayer that is said to form when an NP is introduced into a solution of proteins or biological medium, which could make kinetics analyses even more difficult. Lastly, this study highlights the power of the FCS and FCCS technique to study the kinetics of the interactions between NPs and proteins, which should be considered in future studies designed for biomedical applications.

## CHAPTER FIVE: CONCLUSIONS AND GLOBAL PERSPECTIVE

### 5.1 General Findings

The studies in this thesis examined the interactions between fluorescent polystyrene nanoparticles, called FluoSpheres (FS), of two different sizes, with bovine serum albumin proteins (BSA). Contrary to the current scientific notion of the “protein corona,” the binding ratio of BSA to FS<sub>100</sub> or to FS<sub>200</sub> was found to be quite low. The binding ratio was estimated through two derived approaches, namely the “simplified” and “pseudo-explicit” models used to gain insight from the binding data. The main difference between these two models was that the “pseudo-explicit” method did not use the simplifying assumption that  $\eta^2 N_{\text{protein}}$  was approximately equal to  $\eta N_{\text{protein}}$  for BSA adsorbing onto the surface of a FS. It was deemed that the pseudo-explicit model therefore provided a more representative estimate of the binding ratio between BSA and FS<sub>100</sub> or FS<sub>200</sub>. A maximum binding ratio of approximately 8-10 BSA per FS<sub>100</sub> and 130 BSA per FS<sub>200</sub> was estimated by the pseudo-explicit model, which was much lower than the perceived formation of a protein corona monolayer at the surfaces of NPs. Additionally, TEM images acquired of BSA interacting with FS<sub>100</sub> suggested that not only do the proteins interact with the FS surface, but a stacking of BSA proteins on top of those already adsorbed appears to also occur.

Kinetically, the two systems appeared to follow slightly different kinetics of association. The system composed of BSA interacting with FS<sub>100</sub> appeared to follow first order kinetics, as the determined on-rate constant ( $k_{\text{on}}$ ) did not show a linear dependence on protein or FS concentration across all tested concentration ratios. However, the system composed of BSA interacting with FS<sub>200</sub> appeared to follow pseudo first order kinetics in a possible two-step process. This was determined through analysis of the plots of the

perceived exponential loss in protein concentration over time, and through a linear log-log plot of the  $K_A$  and free protein concentration. Both analyses suggested that the overall reaction to describe protein binding to FS<sub>200</sub> had a square dependence on the protein concentration. In terms of the mechanism of the interaction, it was found that two possible processes contributed to the overall binding of BSA to FS: a binding process and a stacking process. The binding process was thought to involve the association of BSA to the surface of an FS, while the stacking process was thought to involve the stacking of a BSA on top of another BSA protein, already bound to the FS surface. Through analysis of the  $k_{on}$  values determined from the  $G_x(0)$  and from the  $G_p(0)$  for the BSA-FS<sub>200</sub> system, it was observed that  $k_{on-cross} < k_{on-auto}$  up to BSA concentrations of 5000 nM. At higher ratios, however, these two  $k_{on}$  values appeared to converge. Therefore, there appeared to be not only a sphere-dependency, but also a FS size-dependency on the binding and binding mechanism between the FS<sub>100</sub> and FS<sub>200</sub>. This was thought to perhaps be because we could not access low enough BSA to FS<sub>100</sub> ratios to observe the difference in  $k_{on}$  values, because we were already measuring at the convergence. Or, perhaps the BSA does interact slightly differently with the two sizes of FS because the surfaces appear slightly different in terms of the surface chemistry and/or curvature.

The results described in this thesis are significant as they challenge the current scientific understanding of the perceived formation of the protein corona. The results in this thesis also indicate the need for more kinetics analyses to better understand the early stages of hard corona formation, as well as the need for use of more direct, quantitative techniques over more qualitative techniques for better estimations of the binding ratios.<sup>107</sup>

These studies should be considered in the future, so that NPs can be used for their fullest potential in biomedical applications.

## **5.2 Future Studies**

To gain further insight into the interactions between proteins and NPs, further tests involving different sizes of FS NPs should be performed to investigate the suggested size-dependency on the binding ratio. Further experiments could also employ different proteins, such as globulins, to analyze for differences in protein interaction with FS NPs. Competition experiments between two different proteins with FS NPs could be performed to understand more deeply differences in protein binding affinities and assembly kinetics, as well as if different receptors exist on the FS for different proteins. Our group's three-colour FCCS instrument is designed to study the association kinetics of multiple differently labeled proteins and NPs and could be used to track complex formation in real-time.<sup>92,108,109</sup>

As previously discussed in Chapter 1, various factors can influence the binding and binding ratio of proteins to NPs, with two specific examples being the ionic strength of the medium and the temperature. At high ionic strength, the hydrophobic patches on the BSA and FS could be more exposed, and if the binding is not driven by hydrophobic interactions, then low binding ratios could be observed. As the estimated binding ratios were low for the BSA-FS systems described in this thesis, decreasing the ionic strength could result in an increase in the binding ratio. For the studies performed in this thesis, a 10X PBS solution was used for all tested mixtures of proteins and FS NPs. Further studies could employ a PBS solution of lesser ionic strength to analyze for the effect of the ionic strength on the binding ratio between BSA and FS NPs. Another factor that could be further investigated would be the effect of temperature on the BSA-FS binding, as the effect of temperature has

not been deeply investigated in literature thus far, and temperature varies *in-vivo*.<sup>43</sup> It would be of interest and relevance to investigate the BSA-FS binding at normal human body temperature (37 °C), as the experiments performed in this thesis were all conducted at room temperature. Moreover, measuring the  $k_{on}$  as a function of temperature will give insight into the activation energy barrier to binding. Analyzing the thermodynamic and kinetics dependence of the BSA-FS interactions with ionic strength and temperature would further broaden our understanding of the mechanism of interaction and how to best exploit the NP properties.

Also, as discussed in Chapter 1, many studies aimed at understanding protein-NP interactions separate the protein-NP complexes from excess protein and/or NPs in attempts to show protein corona formation. Although this separation raises issues such as shifting the protein-NP equilibrium, it could be of interest to employ a gel electrophoresis of the equilibrated BSA-FS mixtures tested in this thesis. Gel-electrophoresis of the entire mixture, although potentially complex, may not disrupt the equilibrium and could provide qualitative support for the estimated binding ratios, especially for those estimated for the BSA-FS<sub>200</sub> system.

Once the interactions between BSA and FS are more deeply understood *in vitro*, *in vivo* experiments could be performed to analyze the formation of protein-NP complexes.<sup>110-</sup><sup>112</sup> Our group has successfully used the chicken embryo model to study NP deposition in blood vessels *in vivo*<sup>111</sup>, and furthermore, the chicken embryo chorioallantoic membrane has proven to be a good mimic model of angiogenic blood vessels of cancerous tissues. Experiments subjecting bare and protein-coated FS NPs *in vivo* could be performed to yield deeper insight into the potential and efficacy of using NPs for biomedical applications.

## References

1. Walkey, C. D.; Chan, W. C. W., Understanding and controlling the interaction of nanomaterials with proteins in a physiological environment. *Chemical Society Reviews* **2012**, *41* (7), 2780-2799.
2. Mahmoudi, M.; Lynch, I.; Ejtehadi, M. R.; Monopoli, M. P.; Bombelli, F. B.; Laurent, S., Protein-Nanoparticle Interactions: Opportunities and Challenges. *Chemical Reviews* **2011**, *111* (9), 5610-5637.
3. Lynch, I.; Dawson, K. A., Protein-nanoparticle interactions. *Nano Today* **2008**, *3* (1-2), 40-47.
4. Lundqvist, M.; Stigler, J.; Cedervall, T.; Berggard, T.; Flanagan, M. B.; Lynch, I.; Elia, G.; Dawson, K., The Evolution of the Protein Corona around Nanoparticles: A Test Study. *Acs Nano* **2011**, *5* (9), 7503-7509.
5. Walczyk, D.; Bombelli, F. B.; Monopoli, M. P.; Lynch, I.; Dawson, K. A., What the Cell "Sees" in Bionanoscience. *Journal of the American Chemical Society* **2010**, *132* (16), 5761-5768.
6. Tenzer, S.; Docter, D.; Kuharev, J.; Musyanovych, A.; Fetz, V.; Hecht, R.; Schlenk, F.; Fischer, D.; Kiouptsi, K.; Reinhardt, C.; Landfester, K.; Schild, H.; Maskos, M.; Knauer, S. K.; Stauber, R. H., Rapid formation of plasma protein corona critically affects nanoparticle pathophysiology. *Nature Nanotechnology* **2013**, *8* (10), 772-U1000.
7. Capjak, I.; Goreta, S. S.; Jurasin, D. D.; Vrcek, I. V., How protein coronas determine the fate of engineered nanoparticles in biological environment. *Arhiv Za Higijenu Rada I Toksikologiju-Archives of Industrial Hygiene and Toxicology* **2017**, *68* (4), 245-253.
8. Del Pino, P.; Pelaz, B.; Zhang, Q.; Maffre, P.; Nienhaus, G. U.; Parak, W. J., Protein corona formation around nanoparticles - from the past to the future. *Materials Horizons* **2014**, *1* (3), 301-313.
9. Schwille, P., Fluorescence correlation spectroscopy and its potential for intracellular applications. *Cell Biochemistry and Biophysics* **2001**, *34* (3), 383-408.
10. Haustein, E.; Schwille, P., Fluorescence correlation spectroscopy: Novel variations of an established technique. *Annual Review of Biophysics and Biomolecular Structure* **2007**, *36*, 151-169.

11. Feliu, N.; Docter, D.; Heine, M.; del Pino, P.; Ashraf, S.; Kolosnjaj-Tabi, J.; Macchiarini, P.; Nielsen, P.; Alloyeau, D.; Gazeau, F.; Stauber, R. H.; Parak, W. J., In vivo degeneration and the fate of inorganic nanoparticles. *Chemical Society Reviews* **2016**, *45* (9), 2440-2457.
12. Nairi, V.; Medda, S.; Piludu, M.; Casula, M. F.; Vallet-Regi, M.; Monduzzi, M.; Salis, A., Interactions between bovine serum albumin and mesoporous silica nanoparticles functionalized with biopolymers. *Chemical Engineering Journal* **2018**, *340*, 42-50.
13. Hadjidemetriou, M.; Kostarelos, K., NANOMEDICINE Evolution of the nanoparticle corona. *Nature Nanotechnology* **2017**, *12* (4), 288-290.
14. Docter, D.; Westmeier, D.; Markiewicz, M.; Stolte, S.; Knauer, S. K.; Stauber, R. H., The nanoparticle biomolecule corona: lessons learned - challenge accepted? *Chemical Society Reviews* **2015**, *44* (17), 6094-6121.
15. Pulido-Reyes, G.; Leganes, F.; Fernandez-Pinas, F.; Rosal, R., Bio-nano interface and environment: A critical review. *Environmental Toxicology and Chemistry* **2017**, *36* (12), 3181-3193.
16. Barbero, F.; Russo, L.; Vitali, M.; Piella, J.; Salvo, I.; Borrajo, M. L.; Busquets-Fite, M.; Grandori, R.; Bastus, N. G.; Casals, E.; Puentes, V., Formation of the Protein Corona: The Interface between Nanoparticles and the Immune System. *Seminars in Immunology* **2017**, *34* (C), 52-60.
17. Bagchi, P.; Birnbaum, S. M., EFFECT OF PH ON THE ADSORPTION OF IMMUNOGLOBULIN-G ON ANIONIC POLY(VINYLTOLUENE) MODEL LATEX-PARTICLES. *Journal of Colloid and Interface Science* **1981**, *83* (2), 460-478.
18. Muller, R. H.; Ruhl, D.; Luck, M.; Paulke, B. R., Influence of fluorescent labelling of polystyrene particles on phagocytic uptake, surface hydrophobicity, and plasma protein adsorption. *Pharmaceutical Research* **1997**, *14* (1), 18-24.
19. Gessner, A.; Waicz, R.; Lieske, A.; Paulke, B. R.; Mader, K.; Muller, R. H., Nanoparticles with decreasing surface hydrophobicities: influence on plasma protein adsorption. *International Journal of Pharmaceutics* **2000**, *196* (2), 245-249.
20. Monopoli, M. P.; Walczyk, D.; Campbell, A.; Elia, G.; Lynch, I.; Bombelli, F. B.; Dawson, K. A., Physical-Chemical Aspects of Protein Corona: Relevance to in Vitro and

in Vivo Biological Impacts of Nanoparticles. *Journal of the American Chemical Society* **2011**, *133* (8), 2525-2534.

21. Gessner, A.; Lieske, A.; Paulke, B. R.; Muller, R. H., Influence of surface charge density on protein adsorption on polymeric nanoparticles: analysis by two-dimensional electrophoresis. *European Journal of Pharmaceutics and Biopharmaceutics* **2002**, *54* (2), 165-170.

22. Luck, M.; Paulke, B. R.; Schroder, W.; Blunk, T.; Muller, R. H., Analysis of plasma protein adsorption on polymeric nanoparticles with different surface characteristics. *Journal of Biomedical Materials Research* **1998**, *39* (3), 478-485.

23. Li, W.; Liu, T. T.; Li, Z. L.; Wang, Y., Study of the Interaction between a Water-soluble Cationic Fluorescent Conjugated Polymer and Bovine Serum Albumin. *Journal of Solution Chemistry* **2012**, *41* (11), 2009-2016.

24. Satzer, P.; Svec, F.; Sekot, G.; Jungbauer, A., Protein adsorption onto nanoparticles induces conformational changes: Particle size dependency, kinetics, and mechanisms. *Engineering in Life Sciences* **2016**, *16* (3), 238-246.

25. Ross, P. D.; Subramanian, S., THERMODYNAMICS OF PROTEIN ASSOCIATION REACTIONS - FORCES CONTRIBUTING TO STABILITY. *Biochemistry* **1981**, *20* (11), 3096-3102.

26. Mariam, J.; Sivakami, S.; Dongre, P. M., Elucidation of structural and functional properties of albumin bound to gold nanoparticles. *Journal of Biomolecular Structure & Dynamics* **2017**, *35* (2), 368-379.

27. Gessner, A.; Lieske, A.; Paulke, B. R.; Muller, R. H., Functional groups on polystyrene model nanoparticles: Influence on protein adsorption. *Journal of Biomedical Materials Research Part A* **2003**, *65A* (3), 319-326.

28. Kokkinopoulou, M.; Simon, J.; Landfester, K.; Mailander, V.; Lieberwirth, I., Visualization of the protein corona: towards a biomolecular understanding of nanoparticle-cell- interactions. *Nanoscale* **2017**, *9* (25), 8858-8870.

29. Lundqvist, M.; Stigler, J.; Elia, G.; Lynch, I.; Cedervall, T.; Dawson, K. A., Nanoparticle size and surface properties determine the protein corona with possible implications for biological impacts. *Proceedings of the National Academy of Sciences of the United States of America* **2008**, *105* (38), 14265-14270.

30. Lundqvist, M.; Augustsson, C.; Lilja, M.; Lundkvist, K.; Dahlback, B.; Linse, S.; Cedervall, T., The nanoparticle protein corona formed in human blood or human blood fractions. *Plos One* **2017**, *12* (4).
31. Lindman, S.; Lynch, I.; Thulin, E.; Nilsson, H.; Dawson, K. A.; Linse, S., Systematic investigation of the thermodynamics of HSA adsorption to N-iso-propylacrylamide/N-tert-butylacrylamide copolymer nanoparticles. Effects of particle size and hydrophobicity. *Nano Letters* **2007**, *7* (4), 914-920.
32. Aggarwal, P.; Hall, J. B.; McLeland, C. B.; Dobrovolskaia, M. A.; McNeil, S. E., Nanoparticle interaction with plasma proteins as it relates to particle biodistribution, biocompatibility and therapeutic efficacy. *Advanced Drug Delivery Reviews* **2009**, *61* (6), 428-437.
33. Sanchez-Perez, J. A.; Gallardo-Moreno, A. M.; Gonzalez-Martin, M. L.; Vadiillo-Rodriguez, V., BSA adsorption onto nanospheres: Influence of surface curvature as probed by electrophoretic light scattering and UV/vis spectroscopy. *Applied Surface Science* **2015**, *353*, 1095-1102.
34. Li, J. C.; Mao, H. L.; Kawazoe, N.; Chen, G. P., Insight into the interactions between nanoparticles and cells. *Biomaterials Science* **2017**, *5* (2), 173-189.
35. Wang, X. Y.; Wang, X. F.; Wang, M. Z.; Zhang, D.; Yang, Q.; Liu, T.; Lei, R.; Zhu, S. F.; Zhao, Y. L.; Chen, C. Y., Probing Adsorption Behaviors of BSA onto Chiral Surfaces of Nanoparticles. *Small* **2018**, *14* (16).
36. Vaishnav, S. K.; Chandraker, K.; Korram, J.; Nagwanshi, R.; Ghosh, K. K.; Satnami, M. L., Protein nanoparticle interaction: A spectrophotometric approach for adsorption kinetics and binding studies. *Journal of Molecular Structure* **2016**, *1117*, 300-310.
37. Peula, J. M.; Delasnives, F. J., ADSORPTION OF MONOMERIC BOVINE SERUM-ALBUMIN ON SULFONATED POLYSTYRENE MODEL COLLOIDS .1. ADSORPTION-ISOTHERMS AND EFFECT OF THE SURFACE-CHARGE DENSITY. *Colloids and Surfaces a-Physicochemical and Engineering Aspects* **1993**, *77* (3), 199-208.
38. Xu, Z. Z.; Grassian, V. H., Bovine Serum Albumin Adsorption on TiO<sub>2</sub> Nanoparticle Surfaces: Effects of pH and Coadsorption of Phosphate on Protein-Surface Interactions and Protein Structure. *Journal of Physical Chemistry C* **2017**, *121* (39), 21763-21771.

39. Shang, L.; Wang, Y. Z.; Jiang, J. G.; Dong, S. J., pH-dependent protein conformational changes in albumin : gold nanoparticle bioconjugates: A spectroscopic study. *Langmuir* **2007**, *23* (5), 2714-2721.
40. Morrissey, B. W.; Han, C. C., CONFORMATION OF GAMMA-GLOBULIN ADSORBED ON POLYSTYRENE LATTICES DETERMINED BY QUASI-ELASTIC LIGHT-SCATTERING. *Journal of Colloid and Interface Science* **1978**, *65* (3), 423-431.
41. Shan, J. M.; Kim, C.; Zhang, Z. F.; Wang, L. S.; Sun, T., Adsorption of BSA on Carbon-coated Fe<sub>3</sub>O<sub>4</sub> Microspheres Activated with 1-ethyl-3-(3-dimethylaminopropyl)-Carbodiimide Hydrochloride. *Journal of Wuhan University of Technology-Materials Science Edition* **2018**, *33* (1), 1-8.
42. Ledesma, A. E.; Chemes, D. M.; Frias, M. D.; Torres, M. D. G., Spectroscopic characterization and docking studies of ZnO nanoparticle modified with BSA. *Applied Surface Science* **2017**, *412*, 177-188.
43. Mahmoudi, M.; Abdelmonem, A. M.; Behzadi, S.; Clement, J. H.; Dutz, S.; Ejtehadi, M. R.; Hartmann, R.; Kantner, K.; Linne, U.; Maffre, P.; Metzler, S.; Moghadam, M. K.; Pfeiffer, C.; Rezaei, M.; Ruiz-Lozano, P.; Serpooshan, V.; Shokrgozar, M. A.; Nienhaus, G. U.; Parak, W. J., Temperature: The "Ignored" Factor at the NanoBio Interface. *Acs Nano* **2013**, *7* (8), 6555-6562.
44. Bhunia, A. K.; Kamilya, T.; Saha, S., Temperature Dependent and Kinetic Study of the Adsorption of Bovine Serum Albumin to ZnO Nanoparticle Surfaces. *Chemistryselect* **2016**, *1* (11), 2872-2882.
45. Wu, X.; Narsimhan, G., Characterization of secondary and tertiary conformational changes of beta-lactoglobulin adsorbed on silica nanoparticle surfaces. *Langmuir* **2008**, *24* (9), 4989-4998.
46. Fenoglio, I.; Fubini, B.; Ghibaudi, E. M.; Turci, F., Multiple aspects of the interaction of biomacromolecules with inorganic surfaces. *Advanced Drug Delivery Reviews* **2011**, *63* (13), 1186-1209.
47. Duan, Y. K.; Liu, Y.; Shen, W.; Zhong, W. W., Fluorescamine Labeling for Assessment of Protein Conformational Change and Binding Affinity in Protein-Nanoparticle Interaction. *Analytical Chemistry* **2017**, *89* (22), 12160-12167.

48. Rial, R.; Tichnell, B.; Latimer, B.; Liu, Z.; Messina, P. V.; Ruso, J. M., Structural and Kinetic Visualization of the Protein Corona on Bioceramic Nanoparticles. *Langmuir* **2018**, *34* (7), 2471-2480.
49. Wu, X. Y.; Narsimhan, G., Effect of surface concentration on secondary and tertiary conformational changes of lysozyme adsorbed on silica nanoparticles. *Biochimica Et Biophysica Acta-Proteins and Proteomics* **2008**, *1784* (11), 1694-1701.
50. Vertegel, A. A.; Siegel, R. W.; Dordick, J. S., Silica nanoparticle size influences the structure and enzymatic activity of adsorbed lysozyme. *Langmuir* **2004**, *20* (16), 6800-6807.
51. Baral, A.; Satish, L.; Das, D. P.; Sahoo, H.; Ghosh, M. K., Construing the interactions between MnO<sub>2</sub> nanoparticle and bovine serum albumin: insight into the structure and stability of a protein-nanoparticle complex. *New Journal of Chemistry* **2017**, *41* (16), 8130-8139.
52. Norde, W.; Giacomelli, C. E., BSA structural changes during homomolecular exchange between the adsorbed and the dissolved states. *Journal of Biotechnology* **2000**, *79* (3), 259-268.
53. Serebrennikova, Y. M.; Roth, A.; Huffman, D. E.; Smith, J. M.; Lindon, J. N.; Garcia-Rubio, L. H., Multiwavelength Transmission Spectroscopy Revisited for the Characterization of the Protein and Polystyrene Nanoparticle Interactions. *Applied Spectroscopy* **2013**, *67* (1), 86-92.
54. Zeliszewska, P.; Wasilewska, M.; Adamczyk, Z., Monolayers of immunoglobulin G on polystyrene microparticles and their interactions with human serum albumin. *Journal of Colloid and Interface Science* **2017**, *490*, 587-597.
55. Milani, S.; Bombelli, F. B.; Pitek, A. S.; Dawson, K. A.; Radler, J., Reversible versus Irreversible Binding of Transferrin to Polystyrene Nanoparticles: Soft and Hard Corona. *Acs Nano* **2012**, *6* (3), 2532-2541.
56. Nattich-Rak, M.; Adamczyk, Z.; Wasilewska, M.; Sadowska, M., Revealing fibrinogen monolayer conformations at different pHs: Electrokinetic and colloid deposition studies. *Journal of Colloid and Interface Science* **2015**, *449*, 62-71.

57. Fleischer, C. C.; Payne, C. K., Secondary Structure of Corona Proteins Determines the Cell Surface Receptors Used by Nanoparticles. *Journal of Physical Chemistry B* **2014**, *118* (49), 14017-14026.
58. Maiolo, D.; Del Pino, P.; Metrangolo, P.; Parak, W. J.; Bombelli, F. B., Nanomedicine delivery: does protein corona route to the target or off road? *Nanomedicine* **2015**, *10* (21), 3231-3247.
59. Soderquist, M. E.; Walton, A. G., STRUCTURAL-CHANGES IN PROTEINS ADSORBED ON POLYMER SURFACES. *Journal of Colloid and Interface Science* **1980**, *75* (2), 386-397.
60. Baier, G.; Costa, C.; Zeller, A.; Baumann, D.; Sayer, C.; Araujo, P. H. H.; Mailander, V.; Musyanovych, A.; Landfester, K., BSA Adsorption on Differently Charged Polystyrene Nanoparticles using Isothermal Titration Calorimetry and the Influence on Cellular Uptake. *Macromolecular Bioscience* **2011**, *11* (5), 628-638.
61. Lee, S. G.; Ha, J. W., Synthesis of highly carboxylated monodisperse polystyrene microspheres by dispersion polymerization in fluorinated alcohol. *Macromolecular Research* **2016**, *24* (8), 675-683.
62. Romack, T. J.; Maury, E. E.; Desimone, J. M., PRECIPITATION POLYMERIZATION OF ACRYLIC-ACID IN SUPERCRITICAL CARBON-DIOXIDE. *Macromolecules* **1995**, *28* (4), 912-915.
63. Minami, H.; Kimura, A.; Kinoshita, K.; Okubo, M., Preparation of Poly(acrylic acid) Particles by Dispersion Polymerization In an Ionic Liquid. *Langmuir* **2010**, *26* (9), 6303-6307.
64. Thomas, J. B.; Creecy, C. M.; McGinity, J. W.; Peppas, N. A., Synthesis and properties of lightly crosslinked poly((meth)acrylic acid) microparticles prepared by free radical precipitation polymerization. *Polymer Bulletin* **2006**, *57* (1), 11-20.
65. Bunyakan, C.; Hunkeler, D., Precipitation polymerization of acrylic acid in toluene. I: synthesis, characterization and kinetics. *Polymer* **1999**, *40* (23), 6213-6224.
66. Ward, R. S.; Harrison, I.; Leader, R. U.; Williams, A. T., Fluorescent polystyrene microspheres as tracers of colloidal and particulate materials: Examples of their use and developments in analytical technique. *Tracer Hydrology* **1997**, *97*, 99-103.

67. Yaehne, K. Comparing Nanoparticle Physical Properties with Bio-uptake. University of Calgary, 2012.
68. rinzen, F. W.; Bassingthwaight, J. B., Blood flow distributions by microsphere deposition methods. *Cardiovascular Research* **2000**, *45* (1), 13-21.
69. Anetzberger, H.; Thein, E.; Maier, M.; Birkenmaier, C.; Messmer, K., Fluorescent microspheres are reliable for serial bone blood flow measurements. *Clinical Orthopaedics and Related Research* **2004**, (427), 241-248.
70. Carter, D. C.; Chang, B.; Ho, J. X.; Keeling, K.; Krishnasami, Z., PRELIMINARY CRYSTALLOGRAPHIC STUDIES OF 4 CRYSTAL FORMS OF SERUM-ALBUMIN. *European Journal of Biochemistry* **1994**, *226* (3), 1049-1052.
71. He, X. M.; Carter, D. C., ATOMIC-STRUCTURE AND CHEMISTRY OF HUMAN SERUM-ALBUMIN. *Nature* **1992**, *358* (6383), 209-215.
72. Carter, D. C.; Ho, J. X., STRUCTURE OF SERUM-ALBUMIN. *Advances in Protein Chemistry, Vol 45* **1994**, *45*, 153-203.
73. Kragghansen, U., MOLECULAR ASPECTS OF LIGAND-BINDING TO SERUM-ALBUMIN. *Pharmacological Reviews* **1981**, *33* (1), 17-53.
74. Naveenraj, S.; Anandan, S., Binding of serum albumins with bioactive substances - Nanoparticles to drugs. *Journal of Photochemistry and Photobiology C-Photochemistry Reviews* **2013**, *14*, 53-71.
75. Bourassa, P.; Hasni, I.; Tajmir-Riahi, H. A., Folic acid complexes with human and bovine serum albumins. *Food Chemistry* **2011**, *129* (3), 1148-1155.
76. Sugio, S.; Kashima, A.; Mochizuki, S.; Noda, M.; Kobayashi, K., Crystal structure of human serum albumin at 2.5 angstrom resolution. *Protein Engineering* **1999**, *12* (6), 439-446.
77. Huang, B. X.; Kim, H. Y.; Dass, C., Probing three-dimensional structure of bovine serum albumin by chemical cross-linking and mass spectrometry. *Journal of the American Society for Mass Spectrometry* **2004**, *15* (8), 1237-1247.
78. Cai, H. H.; Zhong, X.; Yang, P. H.; Wei, W.; Chen, J. N.; Cai, J. Y., Probing site-selective binding of rhodamine B to bovine serum albumin. *Colloids and Surfaces a-Physicochemical and Engineering Aspects* **2010**, *372* (1-3), 35-40.

79. Huhn, J.; Fedeli, C.; Zhang, Q.; Masood, A.; del Pino, P.; Khashab, N. M.; Papini, E.; Parak, W. J., Dissociation coefficients of protein adsorption to nanoparticles as quantitative metrics for description of the protein corona: A comparison of experimental techniques and methodological relevance. *International Journal of Biochemistry & Cell Biology* **2016**, *75*, 148-161.
80. Terava, J.; Hokkanen, E.; Pihlasalo, S., Nonspecific luminometric assay for monitoring protein adsorption efficiency and coverage on nanoparticles. *Nanoscale* **2017**, *9* (6), 2232-2239.
81. Bhattacharjee, S., DLS and zeta potential - What they are and what they are not? *Journal of Controlled Release* **2016**, *235*, 337-351.
82. Doane, T. L.; Chuang, C. H.; Hill, R. J.; Burda, C., Nanoparticle zeta-Potentials. *Accounts of Chemical Research* **2012**, *45* (3), 317-326.
83. Invitrogen, Molecular Probes Certificate of Analysis. Invitrogen: Thermofisher Scientific ( <https://www.thermofisher.com/order/catalog/product/F8811?SID=srch-hj-f8811>), 2015.
84. Masters, B. R.; So, P. T. C., Antecedents of two-photon excitation laser scanning microscopy. *Microscopy Research and Technique* **2004**, *63* (1), 3-11.
85. Pawlicki, M.; Collins, H. A.; Denning, R. G.; Anderson, H. L., Two-Photon Absorption and the Design of Two-Photon Dyes. *Angewandte Chemie-International Edition* **2009**, *48* (18), 3244-3266.
86. So, P. T. C.; Dong, C. Y.; Masters, B. R.; Berland, K. M., Two-photon excitation fluorescence microscopy. *Annual Review of Biomedical Engineering* **2000**, *2*, 399-429.
87. Oheim, M.; Michael, D. J.; Geisbauer, M.; Madsen, D.; Chow, R. H., Principles of two-photon excitation fluorescence microscopy and other nonlinear imaging approaches. *Advanced Drug Delivery Reviews* **2006**, *58* (7), 788-808.
88. Atkins, P.; Paula, J., *Physical Chemistry*. 7 edition ed.; W. H. Freeman and Company: New York, 2002.
89. Konig, K., Multiphoton microscopy in life sciences. *Journal of Microscopy* **2000**, *200*, 83-104.

90. Heinze, K. G.; Koltermann, A.; Schwille, P., Simultaneous Two-Photon Excitation of Distinct Labels for Dual-Color Fluorescence Crosscorrelation Analysis. *PNAS* **2000**, *97* (19), 10377-10382.
91. Haustein, E.; Schwille, P., Ultrasensitive investigations of biological systems by fluorescence correlation spectroscopy. *Methods* **2003**, *29* (2), 153-166.
92. Swift, J. L.; Heuff, R.; Cramb, D. T., A two-photon excitation fluorescence cross-correlation assay for a model ligand-receptor binding system using quantum dots. *Biophysical Journal* **2006**, *90* (4), 1396-1410.
93. Schwille, P.; Heinze, K. G., Two-photon fluorescence cross-correlation spectroscopy. *Chemphyschem* **2001**, *2* (5), 269-272.
94. Nguyen, T. T.; Swift, J. L.; Burger, M. C.; Cramb, D. T., Effects of Various Small-Molecule Anesthetics on Vesicle Fusion: A Study Using Two-Photon Fluorescence Cross-Correlation Spectroscopy. *Journal of Physical Chemistry B* **2009**, *113* (30), 10357-10366.
95. Chen, Y.; Muller, J. D.; Tetin, S. Y.; Tyner, J. D.; Gratton, E., Probing ligand protein binding equilibria with fluorescence fluctuation spectroscopy. *Biophysical Journal* **2000**, *79* (2), 1074-1084.
96. Chen, Y.; Muller, J. D.; Berland, K. M.; Gratton, E., Fluorescence fluctuation spectroscopy. *Methods-a Companion to Methods in Enzymology* **1999**, *19* (2), 234-252.
97. Swift, J. L.; Burger, M. C.; Massotte, D.; Dahms, T. E. S.; Cramb, D. T., Two-photon excitation fluorescence cross-correlation assay for ligand-receptor binding: Cell membrane nanopatches containing the human mu-opioid receptor. *Analytical Chemistry* **2007**, *79* (17), 6783-6791.
98. Schwille, P.; MeyerAlmes, F. J.; Rigler, R., Dual-color fluorescence cross-correlation spectroscopy for multicomponent diffusional analysis in solution. *Biophysical Journal* **1997**, *72* (4), 1878-1886.
99. Bacia, K.; Kim, S. A.; Schwille, P., Fluorescence cross-correlation spectroscopy in living cells. *Nature Methods* **2006**, *3* (2), 83-89.
100. Bacia, K.; Petrasek, Z.; Schwille, P., Correcting for Spectral Cross-Talk in Dual-Color Fluorescence Cross-Correlation Spectroscopy. *Chemphyschem* **2012**, *13* (5), 1221-1231.

101. Li, R. Investigation of the Interactions between Nanoparticles and Serum Proteins. University of Calgary, 2017.
102. Jiang, J. K.; Oberdorster, G.; Biswas, P., Characterization of size, surface charge, and agglomeration state of nanoparticle dispersions for toxicological studies. *Journal of Nanoparticle Research* **2009**, *11* (1), 77-89.
103. Booth, F., THEORY OF ELECTROKINETIC EFFECTS. *Nature* **1948**, *161* (4081), 83-86.
104. Rocker, C.; Potzl, M.; Zhang, F.; Parak, W. J.; Nienhaus, G. U., A quantitative fluorescence study of protein monolayer formation on colloidal nanoparticles. *Nature Nanotechnology* **2009**, *4* (9), 577-580.
105. Doorley, G. W.; Payne, C. K., Cellular binding of nanoparticles in the presence of serum proteins. *Chemical Communications* **2011**, *47* (1), 466-468.
106. Pollitt, M. J.; Buckton, G.; Brocchini, S.; Alpar, H. O., Calorimetric study of bovine serum albumin dilution and adsorption onto polystyrene particles. *International Journal of Pharmaceutics* **2005**, *298* (2), 333-338.
107. Forest, V.; Pourchez, J., The nanoparticle protein corona: The myth of average. *Nano Today* **2016**, *11* (6), 700-703.
108. Wobma, H. M.; Blades, M. L.; Grekova, E.; McGuire, D. L.; Chen, K.; Chan, W. C. W.; Cramb, D. T., The development of direct multicolour fluorescence cross-correlation spectroscopy: Towards a new tool for tracking complex biomolecular events in real-time. *Physical Chemistry Chemical Physics* **2012**, *14* (10), 3290-3294.
109. Blades, M. L.; Grekova, E.; Wobma, H. M.; Chen, K.; Chan, W. C. W.; Cramb, D. T., Three-Color Fluorescence Cross-Correlation Spectroscopy for Analyzing Complex Nanoparticle Mixtures. *Analytical Chemistry* **2012**, *84* (21), 9623-9631.
110. Caracciolo, G.; Farokhzad, O. C.; Mahmoudi, M., Biological Identity of Nanoparticles In Vivo: Clinical Implications of the Protein Corona. *Trends in Biotechnology* **2017**, *35* (3), 257-264.
111. Yaehne, K.; Tekrony, A.; Clancy, A.; Gregoriou, Y.; Walker, J.; Dean, K.; Nguyen, T.; Doiron, A.; Rinker, K.; Jiang, X. Y.; Childs, S.; Cramb, D., Nanoparticle Accumulation in Angiogenic Tissues: Towards Predictable Pharmacokinetics. *Small* **2013**, *9* (18), 3118-3127.

112. Garcia, K. P.; Zarschler, K.; Barbaro, L.; Barreto, J. A.; O'Malley, W.; Spiccia, L.; Stephan, H.; Graham, B., Zwitterionic-Coated "Stealth" Nanoparticles for Biomedical Applications: Recent Advances in Countering Biomolecular Corona Formation and Uptake by the Mononuclear Phagocyte System. *Small* **2014**, *10* (13), 2516-2529.

## Appendix A

Further examples of  $G_x(0)$  vs time fittings performed for various concentration ratios of BSA interacting with FS<sub>100</sub> or FS<sub>200</sub>.

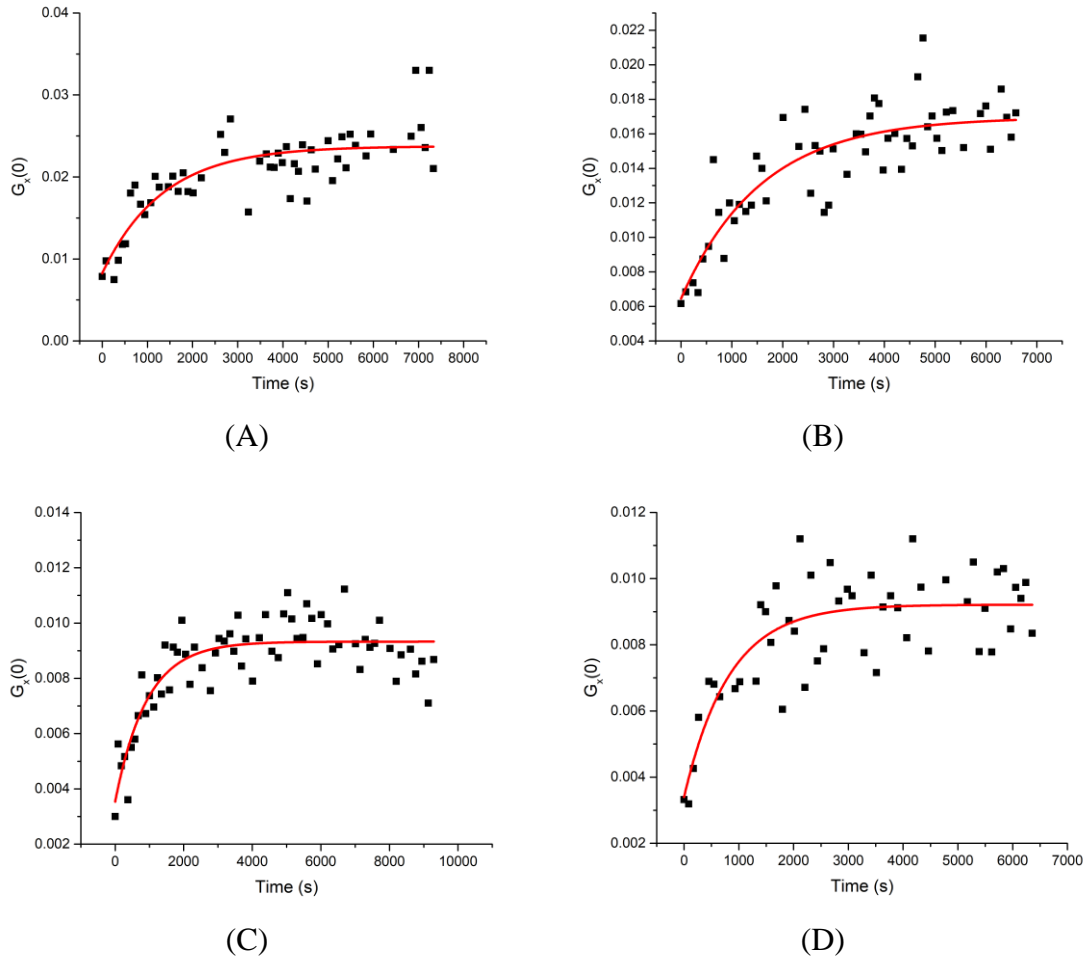
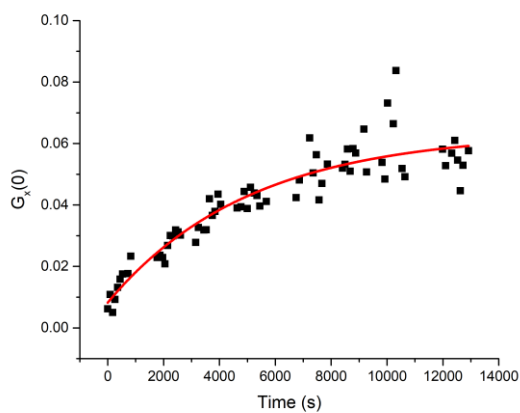
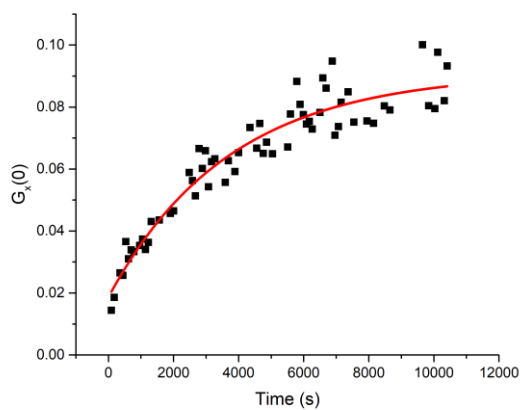


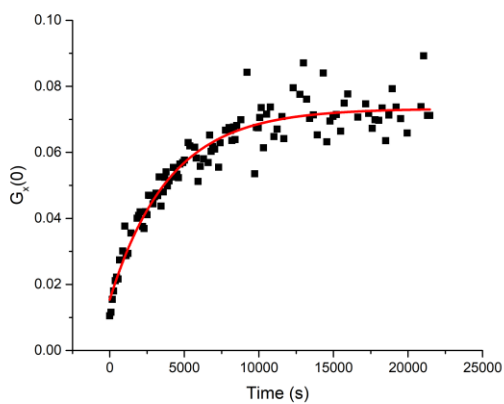
**Figure A1** Examples of various fittings of  $G_x(0)$  data as a function of time for mixtures of 1 nM red-labeled FS<sub>200</sub> with (A) 800 nM BSA, (B) 2400 nM BSA, (C) 3500 nM BSA, and (D) 5000 nM BSA. The line corresponds to the fitting with Equation 4.1.



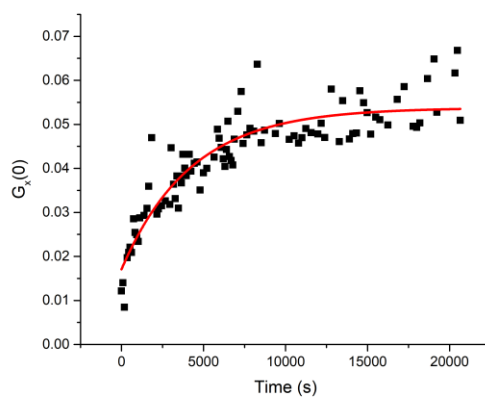
(A)



(B)



(C)



(D)

**Figure A2** Examples of various fittings of  $G_x(0)$  data as a function of time for mixtures of 1 nM yellow-green-labeled FS<sub>200</sub> with (A) 800 nM BSA, (B) 2000 nM BSA, (C) 3500 nM BSA, and (D) 5000 nM BSA. The red line corresponds to the fitting with Equation 4.1.

# Appendix B

## Copyright Permissions

Rightslink Printable License <https://s100.copyright.com/App/PrintableLicenseFrame.jsp?publisherID...>

**ELSEVIER LICENSE  
TERMS AND CONDITIONS**

Jun 29, 2018

---

This Agreement between Ms. Amanda Bishop ("You") and Elsevier ("Elsevier") consists of your license details and the terms and conditions provided by Elsevier and Copyright Clearance Center.

License Number	4378340856872
License date	Jun 29, 2018
Licensed Content Publisher	Elsevier
Licensed Content Publication	Colloids and Surfaces A: Physicochemical and Engineering Aspects
Licensed Content Title	Probing site-selective binding of rhodamine B to bovine serum albumin
Licensed Content Author	Huai-Hong Cai, Xing Zhong, Pei-Hui Yang, Wei Wei, Jianan Chen, Jiye Cai
Licensed Content Date	Dec 3, 2010
Licensed Content Volume	372
Licensed Content Issue	1-3
Licensed Content Pages	6
Start Page	35
End Page	40
Type of Use	reuse in a thesis/dissertation
Portion	figures/tables/illustrations
Number of figures/tables/illustrations	1
Format	both print and electronic
Are you the author of this Elsevier article?	No
Will you be translating?	No
Order reference number	cao2722
Original figure numbers	Scheme 2
Title of your thesis/dissertation	Interactions Between Serum Albumin Proteins and Polystyrene Nanoparticles
Expected completion date	Jun 2018
Estimated size (number of pages)	125
Requestor Location	Ms. Amanda Bishop [REDACTED]
	Calgary, AB [REDACTED] Canada Attn: Ms. Amanda Bishop

1 of 6 6/29/2018 2:31 PM

Publisher Tax ID GB 494 6272 12

Total 0.00 USD

Terms and Conditions

### INTRODUCTION

1. The publisher for this copyrighted material is Elsevier. By clicking "accept" in connection with completing this licensing transaction, you agree that the following terms and conditions apply to this transaction (along with the Billing and Payment terms and conditions established by Copyright Clearance Center, Inc. ("CCC"), at the time that you opened your Rightslink account and that are available at any time at <http://myaccount.copyright.com>).

### GENERAL TERMS

2. Elsevier hereby grants you permission to reproduce the aforementioned material subject to the terms and conditions indicated.

3. Acknowledgement: If any part of the material to be used (for example, figures) has appeared in our publication with credit or acknowledgement to another source, permission must also be sought from that source. If such permission is not obtained then that material may not be included in your publication/copies. Suitable acknowledgement to the source must be made, either as a footnote or in a reference list at the end of your publication, as follows:

"Reprinted from Publication title, Vol /edition number, Author(s), Title of article / title of chapter, Pages No., Copyright (Year), with permission from Elsevier [OR APPLICABLE SOCIETY COPYRIGHT OWNER]." Also Lancet special credit - "Reprinted from The Lancet, Vol. number, Author(s), Title of article, Pages No., Copyright (Year), with permission from Elsevier."

4. Reproduction of this material is confined to the purpose and/or media for which permission is hereby given.

5. Altering/Modifying Material: Not Permitted. However figures and illustrations may be altered/adapted minimally to serve your work. Any other abbreviations, additions, deletions and/or any other alterations shall be made only with prior written authorization of Elsevier Ltd. (Please contact Elsevier at [permissions@elsevier.com](mailto:permissions@elsevier.com)). No modifications can be made to any Lancet figures/tables and they must be reproduced in full.

6. If the permission fee for the requested use of our material is waived in this instance, please be advised that your future requests for Elsevier materials may attract a fee.

7. Reservation of Rights: Publisher reserves all rights not specifically granted in the combination of (i) the license details provided by you and accepted in the course of this licensing transaction, (ii) these terms and conditions and (iii) CCC's Billing and Payment terms and conditions.

8. License Contingent Upon Payment: While you may exercise the rights licensed immediately upon issuance of the license at the end of the licensing process for the transaction, provided that you have disclosed complete and accurate details of your proposed use, no license is finally effective unless and until full payment is received from you (either by publisher or by CCC) as provided in CCC's Billing and Payment terms and conditions. If full payment is not received on a timely basis, then any license preliminarily granted shall be deemed automatically revoked and shall be void as if never granted. Further, in the event that you breach any of these terms and conditions or any of CCC's Billing and Payment terms and conditions, the license is automatically revoked and shall be void as if never

homepage at <http://www.elsevier.com>. All content posted to the web site must maintain the copyright information line on the bottom of each image.

**Posting licensed content on Electronic reserve:** In addition to the above the following clauses are applicable: The web site must be password-protected and made available only to bona fide students registered on a relevant course. This permission is granted for 1 year only. You may obtain a new license for future website posting.

**17. For journal authors:** the following clauses are applicable in addition to the above:

**Preprints:**

A preprint is an author's own write-up of research results and analysis, it has not been peer-reviewed, nor has it had any other value added to it by a publisher (such as formatting, copyright, technical enhancement etc.).

Authors can share their preprints anywhere at any time. Preprints should not be added to or enhanced in any way in order to appear more like, or to substitute for, the final versions of articles however authors can update their preprints on arXiv or RePEc with their Accepted Author Manuscript (see below).

If accepted for publication, we encourage authors to link from the preprint to their formal publication via its DOI. Millions of researchers have access to the formal publications on ScienceDirect, and so links will help users to find, access, cite and use the best available version. Please note that Cell Press, The Lancet and some society-owned have different preprint policies. Information on these policies is available on the journal homepage.

**Accepted Author Manuscripts:** An accepted author manuscript is the manuscript of an article that has been accepted for publication and which typically includes author-incorporated changes suggested during submission, peer review and editor-author communications.

Authors can share their accepted author manuscript:

- immediately
  - via their non-commercial person homepage or blog
  - by updating a preprint in arXiv or RePEc with the accepted manuscript
  - via their research institute or institutional repository for internal institutional uses or as part of an invitation-only research collaboration work-group
  - directly by providing copies to their students or to research collaborators for their personal use
  - for private scholarly sharing as part of an invitation-only work group on commercial sites with which Elsevier has an agreement
- After the embargo period
  - via non-commercial hosting platforms such as their institutional repository
  - via commercial sites with which Elsevier has an agreement

In all cases accepted manuscripts should:

- link to the formal publication via its DOI
- bear a CC-BY-NC-ND license - this is easy to do
- if aggregated with other manuscripts, for example in a repository or other site, be shared in alignment with our hosting policy not be added to or enhanced in any way to appear more like, or to substitute for, the published journal article.

**Published journal article (JPA):** A published journal article (PJA) is the definitive final record of published research that appears or will appear in the journal and embodies all value-adding publishing activities including peer review co-ordination, copy-editing, formatting, (if relevant) pagination and online enrichment.

Policies for sharing publishing journal articles differ for subscription and gold open access articles:

**Subscription Articles:** If you are an author, please share a link to your article rather than the full-text. Millions of researchers have access to the formal publications on ScienceDirect, and so links will help your users to find, access, cite, and use the best available version. Theses and dissertations which contain embedded PJAs as part of the formal submission can be posted publicly by the awarding institution with DOI links back to the formal publications on ScienceDirect.

If you are affiliated with a library that subscribes to ScienceDirect you have additional private sharing rights for others' research accessed under that agreement. This includes use for classroom teaching and internal training at the institution (including use in course packs and courseware programs), and inclusion of the article for grant funding purposes.

**Gold Open Access Articles:** May be shared according to the author-selected end-user license and should contain a [CrossMark logo](#), the end user license, and a DOI link to the formal publication on ScienceDirect.

Please refer to Elsevier's [posting policy](#) for further information.

18. **For book authors** the following clauses are applicable in addition to the above:

Authors are permitted to place a brief summary of their work online only. You are not allowed to download and post the published electronic version of your chapter, nor may you scan the printed edition to create an electronic version. **Posting to a repository:** Authors are permitted to post a summary of their chapter only in their institution's repository.

19. **Thesis/Dissertation:** If your license is for use in a thesis/dissertation your thesis may be submitted to your institution in either print or electronic form. Should your thesis be published commercially, please reapply for permission. These requirements include permission for the Library and Archives of Canada to supply single copies, on demand, of the complete thesis and include permission for Proquest/UMI to supply single copies, on demand, of the complete thesis. Should your thesis be published commercially, please reapply for permission. Theses and dissertations which contain embedded PJAs as part of the formal submission can be posted publicly by the awarding institution with DOI links back to the formal publications on ScienceDirect.

#### **Elsevier Open Access Terms and Conditions**

You can publish open access with Elsevier in hundreds of open access journals or in nearly 2000 established subscription journals that support open access publishing. Permitted third party re-use of these open access articles is defined by the author's choice of Creative Commons user license. See our [open access license policy](#) for more information.

#### **Terms & Conditions applicable to all Open Access articles published with Elsevier:**

Any reuse of the article must not represent the author as endorsing the adaptation of the article nor should the article be modified in such a way as to damage the author's honour or reputation. If any changes have been made, such changes must be clearly indicated.

The author(s) must be appropriately credited and we ask that you include the end user license and a DOI link to the formal publication on ScienceDirect.

If any part of the material to be used (for example, figures) has appeared in our publication

with credit or acknowledgement to another source it is the responsibility of the user to ensure their reuse complies with the terms and conditions determined by the rights holder.

**Additional Terms & Conditions applicable to each Creative Commons user license:**

**CC BY:** The CC-BY license allows users to copy, to create extracts, abstracts and new works from the Article, to alter and revise the Article and to make commercial use of the Article (including reuse and/or resale of the Article by commercial entities), provided the user gives appropriate credit (with a link to the formal publication through the relevant DOI), provides a link to the license, indicates if changes were made and the licensor is not represented as endorsing the use made of the work. The full details of the license are available at <http://creativecommons.org/licenses/by/4.0>.

**CC BY NC SA:** The CC BY-NC-SA license allows users to copy, to create extracts, abstracts and new works from the Article, to alter and revise the Article, provided this is not done for commercial purposes, and that the user gives appropriate credit (with a link to the formal publication through the relevant DOI), provides a link to the license, indicates if changes were made and the licensor is not represented as endorsing the use made of the work. Further, any new works must be made available on the same conditions. The full details of the license are available at <http://creativecommons.org/licenses/by-nc-sa/4.0>.

**CC BY NC ND:** The CC BY-NC-ND license allows users to copy and distribute the Article, provided this is not done for commercial purposes and further does not permit distribution of the Article if it is changed or edited in any way, and provided the user gives appropriate credit (with a link to the formal publication through the relevant DOI), provides a link to the license, and that the licensor is not represented as endorsing the use made of the work. The full details of the license are available at <http://creativecommons.org/licenses/by-nc-nd/4.0>. Any commercial reuse of Open Access articles published with a CC BY NC SA or CC BY NC ND license requires permission from Elsevier and will be subject to a fee.

Commercial reuse includes:

- Associating advertising with the full text of the Article
- Charging fees for document delivery or access
- Article aggregation
- Systematic distribution via e-mail lists or share buttons

Posting or linking by commercial companies for use by customers of those companies.

**20. Other Conditions:**

v1.9

**Questions?** [customercare@copyright.com](mailto:customercare@copyright.com) or +1-855-239-3415 (toll free in the US) or +1-978-646-2777.